12/16/94

SANDIA REPORT

SAND93—4020 • UC—814
Unlimited Release
Printed November 1994

Yucca Mountain Site Characterization Project

Bulk and Mechanical Properties of the Paintbrush Tuff Recovered from Borehole USW NRG-6: Data Report

R. J. Martin, R. H. Price, P. J. Boyd, J. S. Noel

Prepared by
Sandia National Laboratories
Albuquerque, New Mexico 87185 and Livermore, California 94550
for the United States Department of Energy
under Contract DE-AC04-94AL85000

"Prepared by Yucca Mountain Site Characterization Project (YMSCP) participants as part of the Civilian Radioactive Waste Management Program (CRWM). The YMSCP is managed by the Yucca Mountain Project Office of the U.S. Department of Energy, DOE Field Office, Nevada (DOE/NV). YMSCP work is sponsored by the Office of Geologic Repositories (OGR) of the DOE Office of Civilian Radioactive Waste Management (OCRWM)."

Issued by Sandia National Laboratories, operated for the United States Department of Energy by Sandia Corporation.

Available to DOE and DOE contractors from
Office of Scientific and Technical Information
PO Box 62
Oak Ridge, TN 37831

Prices available from (615) 576-8401, FTS 626-8401

Available to the public from
National Technical Information Service
US Department of Commerce
5285 Port Royal Rd
Springfield, VA 22161

NTIS price codes
Printed copy: A06
Microfiche copy: A01

DISCLAIMER

Portions of this document may be illegible in electronic image products. Images are produced from the best available original document.

SAND93-4020
Unlimited Release
Printed November 1994

Distribution
Category UC-814

BULK AND MECHANICAL PROPERTIES OF THE PAINTBRUSH TUFF RECOVERED FROM BOREHOLE USW NRG-6: DATA REPORT

R. J. Martin[1], R. H. Price[2], P. J. Boyd[1], J. S. Noel[1]

[1]New England Research, Inc.
White River Junction, Vermont 05001

[2]YMP Performance Assessment Applications Department
Sandia National Laboratories
Albuquerque, New Mexico 87185

ABSTRACT

Experimental results are presented for bulk and mechanical properties measurements on specimens of the Paintbrush tuff recovered from borehole USW NRG-6 at Yucca Mountain, Nevada. Measurements have been performed on four thermal/mechanical units, TCw, PTn, TSw1, and TSw2. On each specimen the following bulk properties have been reported: dry bulk density, saturated bulk density, average grain density, and porosity. Unconfined compression to failure, confined compression to failure, and indirect tensile strength tests were performed on selected specimens recovered from the borehole. In addition, compressional and shear wave velocities were measured on specimens designated for unconfined compression and confined compression experiments. Measurements were conducted at room temperature on nominally water saturated specimens; however, some specimens of PTn were tested in a room dry condition. The nominal strain rate for the fracture experiments was 10^{-5} s^{-1}.

CONTENTS

List of Figures

List of Tables

This report was prepared for the Yucca Mountain Site Characterization Project. The scientific investigation discussed in this report is covered under the description of work for WBS number 1.2.3.2.7.1.3, QA Grading Report #1.2.3.2.7.1.3, Revision 00. The planning documents that guided this work activity are Site Characterization Plan Section 8.3.1.15.1.3; Study Plan SP-8.3.1.15.1.3, Revision 0; and Work Agreement WA-0090. The information and data documented in this report were collected under a fully qualified QA Program and may be used in licensing the repository.

1.0 INTRODUCTION

An integral part of the licensing procedure for the potential nuclear waste repository at Yucca Mountain, Nevada, involves prediction of the *in situ* rheology for the design and construction of the facility and the emplacement of canisters containing radioactive waste. The data used to model the thermal and mechanical behavior of the repository and surrounding lithologies include dry and saturated bulk densities, average grain density, porosity, compressional and shear wave velocities, elastic moduli, and compressional and tensional fracture strengths. In this study, a suite of experiments was performed on cores recovered from the USW NRG-6 borehole drilled in support of the Exploratory Studies Facility (ESF) at Yucca Mountain. USW NRG-6 was drilled to a depth of 1,100 feet through four thermal/mechanical units of Paintbrush tuff. The thermal/mechanical stratigraphy was defined by Ortiz et al. (1985) to group rock horizons of similar properties for the purpose of simplifying modeling efforts. The relationship between the geologic stratigraphy and the thermal/mechanical stratigraphy is presented in Figure 1. The tuff samples in this study have a wide range of welding characteristics (usually reflected in sample porosity), and a smaller range of mineralogy and petrology characteristics. Generally, the samples are silicic, ash-fall tuffs that exhibit large variability in their elastic and strength properties (see Price and Bauer, 1985).

Seventy-eight cores from USW NRG-6 were sent to New England Research, Inc., for bulk and baseline mechanical property measurements. A breakdown of the samples according to tests performed is given below:

Type of Test	**Number of Samples Tested**
Average Grain Density	78
Unconfined Compression	48
Confined Compression	20
Indirect Tensile Strength	39

On thirteen cores there was insufficient material or the material was of such poor quality that mechanical tests could not be performed. On these cores, only the average grain density and porosity were determined. Some of the raw cores were also prepared for use in thermal properties measurements.

USW NRG-6
Stratigraphic and Thermal/Mechanical Units Summary

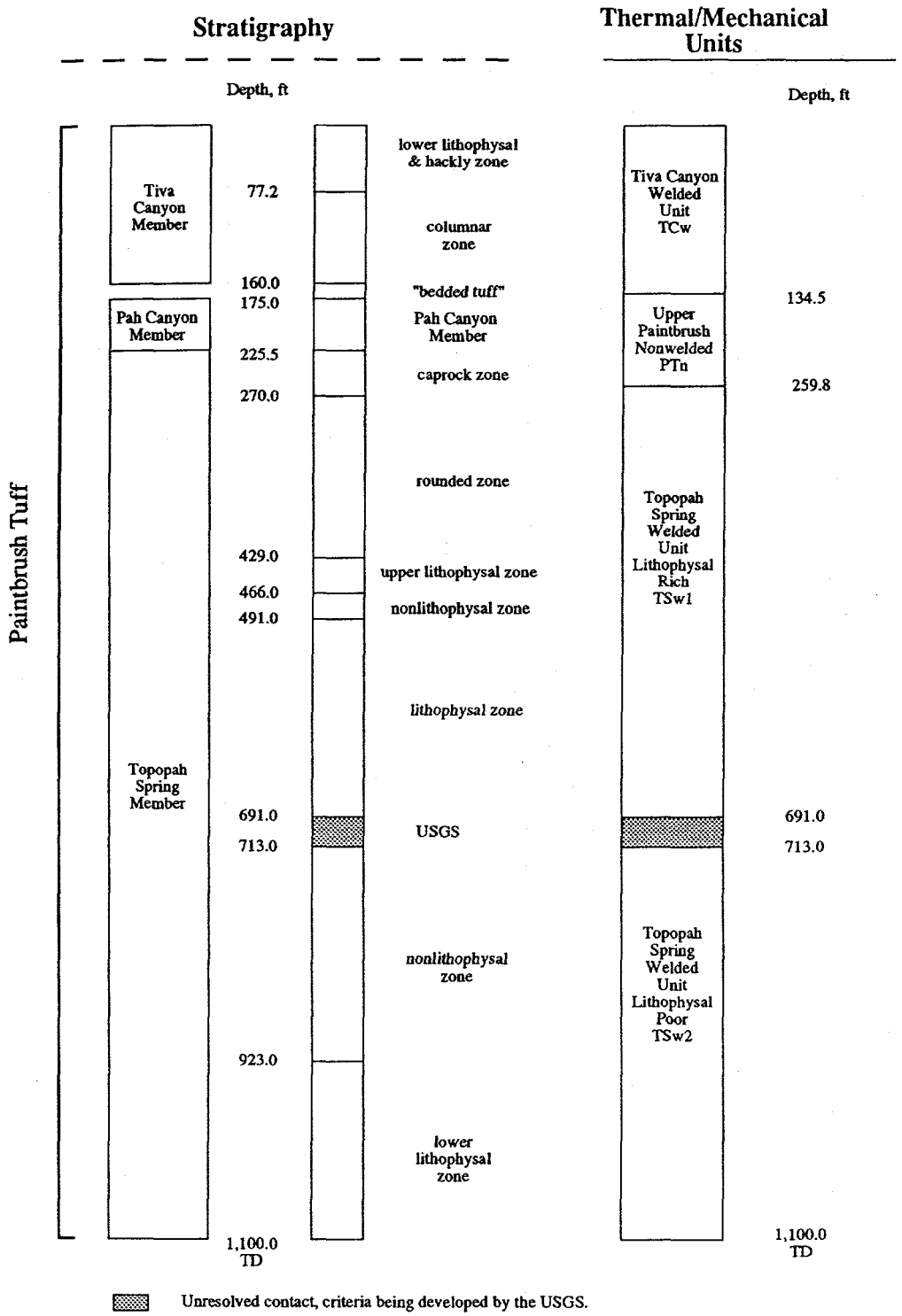

Figure 1: The correlation between the stratigraphic and thermal/mechanical units for borehole USW NRG-6 at Yucca Mountain, Nevada (per preliminary stratigraphy by J.F.T. Agapito and Associates, Inc., 10-28-93).

2.0 EXPERIMENTAL PROCEDURE

Measurements were performed on 78 specimens prepared from core recovered from borehole USW NRG-6. When the core was received it was examined to determine the best utilization of the rock material to obtain the maximum mechanical data. The size of the specimen for each type of measurement was a major part of the selection criteria. The nominal dimensions of the cylindrical rock specimens for each of the mechanical tests are given below:

Test	Length (mm)	Diameter (mm)
Indirect Tensile Strength	38.1	50.8
Unconfined Compression	101.6	50.8
Confined Compression	50.8	25.4

The length and diameter have a tolerance of $\pm$ 0.125 mm. The ends of the cylinders were parallel to within 0.025 mm.

Dry, and saturated (with a few exceptions) bulk densities were measured on each of the specimens prepared for unconfined compression, confined compression, and indirect tensile strength tests. Average grain density was determined with the water pycnometry technique using pieces remaining from the subcoring attendant to the preparation of the test specimens.

2.1 Sample Preparation

All specimens prepared for unconfined compression, confined compression, and indirect tensile strength testing were ground, right circular cylinders with dimensions listed above. The dimensions of the specimens were checked and verified according to the Sandia National Laboratories (SNL) Technical Procedure (TP) 51 entitled "Preparing Cylindrical Samples, Including Inspection of Dimensional and Shape Tolerances".

In some cases more than one specimen was obtained from a core. This was particularly true for the confined compression tests. This approach was adopted, on a limited basis, for several reasons. The tuff is very heterogeneous. Testing a limited number of specimens at confining pressures of 5, or 10 MPa may not reflect the singular effect of pressure on fracture strength and elastic constants. The determination of the influence of pressure is further complicated by limited sample availability. Certain standard test methods suggest that measurements should be carried out on specimens greater than

47 mm in diameter, but they allow for smaller specimens, if deemed appropriate, as long as the decision is documented. If the latter approach is adopted, the influence of the smaller specimen volume must be incorporated into the engineering analysis of the data. By preparing a statistically significant number of 25.4 mm diameter specimens from raw core, the effect of pressure could be more clearly distinguished without the complicating effects of variable porosity and pore geometry. A core of the TCw thermal mechanical unit, recovered from a depth of 22.2 to 23.1 feet was of sufficient quality and homogeneity to machine 12 specimens for confined compression experiments. Similarly, eight specimens were machined from a core of the TSw1 thermal/mechanical unit, recovered from a depth of 416.0 to 417.0 feet. Subdivisions of these cores were treated as new specimens and a Chain-of-Custody form was prepared for each piece of material generated in the subdivision process (per SNL QAIP 20-03, "Sample Control"). The prepared specimens were labeled and stored in containers until the measurement sequence was initiated.

The general measurement sequence for each specimen is given below:

Dimensions measurement
Specimen description
CT Scan (unconfined compression specimens only)
Drying specimen to a constant weight
Dry bulk density measurement
Compressional and shear wave velocities for the dry condition (all unconfined and representative confined compression specimens)
Saturating specimen to a constant weight with water
Saturated bulk density measurement
Compressional and shear wave velocities for the saturated state (all unconfined and representative confined compression specimens)
Mechanical testing (unconfined compression, confined compression, or indirect tensile strength tests)
Description of post failure condition of the specimen
Post-test photograph taken

Average grain density measurements were performed concurrently with the other activities.

2.2 CT Scans of Each Specimen Tested in Unconfined Compression

Prior to testing, a computerized tomography (CT) scan was performed on each

specimen designated for testing in unconfined compression. Since CT scans are sensitive to variations in density, this visual representation permits an initial qualitative examination of the distribution of pores and low density zones throughout the rock specimen and provides data for more quantitative analyses, if desired. Given the presence of lithophysae and vapor-phase altered zones within the tuff, the CT scan is a particularly useful technique for evaluating the effects these features may have on the mechanical properties of the tuff at the laboratory scale.

2.3 Drying, Saturation, Bulk Density, Average Grain Density, and Porosity

The dry and saturated bulk densities, average grain density, and porosity were determined for each specimen prepared for a mechanical test. The procedures were developed in accordance with ASTM D 854 "Standard Test Method for Specific Gravity of Soils" and ASTM C 135 "Standard Test Method for True specific Gravity of Refractory Materials by Water Immersion".

2.3.1 Procedure for Drying a Specimen

The specimen was dried to a constant weight and its dry bulk density determined. Drying was carried out at 110 ± 5 °C according to SNL TP-65, "Drying Geologic Specimens to a Constant Weight". Once the mass change for successive drying cycles had stabilized to within ± 0.05 percent, the dry bulk density, ρ_{db}, was computed.

Previous studies have shown that drying at 110 °C produces no noticeable damage (microcracks) in welded tuff. This was demonstrated by measuring compressional and shear wave velocities before and after heating a TSw2 specimen to 110 °C. Thermal cycling produced no reduction in the velocities suggesting no thermally induced microcracking. If microcracks develop due to differential thermal expansion, the velocities will decrease.

Each specimen is dried in an oven controlled to an accuracy of ± 5 °C. The procedure for drying is outlined below.

1) Place the specimen in the oven. Increase the temperature in the oven to 110 ± 5 °C at a rate less than or equal to 2 °C min^{-1}.

2) Maintain the specimen at 110 ± 5 °C for 120 to 128 hours. Reduce the temperature in the oven at a rate of less than or equal to 2 °C min^{-1} until the oven

temperature is between ambient and 40 °C.

3) Remove the specimen from the drying oven and weigh it three times. The specimen should be weighed within 15 seconds of removal from the oven. Calculate the mean dry mass of the specimen for the three measurements.

4. Repeat steps 1 through 3.

5) Calculate the mass change of the specimen for the successive drying cycles. If the change in mass for successive drying cycles is less than or equal to 0.05% the process has met the specification and oven drying of the specimen is terminated. If the mass change is greater than 0.05% steps 1 through 3 must be repeated until the specification is met.

6) Compute the dry bulk density by dividing the dry mass by the specimen volume.

2.3.2 Procedure for Water Saturation

With the exception of some very friable specimens, the mechanical tests were performed on water saturated specimens. Saturation of the specimens was achieved in a two-stage process. First, the specimen was pressure saturated at 10 MPa for a minimum of 1 hour. Next, a minimum of two vacuum saturation cycles were performed, according to SNL TP-64, "Procedure for Vacuum Saturation of Geologic Core Samples". Once the mass change for successive saturation cycles had stabilized to within ± 0.05 percent, the saturated bulk density, ρ_{sb}, was computed. The specimens were stored in distilled water following saturation and prior to testing. Some specimens from thermal/mechanical unit PTn were not saturated due to their friable nature, and the apparent presence of clay. Therefore saturated bulk density data was not obtained and these specimens were tested in unconfined compression and indirect tension in a room dry condition.

A brief synopsis of the procedure for saturation follows:

1) Place the specimen in a pressure vessel filled with distilled water.

2) Pressurize the vessel to 10 MPa and hold constant for at least one hour.

3) Remove the specimen from the pressure vessel, blot it with a damp lint free

paper towel.

4) Weigh the specimen within 15 seconds of blotting. Record the mass of the specimen in the laboratory notebook.

5) Place the specimen in a container filled with distilled water.

6) Place the water filled container with the specimen in a vacuum chamber.

7) Apply a vacuum to the vacuum chamber.

8) Vacuum saturate the specimen for at least 30 hours.

9) Turn off the vacuum pump, open the valve on the vacuum chamber and allow the pressure to equilibrate with atmospheric conditions.

10) Keep the specimen submerged in water at ambient pressure for at least 16 hours.

11) Remove the specimen from the container and blot it with a damp lint free paper towel.

12) Weigh the specimen within 15 seconds of blotting. Record the mass of the specimen on the vacuum saturation data sheet.

13) Return the specimen to the water filled container and repeat steps 11 and 12. Calculate the mean saturated mass of the specimen for the two measurements.

14) Return the specimen to the water filled container and repeat the vacuum saturation procedure in steps 6 through 13. Calculate the mass change for each successive vacuum saturation cycle. If the mass change for successive vacuum saturation cycles is less than or equal to 0.05% the process has met the specification and the saturation procedure is terminated. If the mass change is greater than 0.05% steps 6 through 13 must be repeated until the specification is met.

15) Store the specimen in distilled water at ambient pressure and temperature until it is ready for mechanical testing.

16) Compute the saturated bulk density by dividing the saturated mass by the

specimen volume.

2.3.3 Average Grain Density Measurement Using Water Pycnometry

The average grain density of each core received from the USW NRG-6 borehole was measured using the water pycnometry method. The technique employs a two-stage measurement. First, the mass of a dry, powdered specimen is measured. Next, the volume of the powder is determined. These two measurements are combined to compute the average grain density.

Pieces of core with a mass of approximately 20 to 50 grams are ground to a powder with a particle size of 1.5 mm or less. The powder is dried according to SNL TP-65.

The powdered specimen of tuff is added to a dry, calibrated, water pycnometer with a nominal volume of 100 ml. The step-by-step procedure presented below produces measurements of the dry mass of the powdered specimen and the corresponding volume of the specimen. The technique has been verified using quartz powders with a well characterized density.

1. Pulverize approximately 20 to 50 g of the specimen to a particle size of 1.5 mm or less. The powder is dried in an aluminum drying pan according to SNL TP-65, except cooling is not allowed at any time in order to minimize rehydration.

2. Add the dried sample to a calibrated, clean, dry and numbered pycnometer by pouring it through a clean, dry transfer funnel.

3. Weigh the pycnometer with the dry sample immediately (do not allow it to cool).

4. Add 50 to 60 ml of distilled water to the pycnometer and swirl it to moisten all of the sample powder.

5. Place the pycnometer, with the sample, in an active vacuum for a minimum of 16 hours. For the first one or two hours, watch the pycnometer to ensure that the boiling action does not displace any of the sample from the pycnometer. The vacuum should be regulated depending upon the observed phenomena.

6. Remove the pycnometer from the vacuum chamber and pour additional deaired water into the pycnometer until the water level is just below the scribe line. Note that pouring water down the neck reduces the likelihood of entrapping air into the

water as it is added to the pycnometer.

7. Use a pipette to add water until the bottom of the meniscus is at the height of the scribe line. It may be necessary to raise the water level higher than the scribe line, to wet the sides of the pycnometer for a suitable meniscus. In this case, water is removed to obtain the correct reading.

8. Use a cotton swab to dry the inside of the neck of the pycnometer.

9. Use a lint free wipe to clean and dry the exterior of the pycnometer.

10. Weigh the pycnometer and its contents.

11. Measure the water temperature in the pycnometer to the nearest 0.2 ^{o}C.

12. Calculate the average grain density (ρ_g) of the specimen using the water pycnometer grain density measurement sheet (Figure 2).

13. Pour the sample and water into a clean container to allow the water to evaporate.

14. Store the sample powder in a container to maintain it in its original condition.

2.3.4 Dry Bulk Density, Saturated Bulk Density, and Porosity

The dry bulk density, ρ_{db}, is obtained by computing the volume of a test specimen from its external dimensions and dividing it into the mass measured in a dry condition. The density corresponding to the measurement in the saturated condition is the saturated bulk density, ρ_{sb}. Preferably, porosity, ϕ, is computed using the following relation:

$$\phi = \frac{\rho_g - \rho_{db}}{\rho_g} \times 100\%$$

Alternatively, the porosity can be calculated from the dry bulk density and saturated bulk density according to:

$$\phi = \frac{\rho_{sb} - \rho_{db}}{\rho_w} \times 100\%$$

where ρ_w is the density of water.

Bulk Properties
Yucca Mountain Project
WATER PYCNOMETER GRAIN DENSITY MEASUREMENT
per TP-___229 Rev. 0____

SAMPLE ID:_____

WATER PYCNOMETER ID:_____

Date of latest calibration:_____Nominal Pycnometer Volume:_____

DATA:

Dry Pyc. Wt.:_____g (A) Dry Pyc. + Dry Sample Wt.:_____g (B)

Dry Sample Wt.:_____g (C) = B-A

Wt. Pyc. + Sample + Water:_____g (D)

Water Temperature:_____°C (E) Water Density at (E) (See Below):_____g/cc (F)

Wt. Water Only:_____g (G) = D-B

Volume Water:_____cc (H) = G/F

Volume Pyc. at (E) from Calibration:_____cc (I)

Volume Sample:_____cc (J) = I-H

Sample Grain Density:_____g/cc (K) = C/J

Absolute Density of Water
(From Lange's Handbook of Chemistry, edited by J. Dean, 11th Edition, Sect. 10-127)

Temp °C	Density	Temp °C	Density	Temp °C	Density	Temp °C	Density
18.0	0.998595	20.8	0.998035	23.6	0.997394	26.4	0.996676
18.2	0.998553	21.0	0.997992	23.8	0.997345	26.6	0.996621
18.4	0.998520	21.2	0.997948	24.0	0.997296	26.8	0.996567
18.6	0.998482	21.4	0.997904	24.2	0.997246	27.0	0.996512
18.8	0.998444	21.6	0.997850	24.4	0.997196	27.2	0.996457
19.0	0.998405	21.8	0.997815	24.6	0.997146	27.4	0.996401
19.2	0.998365	22.0	0.997770	24.8	0.997095	27.6	0.996345
19.4	0.998325	22.2	0.997724	25.0	0.997044	27.8	0.996289
19.6	0.998285	22.4	0.997678	25.2	0.996992	28.0	0.996232
19.8	0.998244	22.6	0.997632	25.4	0.996941	28.2	0.996175
20.0	0.998203	22.8	0.997585	25.6	0.996888	28.4	0.996118
20.2	0.998162	23.0	0.997535	25.8	0.996835	28.6	0.996060
20.4	0.998120	23.2	0.997490	26.0	0.996783	28.8	0.996002
20.6	0.998078	23.4	0.997442	26.2	0.996729	29.0	0.995944

Operator: Print/Sign:_____Date/Time:_____

Figure 2: Bulk properties worksheet used to record measurements and reduce data for the computation of average grain density.

2.4 Compressional and Shear Wave Velocity Measurements

Compressional and shear wave velocities were measured on right circular cylinders with a nominal length to diameter ratio of 2:1. The velocities were measured for both dry and water saturated conditions at ambient temperature in a benchtop apparatus. Specimens were dried at 110 °C according to SNL TP-65 (as in Section 2.3.1). Earlier investigations have shown that heating specimens of Topopah Spring Member tuff to 110 °C does not damage them by the formation of microcracks.

The compressional and shear wave velocity measurements are used for two main purposes. First, a measure of the specimen anisotropy can be directly obtained by comparing the compressional and shear wave velocities measured both parallel and normal to the core axis. Second, compressional and shear wave velocity data, combined with the density of the specimen, are used to compute Young's modulus and Poisson's ratio. These elastic moduli will be referred to as dynamic moduli in subsequent discussions. The dynamic moduli can then be compared with the moduli computed for the data on the unconfined compression tests conducted at a strain rate of 10^{-5} s^{-1}. The elastic constants computed from stress and strain measurements in a deformational experiment are often referred to as static. For porous rocks, the dynamic moduli are greater than the static moduli measured during the constant strain rate experiments, and therefore serve as an upper bound on the static moduli (Simmons and Brace, 1965; Cheng and Johnston, 1981; Haupt et al., 1992).

A self-contained ultrasonic measuring system is used to perform the velocity measurements. A tuff specimen is placed between a matched set of ultrasonic transducers. One transducer serves as the source; the second as the receiver (Figure 3). The travel time through the rock is divided by the sample length to compute the velocity.

Each ultrasonic transducer contains one compressional and one or two polarized shear wave elements. For the measurements parallel to the core axis one compressional and two orthogonally polarized shear waves are propagated. For measurements normal to the core axis, one compressional and one polarized shear wave velocity are measured. The polarization direction of the shear wave propagating normal to the core axis is parallel to the axis of the core.

The transducers are constructed using piezoelectric crystals with a resonant frequency of 1 MHz. The multicomponent piezoelectric crystals are bonded to a titanium substrate. Titanium has been selected because it has a good acoustical impedance match both to the rock and to the piezoelectrical crystals. The source crystal is excited with a fast

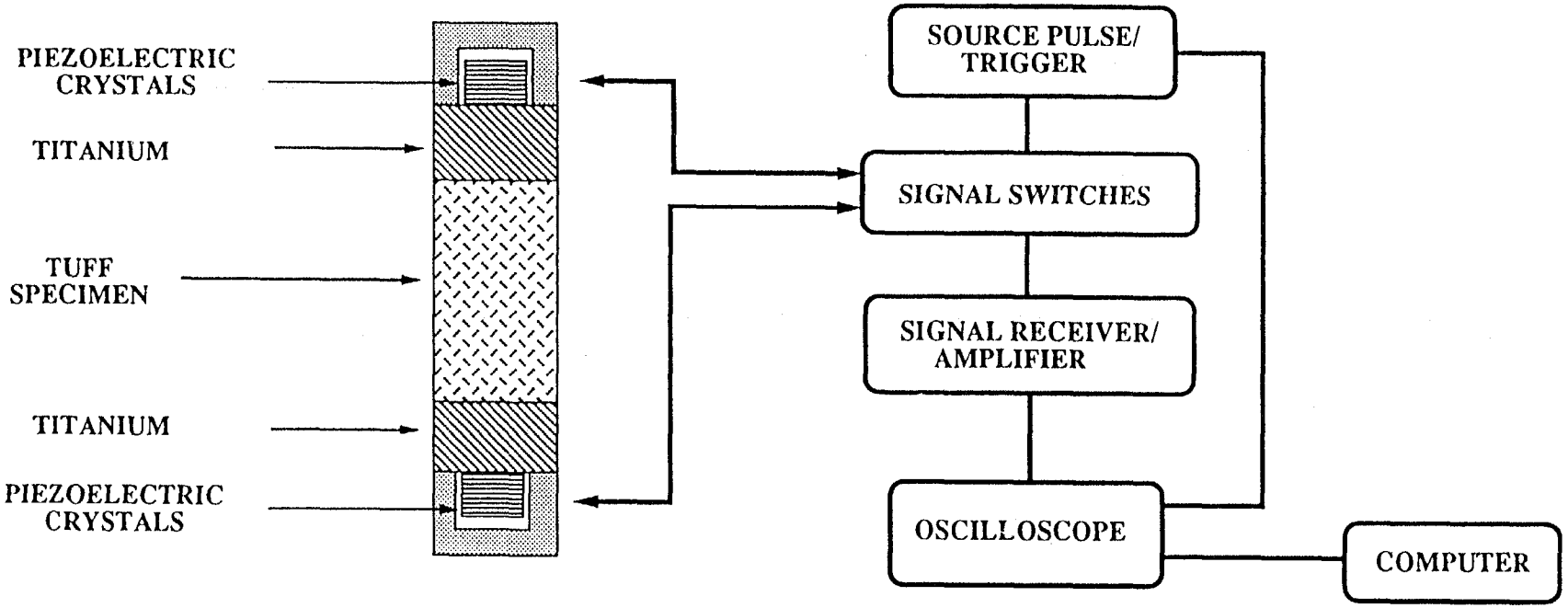

Figure 3: Schematic diagram of the geometry used to measure compressional and shear wave velocities in tuff. The diagram shows the setup for the measurement of velocities parallel to the core axis.

rise time pulse generator. The crystal produces a broad band ultrasonic pulse propagated through the adjacent titanium substrate, the rock, the titanium at the opposite end of the core, and into the receiver crystal. The received electrical signal is then amplified and filtered through the receiving section of the pulser-receiver and displayed on a digital storage oscilloscope. The signals are amplified, and high pass filtered above 0.3 MHz. The time series displayed on the oscilloscope is then digitized and transferred to a computer for subsequent analysis including picking the first arrival of the compressional and shear wave energy to compute the compressional and shear wave velocities. The accuracy of the travel time is ± 0.02 microseconds.

A diagram of the system is shown in Figure 4. Pneumatic actuators couple the transducer assemblies in both the axial and radial directions. The stress across the interface for both the matched transducer pairs is identical; this is accomplished by adjusting the loading areas in the pneumatic actuators. The titanium pieces for the radial transducers are concave to mate with the rock surface. Because of the geometry of the interface, only polarizations parallel to the core axis are propagated for shear waves in the radial direction.

2.4.1 Detailed Procedure for Compressional and Shear Wave Velocity Measurements

The detailed procedure for measuring compressional and shear wave velocities on dry and water saturated tuff specimens is presented below.

1. The tuff sample is a ground, right circular cylinder with a nominal length to diameter ratio of 2:1. The sample is machined to meet or exceed the tolerances specified in SNL TP-51.

2. Coat the ends of the specimen with a shear wave couplant. Shear wave couplant is a viscous substance that facilitates the propagation of shear waves across the specimen-titanium interface. Shear wave couplant is also applied at the midpoint of the specimen where the velocities normal to the specimen axis are measured.

3. Position the specimen in the ultrasonic velocity measuring apparatus. Ensure that the specimen is lined up with the transducers in the axial direction.

4. Increase the pressure in the pneumatic actuators to load the axial and radial transducer assemblies to the specimen. Ensure that the specimen has not shifted during this procedure and that the specimen is well coupled to the transducer

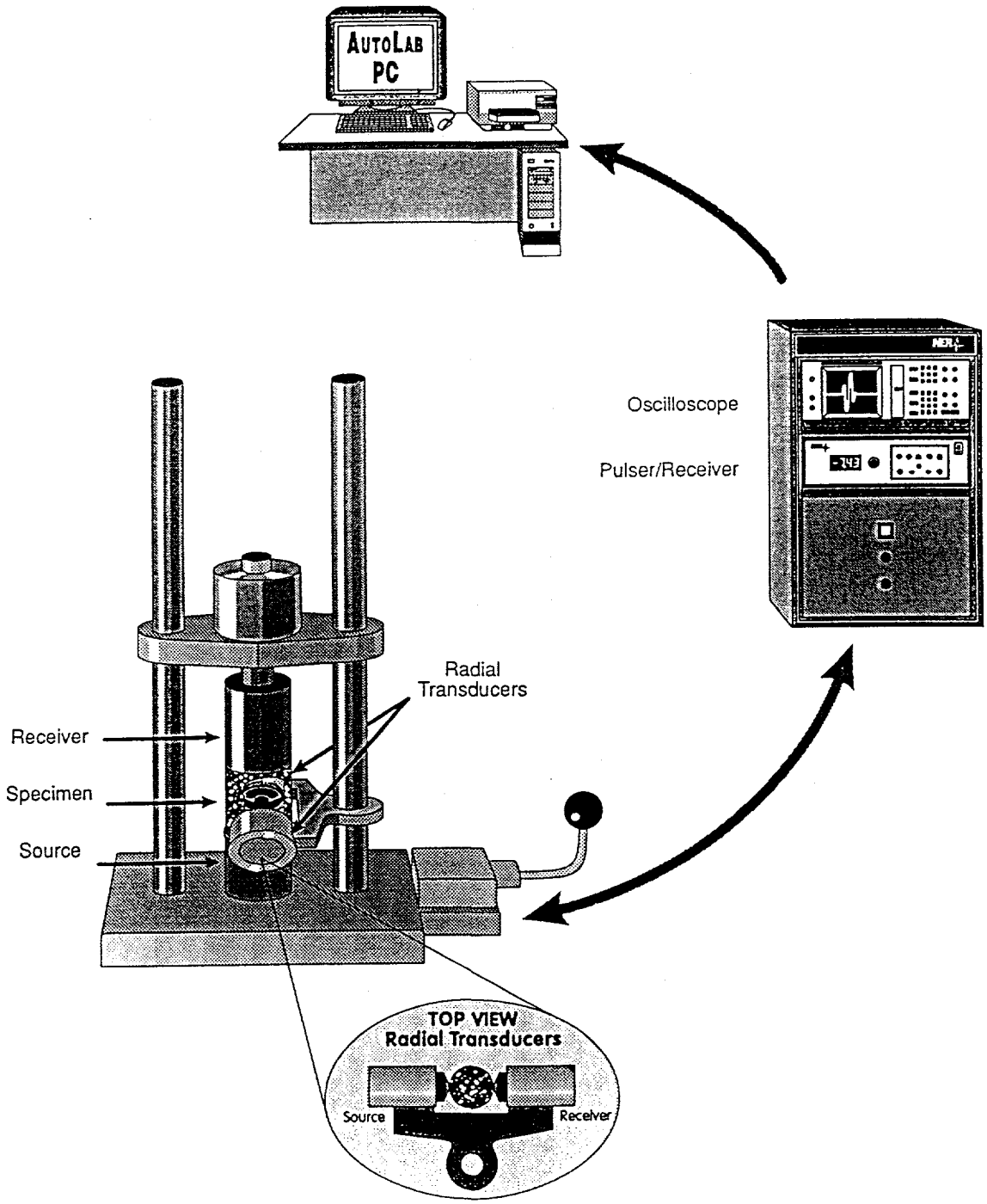

Figure 4: Schematic of the apparatus used to measure ultrasonic velocities parallel and normal to the core axis under ambient conditions prior to testing in unconfined compression.

assembly.

5. Turn on the data acquisition system. First, set the signal selection switch for a compressional (P) wave along the axis of the specimen. Observe the received signal on the digital oscilloscope. Adjust the pulse excitation signal gain and/or attenuation to obtain a well-defined signal.

6. Initiate the data acquisition software to store the waveform; capture and store the waveform.

7. Capture the two shear (S1 and S2) wave polarizations with a propagation direction parallel to the core axis, and the compressional and shear wave signals for the propagation direction normal to the core axis, following the same procedure used for the compressional wave in steps 5 and 6.

8. Compute the compressional and shear wave velocities by determining the travel time through the specimen and dividing it into the sample length. The travel time is determined by picking the time of the first arrival of the compressional or shear wave energy. The measured travel times are reduced by the travel time through the titanium substrates. The corrected travel time is then divided into the sample length to determine the velocity.

9. Print the stored waveforms, along with the computed compressional and shear wave velocities, and place the data in the scientific notebook.

10. Compute the dynamic Young's modulus (E) and Poisson's ratio (ν) from the velocity data collected parallel to the core axis and the bulk density of the specimen for the measurement condition. The dynamic elastic moduli are computed as follows:

$$E = [\rho V_s^2 (3V_p^2 - 4V_s^2)/(V_p^2 - V_s^2)]$$

$$\nu = (V_p^2 - 2V_s^2)/[2(V_p^2 - V_s^2)]$$

where

V_p = compressional wave velocity, km s^{-1}

V_s = average shear wave velocity, km s^{-1}

ρ = bulk density for the measurement conditions, g cm^{-3}

2.5 Unconfined Compression to Failure

The unconfined compression experiments were performed on right-circular cylinders of tuff with a nominal length to diameter ratio of 2:1, at a constant axial strain rate of 10^{-5} s^{-1} at room temperature. System checks of the entire test system were conducted during this experimental series in order to establish the performance of the system using an aluminum specimen with the same nominal dimensions as the tuff test specimens.

A description of the equipment and an overview of the test procedures places the step-by-step procedures in the proper context. All the compression tests were carried out in a servo-controlled hydraulic loading frame with a capacity of 1.1×10^6 N. The servo-controller is a self-contained digital unit, which operates in either force or displacement feedback. The rate at which the reference signal is updated can be varied from 10^{-5} to 10^3 times per second. The loading rate or displacement rate depends on the range of the feedback transducers and the time between steps. The feedback transducers are conditioned with amplifiers in the servo-control unit and balanced so that the full-scale output of the transducer corresponds to the maximum range of the reference signal generator. The full scale output (10 V) is divided into 2^{12} discrete steps.

Figure 5 is a schematic diagram of an instrumented specimen. The test assembly consists of the specimen positioned between hardened steel end caps. The specimen is jacketed in a flexible membrane in order to maintain its moisture level.

For this experimental series, five outputs from a variety of transducers were monitored. The output from each device is conditioned, amplified, converted to digital format, and recorded as a function of time. The outputs from the devices were recorded with a microcomputer acquisition system. Each channel is sampled at a frequency of 4 Hz.

For constant strain rate tests the loading frame is operated in displacement feedback. The displacement can be controlled to within $\pm 10^{-3}$ mm when the system is in the displacement mode. The accuracy and the reproducibility of the strain rate in this system is $\pm$ 0.5 percent.

During each test the axial and radial displacements of the specimen were measured with Linear Variable Differential Transformers (LVDTs). A schematic of their arrangement is shown in Figure 5. Two LVDTs monitor the axial displacement. The LVDT barrels are secured in a ring which is attached one specimen radius from the upper end of the specimen. The cores for the displacement transducers are on extended rods which attach to a second ring separated from the first by one specimen diameter. The second ring is

Axial and Radial Deformation Instrumentation

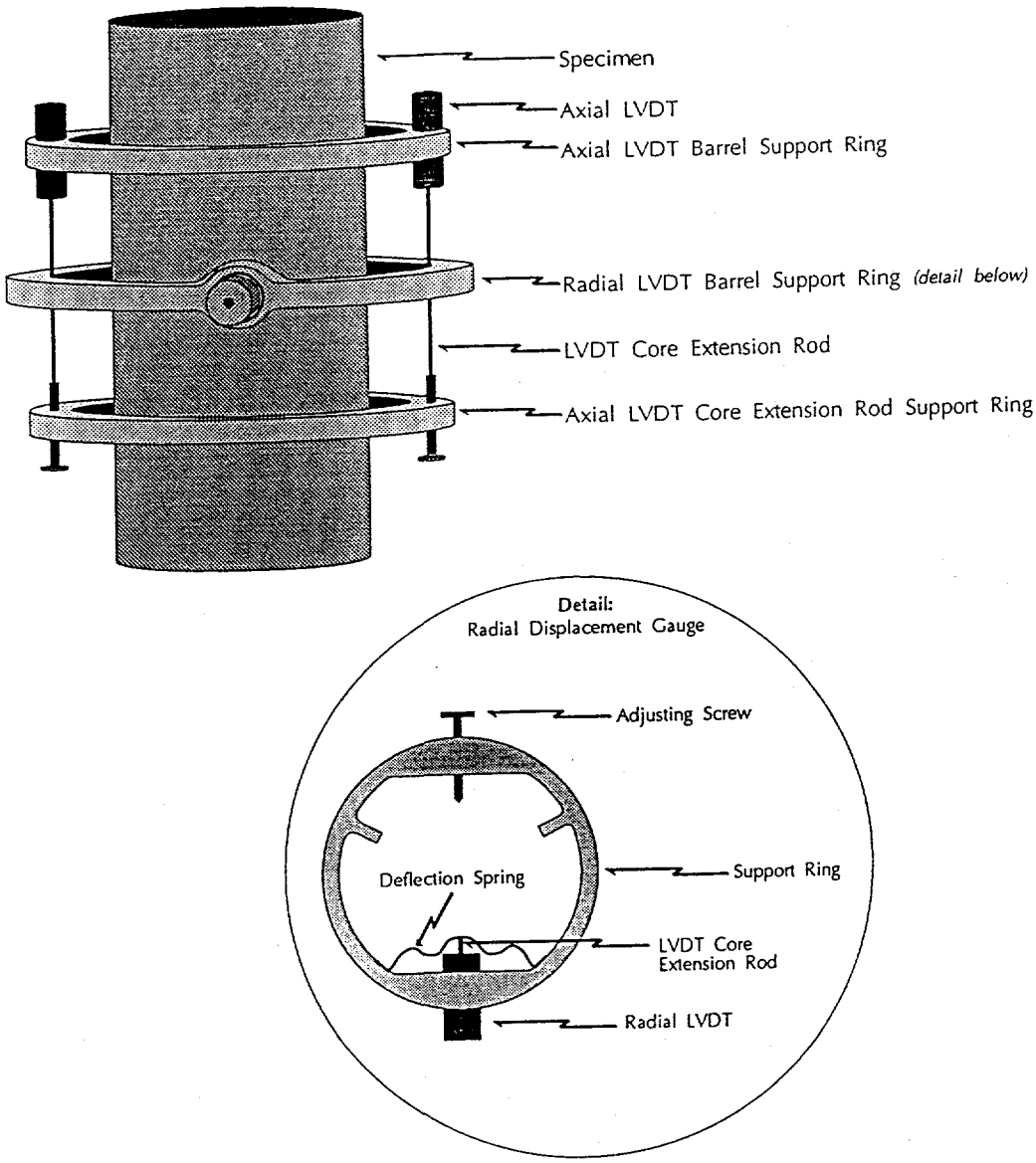

Figure 5: Schematic of the transducer configuration used to measure the axial and radial displacement of specimens during unconfined and confined compression tests.

mounted approximately one specimen radius from the lower end of the specimen.

The most direct way to measure radial strain is with the radial displacement gage developed by Holcomb and McNamee (1984). Their gage consists of an LVDT mounted in a ring which is spring loaded against the surface of the specimen (Figure 5). The core of the LVDT is connected to the spring. As the specimen diameter changes, the spring deflects, changing the position of the core within the barrel of the LVDT in direct proportion to the radial displacement.

The force on the test column is measured with a load cell. The accuracy of the load cell is better than 0.5 percent of its full-scale output; the combined linearity and hysteresis are better than 1.0 percent. The position of the hydraulic piston is observed with a displacement transducer. This transducer provides feedback control in constant strain rate tests and is continuously monitored along with all the transducer outputs. The hydraulic piston advances at a constant rate; this is equivalent to deforming the specimen at a constant strain rate only in the linear portion of the stress-strain curve.

Checks of the entire test system are made using a sample of 6061-T6511 aluminum with the same nominal dimensions as the test specimens. One check is performed before the experiments on a suite of tuff samples, and then after each group of ten tuff samples. Each check was performed at the same conditions as the experiments on the tuff specimens: a nominal strain rate of 10^{-5} s^{-1}, at ambient temperature.

2.5.1 Experimental Procedures For Unconfined Compression Tests

Specimens of tuff were tested to failure at a constant strain rate of 10^{-5} s^{-1}, under ambient temperature and pressure conditions. The following sections include the step-by-step procedures for the mechanical experiments based on SNL TP 219 "Unconfined Compression Experiments at 22 °C and a Strain Rate of 10^{-5} s^{-1}". The test procedure relies on ASTM Standard Method D 3148 " Standard Test Method for Elastic Moduli of Intact Rock Core Specimens in Uniaxial Compression" and ISRM procedure "Suggested Methods for Determining the Uniaxial Compressive Strength and Deformability of Rock Materials."

1. Each tuff specimen is machined according to SNL TP-51, dried according to SNL TP-65, and saturated according to SNL TP-64 (unless saturation would cause the specimen to disintegrate). Velocity measurements are performed after the drying and saturation procedures.

2. List all transducers used for each experiment. The information includes the serial

numbers of the device, signal conditioning amplifier number, the computer channel on which the output is recorded, and the scaling factor for the amplified output.

3. Visually inspect the test specimen and note any surface irregularities and imperfections.

4. Jacket the saturated specimen in a thin, flexible membrane. The membrane is extended 12 mm beyond each end of the specimen. Hardened steel end caps are then positioned at each end of the specimen.

5. Position the ring supporting the two axial LVDT barrels approximately one specimen radius from the upper end of the specimen. Carefully center the ring so that it is concentric with the specimen.

6. Position the LVDT ring used to measure the radial displacement at the midpoint of the specimen. The supporting ring for the LVDT (with a range of $\pm$ 1.25 mm) is positioned in such a way to ensure that the line between the adjusting screw on the ring and the axis of the core barrel of the LVDT passes through the axis of the specimen and is perpendicular to the axis of the specimen.

7. Position the lower support ring for the axial LVDT concentrically about the specimen approximately one specimen diameter from the upper ring. This ring supports the stainless steel extension rods for the LVDT cores. Ensure that the axes of the LVDT core barrels are aligned parallel with the axis of the specimen. The extension rods are supported with adjusting screws that are secured with locking nuts.

8. Measure the center-to-center separation of the axial LVDT support rings with a caliper-micrometer. Record this value in the scientific notebook.

9. Place the specimen assembly on the base plug of the load frame.

10. Connect the two axial LVDTs and the radial LVDT to the electrical leads in the base plug.

11. Advance the loading piston, in displacement control, until a small load is exerted on the specimen column (just enough to hold the specimen securely in position).

12. Make the final mechanical adjustments on the LVDTs. Each LVDT is adjusted so that its initial amplified output is approximately 0.10 V. Note that all the LVDTs are wired so that increasing the specimen diameter and shortening the specimen assembly results in an increasing positive output voltage.

13. Retract the hydraulic piston until there is no force on the loading column.

14. Initiate data acquisition. The amplified outputs from five transducers are monitored and recorded using a microprocessor-based data acquisition system. The transducers that are monitored include the three LVDTs, the feedback displacement transducer, and the force cell. All the channels are sampled every 0.25 seconds. Data is stored when the output of one channel deviates from the previous value by a preselected threshold. The threshold for each channel is independently set prior to the experiment.

15. Adjust the setting on the displacement rate controller to the displacement rate that corresponds to a nominal strain rate of 10^{-5} s^{-1}. After a final check of all the transducer values, start loading the specimen.

16. Load the specimen to failure.

17. Remove the specimen from the press and examine the manner in which it failed. Record the observations in the scientific notebook. Photograph the specimen. Ensure that the field of view of the photograph includes the specimen identification, TP identification, scale, date, type of test performed, and NER identification.

18. Return the specimen to its original container, and return it to storage.

19. Reduce the data. The following elastic constants are computed:

    (a) Young's modulus, E
    $E = \Delta$ (axial stress) / Δ (axial strain)

    (b) Poisson's ratio, ν
    $\nu = \Delta$ (radial strain) / Δ (axial strain)

    The elastic constants are computed by performing a least-squares linear fit to the data collected between 10 and 50 percent of the fracture strength. Axial stress is computed by dividing the axial force by the initial cross sectional area of the

specimen. Stress is reported in MPa. Axial strain is obtained by dividing the average axial displacement of the axial LVDT support rings by the original ring separation distance. Radial strain is computed by dividing the change in radial displacement observed by the radial LVDT by the initial specimen diameter. All strains are reported in millistrain.

2.6 Confined Compression to Failure

Confined compression tests were carried out on specimens from cores with sufficient uniform material that numerous specimens could be obtained. The specimens had a length to diameter ratio of 2:1 with a diameter of 25.4 mm and were tested in a saturated condition. The general procedure for testing these specimens was the same as that described for the unconfined compression tests except that the specimens were jacketed in copper and deformed in a pressure vessel at a fixed confining pressure. The procedure was based on TP-219 and conforms to ISRM "Suggested Methods for Determining the Strength of Rock Materials in Triaxial Compression" and ASTM D 2664-86 "Triaxial Compressive Strength of Undrained Rock Core Specimens Without Pore Pressure Measurements". The series of tests were designed so that at least three specimens were tested for each confining pressure. Specimens were tested at confining pressures of 0, 5, and 10 MPa.

Each specimen was jacketed in dead soft copper 0.13 mm thick. The jacket was seated to the rock specimen by subjecting it to a hydrostatic pressure of 10 MPa. Once the jacket was seated, it was visually inspected to ensure that there were no holes that would permit leakage of the confining medium into the rock core during the test. Next, the specimen was instrumented using the same arrangement utilized for the unconfined compression tests (Figure 5).

The instrumented specimen was mounted on the base plug of a 50 MPa capacity pressure vessel. The LVDTs were adjusted. Once the LVDTs were on scale and functioning properly, the base plug of the pressure vessel containing the instrumented specimen assembly was inserted into the pressure vessel. Next, the confining pressure was exerted on the specimen using a servo-controlled hydraulic intensifier. The confining medium was argon gas. The confining pressure was allowed to stabilize. The confining pressure was held constant during the remainder of the experiment to within $\pm$ 0.1 MPa.

Once the confining pressure reached thermal equilibrium the specimen was monotonically loaded to failure at a strain rate of 10^{-5} s^{-1}. After the specimen failed, the

confining pressure was released and the specimen was removed and inspected. The data was reduced to determine Young's modulus, Poisson's ratio, and fracture strength. Young's modulus and Poisson's ratio are computed in the same manner as for the unconfined compression tests, between 10 and 50 percent of the stress difference at failure.

2.7 Indirect Tensile Strength Tests

Indirect tensile strength tests, commonly referred to as Brazil tests, were carried out using a procedure adhering to ASTM D-3967 "Splitting Tensile Strength of Intact Rock Core Specimens". The test is quite simple in principle. A load is applied to a cylindrical specimen with its axis normal to the loading direction. A tensile stress develops in the center of the cylinder. The specimen fails by an extension fracture along the diametral loading plane. The force is increased until the specimen fails. The strength is computed from the force at failure.

The tests were performed in the servo-controlled load frame used for the unconfined and confined compression tests. For these measurements the only transducer was a load cell with a capacity of 4.5×10^4 N. A schematic diagram of the setup is shown in Figure 6.

The specimens were right circular cylinders, ground to the dimensions and tolerances listed in Section 2.0. The dry bulk density and saturated bulk density were measured prior to testing. In general, specimens were tested in a water saturated condition except for some specimens of the PTn thermal/mechanical unit.

To obtain reproducible and accurate data, it is important that the loading axis of the test frame passes through the axis of the specimen. As an aid in the alignment of the specimen in the loading column, diametral lines are scribed on the bearing surfaces.

2.7.1 Experimental Procedures for Indirect Tensile Strength Tests

The detailed procedure developed according to ASTM D-3967 is presented below.

1. Each tuff specimen was machined according to SNL TP-51, dried according to SNL TP-65, and saturated according to SNL TP-64 (unless saturation would cause the specimen to disintegrate). All initial conditions were documented.

2. Mark diametral lines on the ends of the specimen.

3. Cut 2.5 cm wide by 4.0 cm long (slightly longer than the specimens) pieces of

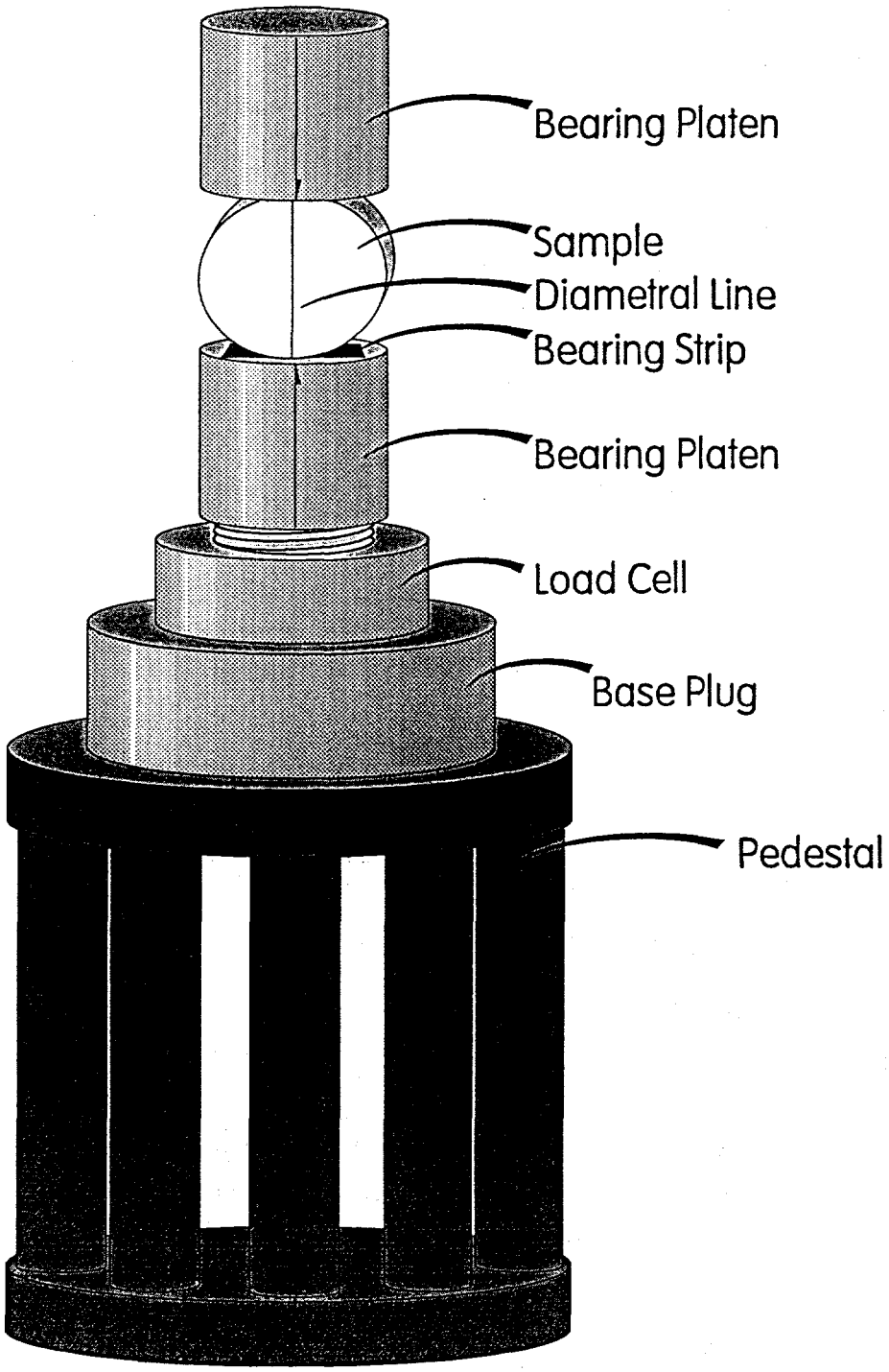

Figure 6: Schematic of the loading arrangement and sample geometry used for the indirect tensile strength tests.

notepad-backing cardboard approximately 0.89 mm thick for bearing strips.

4. Place one bearing strip onto the bottom bearing platen with its length parallel to the diametral line scribed onto the platen.

5. Place the specimen onto the bearing strip making certain its full length is supported by the bearing strip. Align the axis of the specimen parallel to the line scribed onto the platen (lines on both ends of the specimen line up with the line scribed on the platen).

6. Place the second bearing strip onto the top of the specimen making certain it will support the full length of the specimen.

7. Advance the loading piston, in displacement control, until a small load is applied (just enough to hold the specimen and the bearing strips in place while positioning them).

8. Make final adjustments to the specimen's position to ensure the diametral plane of the two lines marked onto the specimen line up with the center of thrust (lines scribed onto the top and bottom bearing planes), and its midpoint along its length is also lined up to within $\pm$ 0.025 mm of the center of the bearing platens. The midpoint is centered by repeatedly measuring the distance from the specimen ends to the edge of the bearing platens and adjusting its position until they are equal.

9. Initiate the data acquisition system.

10. Load the specimen monotonically to failure in displacement control at the same rate used for the unconfined compression tests. Once the specimen fails, data acquisition is terminated and any remaining load is removed. The specimen is removed from the loading column, described, and photographed.

11. Calculate the indirect tensile strength using the formula:

$$\sigma_t = 2F/\pi L D$$

where

F = applied force

L= specimen length

D= specimen diameter.

The indirect tensile strength is reported in MPa.

3.0 RESULTS

The results of the bulk properties measurements and the mechanical tests are presented in Tables 1, 2, 3, and 4. Table 1 presents the data associated with the unconfined compression tests. The data include dry bulk density, saturated bulk density, average grain density, porosity, compressional and shear wave velocities for the dry and saturated conditions, both parallel [axial] and normal [radial] to the core axis, static Young's modulus, static Poisson's ratio, axial stress at failure, and axial strain at failure. These data have been grouped according to depth. The thermal/mechanical unit is indicated for each specimen. For some specimens, saturated bulk density was not measured and reliable compressional and shear wave velocities were not obtained due to poor signal quality. The absence of the data is reflected in Tables 1, 2, and 3.

The porosity reported in Tables 1, 2, 3 and, 4 is the total porosity including occluded porosity. The value is computed from the grain density and dry bulk density. The total porosity is most applicable when elastic constants and strength characteristics are measured. The porosity computed from the dry and saturated bulk densities is typically lower than the total porosity and reflects the interconnected porosity. The latter value is applicable when considering fluid transport properties.

Table 2 presents the data for the confined compression tests. The dry bulk density, saturated bulk density, average grain density, porosity, compressional and shear wave velocities for propagation parallel to the specimen axis at one confining pressure, confining pressure at which the sample was tested, static Young's modulus, static Poisson's ratio, axial stress difference at failure, and axial strain difference at failure are presented as a function of depth for the two suites of confined compression tests performed on core recovered from depths of 22.2 to 23.1 feet (TCw) and 416.0 to 417.0 feet (TSw1).

Table 3 presents the results of the indirect tensile strength tests. The data are presented as a function of depth and include dry bulk density, saturated bulk density, average grain density, porosity, and indirect tensile strength. The thermal/mechanical unit for each specimen is also indicated. No compressional or shear wave velocities were measured on these specimens.

Table 4 lists the specimens for which only average grain density, dry bulk density, and porosity were measured. The thermal/mechanical unit for each of these specimens is indicated.

Table 1

SUMMARY DATA SHEET: NRG-6 BOREHOLE

Unconfined Compression Tests

Sample IDs are shortened from the "NRG-6-Depth-SNL-Subdivision" Format
Test Conditions: Saturated samples (except as noted), ambient pressure and temperature, and a nominal strain rate of 10E-5 sE-1
Nominal Sample Dimensions: Length = 101.60 mm; Diameter = 50.80 mm

Depth, ft:	22.2	23.4	98.1	98.1	111.0	111.0	143.5	151.2	161.4 *	169.5 *
T/M Unit:	TCw	TCw	TCw	TCw	TCw	TCw	PTn	PTn	PTn	PTn
Date Tested:	5/11/93	5/13/93	5/13/93	5/13/93	5/13/93	5/13/93	5/10/93	5/10/93	5/5/93	5/5/93
Dry Bulk Density (g/cc):	2.354	2.356	2.309	2.305	2.219	2.236	1.897	1.431	1.490	1.501
Saturated Bulk Density (g/cc):	2.399	2.404	2.371	2.369	2.325	2.332	2.065	1.815		
Average Grain Density (g/cc):	2.496	2.491	2.493	2.493	2.497	2.497	2.439	2.416	2.423	2.498
Porosity via Grain Density (%):	5.7	5.4	7.4	7.5	11.1	10.5	22.2	40.8	38.5	39.9
Dry P Velocity (km/s):	4.682	4.728	4.370	4.355	4.157	4.190	3.750	2.875		
Dry S1 Velocity (km/s):	2.901	2.940	2.671	2.662	2.634	2.602	2.464	1.903		
Dry S2 Velocity (km/s):	2.895	2.929	2.672	2.660	2.527	2.601	2.444	1.887		
Dry Radial P Velocity (km/s):										
Dry Radial S Velocity (km/s):										
Sat. P Velocity (km/s):	4.704	4.729	4.402	4.395	4.233	4.230	3.507			
Sat. S1 Velocity (km/s):	2.839	2.860	3.170	2.595	2.384	2.512	2.645			
Sat. S2 Velocity (km/s):	2.818	2.846	3.143	2.589	2.359	2.525	2.644			
Saturated Radial P Velocity, km/s	4.689	4.710	4.432	4.422	4.252	4.343	4.027			
Saturated Radial S Velocity, km/s	2.928	2.877	2.616	2.627	2.359	2.495	1.235			
Static Young's modulus (GPa):	36.7	39.0	30.0	29.2	23.1	26.5	14.8	5.9	2.9	2.4
Static Poisson's ratio:	0.22	0.22	0.24	0.25	0.21	0.21	0.13	0.13	0.16	0.12
Ultimate Axial Stress (MPa):	313.6	303.7	245.6	242.2	78.2	114.1	61.8	11.3	3.5	5.9
Ax. Strn at Ult. Ax. Sts. (milstrn):		8.38	8.58	8.72	3.60	5.03	7.38	2.40	2.69	3.36

* Specimen tested room dry.
P is the compressional wave; S1 and S2 are the two orthogonally polarized shear waves.
Elastic properties are calculated between 10 and 50 percent of the ultimate differential axial stress.

Table 1 (Continued)

SUMMARY DATA SHEET: NRG-6 BOREHOLE

Unconfined Compression Tests

Sample IDs are shortened from the "NRG-6-Depth-SNL-Subdivision" Format
Test Conditions: Saturated samples (except as noted), ambient pressure and temperature, and a nominal strain rate of 10E-5 sE-1
Nominal Sample Dimensions: Length = 101.60 mm; Diameter = 50.80 mm

Depth, ft:	174.0 *	182.2 *	187.0 *	222.0 *	227.9 *	241.5 *	276.2	304.4	316.3	318.2
T/M Unit:	PTn	PTn	PTn	PTn	PTn	PTn	TSw1	TSw1	TSw1	TSw1
Date Tested:	5/5/93	5/10/93	5/5/93	5/5/93	5/10/93	5/5/93	5/13/93	5/13/93	5/14/93	5/14/93
Dry Bulk Density (g/cc):	1.100	1.039	1.113	1.396	1.027	1.027	2.304	2.270	2.192	2.194
Saturated Bulk Density (g/cc):							2.387	2.369	2.331	2.327
Average Grain Density (g/cc):	2.413	2.392	2.383	2.489	2.364	2.456	2.565	2.559	2.593	2.585
Porosity via Grain Density (%):	54.4	56.6	53.3	43.9	56.6	58.2	10.2	11.3	15.5	15.1
Dry P Velocity (km/s):							4.355	4.193	3.580	3.623
Dry S1 Velocity (km/s):							2.589	2.572	2.221	2.231
Dry S2 Velocity (km/s):							2.590	2.568	2.206	2.208
Dry Radial P Velocity (km/s):										
Dry Radial S Velocity (km/s):										
Sat. P Velocity (km/s):							4.632	4.545	4.116	4.104
Sat. S1 Velocity (km/s):							3.273	3.232		
Sat. S2 Velocity (km/s):							3.249	3.186		
Saturated Radial P Velocity, km/s							4.681	4.570	4.247	
Saturated Radial S Velocity, km/s								3.098		
Static Young's modulus (GPa):	1.2	0.8	1.3	1.5	0.7	0.5	33.2	28.1	22.0	22.4
Static Poisson's ratio:	0.21	0.23	0.34	0.23	0.23	0.29	0.21	0.21	0.26	0.27
Ultimate Axial Stress (MPa):	4.3	3.3	4.1	4.8	2.7	2.1	118.6	102.2	79.2	77.2
Ax. Strn at Ult. Ax. Sts. (milstrn):	4.43	3.25	3.94	3.90	4.95	5.46	3.75	4.08	4.26	4.40

* Specimen tested room dry.
P is the compressional wave; S1 and S2 are the two orthogonally polarized shear waves.
Elastic properties are calculated between 10 and 50 percent of the ultimate differential axial stress.

Table 1 (Continued)

SUMMARY DATA SHEET: NRG-6 BOREHOLE

Unconfined Compression Tests

Sample IDs are shortened from the "NRG-6-Depth-SNL-Subdivision" Format
Test Conditions: Saturated samples (except as noted), ambient pressure and temperature, and a nominal strain rate of 10E-5 sE-1
Nominal Sample Dimensions: Length = 101.60 mm; Diameter = 50.80 mm

Depth, ft:	328.7	328.7	354.4	372.6	373.1	391.6	395.2	397.0	407.2	420.8
T/M Unit:	TSw1	TSw1	TSw1	TSw1	TSw1	TSw1	TSw1	TSw1	TSw1	TSw1
Date Tested:	5/14/93	5/14/93	5/28/93	5/28/93	5/28/93	5/28/93	5/28/93	5/28/93	5/28/93	5/28/93
Dry Bulk Density (g/cc):	2.166	2.182	2.163	2.173	2.145	2.223	2.229	2.246	2.228	2.201
Saturated Bulk Density (g/cc):	2.311	2.327	2.303	2.302	2.290	2.336	2.332	2.353	2.327	2.309
Average Grain Density (g/cc):	2.593	2.593	2.588	2.567	2.572	2.563	2.543	2.559	2.546	2.536
Porosity via Grain Density (%):	16.5	15.9	16.4	15.4	16.6	13.3	12.4	12.2	12.5	13.2
Dry P Velocity (km/s):	3.705	3.706	3.510	3.631	3.555	3.862	3.745	3.797	3.888	3.747
Dry S1 Velocity (km/s):	2.430	2.289	2.242	2.264	2.250	2.376	2.277	2.319	2.286	2.208
Dry S2 Velocity (km/s):	2.215	2.293	2.169	2.310	2.234	2.380	2.292	2.325	2.288	2.222
Dry Radial P Velocity (km/s):				3.918	3.912	3.946	3.916		4.197	3.982
Dry Radial S Velocity (km/s):				2.367	1.972	2.420	2.401		2.531	2.502
Sat. P Velocity (km/s):	4.102	4.203	3.956	4.010	3.878	4.139	4.016	4.033	4.051	3.908
Sat. S1 Velocity (km/s):			2.223		2.075					
Sat. S2 Velocity (km/s):					2.091					
Saturated Radial P Velocity, km/s		4.358	4.238	4.365		4.235	4.235		4.433	4.125
Saturated Radial S Velocity, km/s										
Static Young's modulus (GPa):	21.5	23.8	17.0	15.1	21.2	20.6	21.8	20.6	20.1	12.2
Static Poisson's ratio:	0.29	0.24	0.15	0.16	0.25	0.22	0.21	0.29	0.27	0.33
Ultimate Axial Stress (MPa):	73.2	72.8	32.4	33.3	68.8	58.3	48.4	60.4	56.8	36.2
Ax. Strn at Ult. Ax. Sts. (milstrn):	3.92	3.75	3.51	2.72	3.79	3.34	2.54	4.27	3.12	3.70

P is the compressional wave; S1 and S2 are the two orthogonally polarized shear waves.
Elastic properties are calculated between 10 and 50 percent of the ultimate differential axial stress.

Table 1 (Continued)

SUMMARY DATA SHEET: NRG-6 BOREHOLE

Unconfined Compression Tests

Sample IDs are shortened from the "NRG-6-Depth-SNL-Subdivision" Format
Test Conditions: Saturated samples (except as noted), ambient pressure and temperature, and a nominal strain rate of 10E-5 sE-1
Nominal Sample Dimensions: Length = 101.60 mm; Diameter = 50.80 mm

Depth, ft:	427.0	488.0	662.2	687.5	720.7	742.3	742.9	762.9	773.5	784.8
T/M Unit:	TSw1	TSw1	TSw1	TSw1	TSw2	TSw2	TSw2	TSw2	TSw2	TSw2
Date Tested:	5/28/93	7/27/93	7/27/93	7/27/93	7/27/93	7/27/93	7/27/93	7/27/93	7/27/93	7/27/93
Dry Bulk Density (g/cc):	2.172	2.219	2.146	2.222	2.292	2.249	2.275	2.309	2.264	2.270
Saturated Bulk Density (g/cc):	2.292	2.324	2.292	2.336	2.367	2.351	2.367	2.400	2.359	2.356
Average Grain Density (g/cc):	2.527	2.504	2.534	2.535	2.504	2.526	2.528	2.552	2.523	2.511
Porosity via Grain Density (%):	14.1	11.4	15.3	12.4	8.5	11.0	10.0	9.5	10.3	9.6
Dry P Velocity (km/s):	3.463	4.299	4.421	4.352	4.629	4.393	4.395	4.471	4.575	4.432
Dry S1 Velocity (km/s):	2.228	2.684			2.928	2.766	2.780	2.831	2.886	2.818
Dry S2 Velocity (km/s):	2.179	2.679			2.919	2.774	2.810	2.812	2.891	2.824
Dry Radial P Velocity (km/s):	4.035	4.157	4.261	4.403	4.624	4.405	4.259	4.492	4.575	4.436
Dry Radial S Velocity (km/s):	2.456	2.649	2.682		2.916	2.769	2.814	2.848	2.878	2.823
Sat. P Velocity (km/s):	3.817	4.334	4.447	4.467	4.632	4.408	4.407	4.518	4.574	4.436
Sat. S1 Velocity (km/s):										
Sat. S2 Velocity (km/s):										
Saturated Radial P Velocity, km/s	4.080	4.214		4.486	4.634	4.427	4.311	4.540	4.578	4.432
Saturated Radial S Velocity, km/s										2.703
Static Young's modulus (GPa):	14.2	33.3	29.2	24.6	37.1	30.6	32.4	29.2	36.2	29.7
Static Poisson's ratio:	0.19	0.21	0.38	0.12	0.19	0.20	0.22	0.18	0.23	0.17
Ultimate Axial Stress (MPa):	43.4	149.4	50.4	95.8	235.5	162.3	212.8	112.1	117.4	223.0
Ax. Strn at Ult. Ax. Sts. (milstrn):	3.94	8.76	2.79	4.37	6.82	7.03	7.37	4.85	2.90	9.46

P is the compressional wave; S1 and S2 are the two orthogonally polarized shear waves.
Elastic properties are calculated between 10 and 50 percent of the ultimate differential axial stress.

Table 1 (Continued)

SUMMARY DATA SHEET: NRG-6 BOREHOLE

Unconfined Compression Tests

Sample IDs are shortened from the "NRG-6-Depth-SNL-Subdivision" Format
Test Conditions: Saturated samples (except as noted), ambient pressure and temperature, and a nominal strain rate of 10E-5 sE-1
Nominal Sample Dimensions: Length = 101.60 mm; Diameter = 50.80 mm

Depth, ft:	785.6	806.8	848.0	953.2	963.3	971.4	985.7	1017.8
T/M Unit:	TSw2	TSw2	TSw2	TSw2	TSw2	TSw2	TSw2	TSw2
Date Tested:	7/28/93	7/28/93	7/28/93	7/28/93	7/28/93	7/28/93	7/29/93	7/29/93
Dry Bulk Density (g/cc):	2.274	2.309	2.322	2.099	2.165	2.227	2.301	2.246
Saturated Bulk Density (g/cc):	2.359	2.379	2.420	2.259	2.306	2.335	2.397	2.359
Average Grain Density (g/cc):	2.507	2.509	2.605	2.548	2.542	2.542	2.554	2.572
Porosity via Grain Density (%):	9.3	8.0	10.9	17.6	14.8	12.4	9.9	12.7
Dry P Velocity (km/s):	4.506	4.661	4.433	4.054		4.511	4.494	4.456
Dry S1 Velocity (km/s):	2.860	2.946		2.408		2.812	2.805	2.786
Dry S2 Velocity (km/s):	2.873	2.942		2.459				2.802
Dry Radial P Velocity (km/s):	4.435	4.686	4.644	4.351		4.477	4.459	4.408
Dry Radial S Velocity (km/s):	2.845	2.950	2.807			2.836	2.796	2.746
Sat. P Velocity (km/s):	4.479	4.662	4.589	4.254		4.607	4.573	4.541
Sat. S1 Velocity (km/s):								
Sat. S2 Velocity (km/s):								
Saturated Radial P Velocity, km/s	4.435	4.656	4.725	4.427		4.614	4.588	4.500
Saturated Radial S Velocity, km/s		2.903						
Static Young's modulus (GPa):	30.1	31.7	34.6	16.9	19.3	27.4	37.6	27.4
Static Poisson's ratio:	0.16	0.16	0.19	0.11	0.31	0.19	0.25	0.23
Ultimate Axial Stress (MPa):	218.6	261.9	175.5	31.6	56.3	97.3	177.3	84.9
Ax. Strn at Ult. Ax. Sts. (milstrn):	7.94	8.05	5.52	4.56	3.86	4.48	4.96	3.29

P is the compressional wave; S1 and S2 are the two orthogonally polarized shear waves.
Elastic properties are calculated between 10 and 50 percent of the ultimate differential axial stress.

Table 2

SUMMARY DATA SHEET: NRG-6 BOREHOLE

Confined Compression Tests

Sample IDs are shortened from the "NRG-6-Depth-SNL-Subdivision" Format
Test Conditions: Saturated samples, ambient temperature, and a nominal strain rate of 10E-5 sE-1.
Nominal Sample Dimensions: Length = 50.80 mm; Diameter = 25.40 mm.

Depth, ft:	22.2-B	22.2-C	22.2-D	22.2-E	22.2-F	22.2-G	22.2-H	22.2-I	22.2-J	22.2-K	22.2-L	22.2-M
T/M Unit:	TCw	TCw	TCw	TCw	TCw	TCw	TCw	TCw	TCw	TCw	TCw	TCw
Date Tested:	6/14/93	6/14/93	6/14/93	6/15/93	6/15/93	6/15/93	6/15/93	6/15/93	6/16/93	6/16/93	6/16/93	6/16/93
Dry Bulk Density (g/cc):	2.357	2.351	2.329	2.363	2.368	2.367	2.354	2.360	2.358	2.363	2.367	2.363
Saturated Bulk Density (g/cc):	2.409	2.403	2.393	2.414	2.418	2.417	2.406	2.412	2.410	2.414	2.419	2.413
Average Grain Density (g/cc):	2.496	2.496	2.496	2.496	2.496	2.496	2.496	2.496	2.496	2.496	2.496	2.496
Porosity via Grain Density (%):	5.6	5.8	6.7	5.3	5.1	5.2	5.7	5.5	5.5	5.3	5.2	5.3
Sat. P Velocity at 10 MPa (km/s):	4.789	4.792	4.731	4.818	4.830	4.842	N/A	N/A	N/A	N/A	N/A	N/A
Sat. S1 Velocity at 10 MPa (km/s):	2.819	2.872	2.815	2.862	2.849	2.854	N/A	N/A	N/A	N/A	N/A	N/A
Sat. S2 Velocity at 10 MPa (km/s):	2.815	2.867	2.804	2.853	2.844	2.852	N/A	N/A	N/A	N/A	N/A	N/A
Confining Pressure (MPa):	10	10	10	10	5	5	5	5	0	0	0	0
Static Young's modulus (GPa):	36.9	38.1	35.6	38.3	36.4	37.4	36.8	36.3	37.2	37.4	36.4	36.7
Static Poisson's ratio:	0.23	0.20	0.21	0.21	0.22	0.22	0.21	0.20	0.21	0.20	0.22	0.22
Ultimate Diff. Axial Stress (MPa):	429.7	424.6	333.4	407.3	390.5	386.2	391.8	302.1	315.8	284.2	313.8	332.4
Ax. Strn at Ult. Ax. Sts. (milstrn):	14.06	13.04	11.98	13.33	12.28	11.67	12.36	8.70	9.24	8.55	9.32	9.75

P is the compressional wave; S1 and S2 are the two orthogonally polarized shear waves.
Elastic properties are calculated between 10 and 50 percent of the ultimate differential axial stress.

Table 2 (Continued)

SUMMARY DATA SHEET: NRG-6 BOREHOLE

Confined Compression Tests

Sample IDs are shortened from the "NRG-6-Depth-SNL-Subdivision" Format
Test Conditions: Saturated samples, ambient temperature, and a nominal strain rate of 10E-5 sE-1.
Nominal Sample Dimensions: Length = 50.80 mm; Diameter = 25.40 mm.

Depth, ft:	416.0-B	416.0-C	416.0-D	416.0-E	416.0-F	416.0-G	416.0-H	416.0-I
T/M Unit:	TSw1	TSw1	TSw1	TSw1	TSw1	TSw1	TSw1	TSw1
Date Tested:	6/17/93	6/17/93	6/17/93	6/17/93	6/17/93	6/18/93	6/18/93	6/18/93
Dry Bulk Density (g/cc):	2.262	2.266	2.213	2.267	2.239	2.197	2.235	2.230
Saturated Bulk Density (g/cc):	2.363	2.366	2.334	2.367	2.341	2.322	2.336	2.338
Average Grain Density (g/cc):	2.546	2.546	2.546	2.546	2.546	2.546	2.546	2.546
Porosity via Grain Density (%):	11.2	11.0	13.1	11.0	12.1	13.7	12.2	12.4
Sat. P Velocity at 10 MPa (km/s):	4.437	4.396	4.373	4.397	N/A	N/A	N/A	N/A
Sat. S1 Velocity at 10 MPa (km/s):	2.478	2.436	2.345	2.461	N/A	N/A	N/A	N/A
Sat. S2 Velocity at 10 MPa (km/s):	2.486	2.437	2.309	2.464	N/A	N/A	N/A	N/A
Confining Pressure (MPa):	10	10	10	10	5	5	5	5
Static Young's modulus (GPa):	17.9	19.3	21.0	8.4	12.3	13.7	17.1	16.3
Static Poisson's ratio:	0.34	0.30	0.28	0.22	0.45	-0.02	0.21	0.21
Ultimate Diff. Axial Stress (MPa):	109.9	137.9	20.1	51.1	72.1	34.6	79.7	53.8
Ax. Strn at Ult. Ax. Sts. (milstrn):	8.62	9.13	1.09	9.83	11.16	N/A	7.01	5.28

P is the compressional wave; S1 and S2 are the two orthogonally polarized shear waves.
Elastic properties are calculated between 10 and 50 percent of the ultimate differential axial stress.

Table 3

SUMMARY DATA SHEET: NRG-6 BOREHOLE

Indirect Tensile Strength (Brazil) Tests

Sample IDs are shortened from the "NRG-6-Depth-SNL-Subdivision" Format
Test Conditions: Saturated samples (except as noted), ambient pressure and temperature.
Nominal Sample Dimensions: Length = 38.10 ; Diameter = 50.80 mm.

Depth, ft:	23.4	23.4	98.1	98.1	111.0	111.0	145.7	151.2	174.0*	182.2*
T/M Unit:	TCw	TCw	TCw	TCw	TCw	TCw	PTn	PTn	PTn	PTn
Date Tested:	6/3/93	6/3/93	6/3/93	6/3/93	6/3/93	6/3/93	6/3/93	6/3/93	6/3/93	6/3/93
Dry Bulk Density (g/cc):	2.352	2.355	2.311	2.308	2.238	2.219	1.717	1.430	1.070	1.062
Saturated Bulk Density (g/cc):	2.400	2.403	2.378	2.375	2.336	2.321	1.912	1.821	N/A*	N/A*
Average Grain Density (g/cc):	2.491	2.491	2.493	2.493	2.497	2.497	2.443	2.416	2.413	2.392
Porosity via Grain Density (%):	5.6	5.5	7.3	7.4	10.4	11.1	29.7	40.8	55.7	55.6
Ultimate Tensile Stress (MPa):	16.0	13.2	10.6	11.3	8.2	12.1	4.5	1.9	0.3	0.4

Depth, ft:	222.0*	241.5*	276.2	304.4	318.2	355.4	373.6	392.6	395.0	397.5
T/M Unit:	PTn	PTn	TSw1	TSw1	TSw1	TSw1	TSw1	TSw1	TSw1	TSw1
Date Tested:	6/3/93	6/3/93	6/3/93	6/3/93	6/3/93	6/3/93	6/3/93	6/3/93	6/4/93	6/4/93
Dry Bulk Density (g/cc):	1.331	0.997	2.307	2.288	2.220	2.171	2.197	2.230	2.261	2.252
Saturated Bulk Density (g/cc):	N/A*	N/A*	2.382	2.371	2.349	2.319	2.321	2.335	2.363	2.356
Average Grain Density (g/cc):	2.489	2.456	2.565	2.559	2.585	2.582	2.568	2.546	2.553	2.554
Porosity via Grain Density (%):	46.5	59.4	10.1	10.6	14.1	15.9	14.5	12.4	11.4	11.8
Ultimate Tensile Stress (MPa):	0.3	0.2	8.4	9.3	7.6	5.3	6.6	6.5	6.8	4.7

*Specimen tested room dry.

Table 3 (Continued)

SUMMARY DATA SHEET: NRG-6 BOREHOLE

Indirect Tensile Strength (Brazil) Tests

Sample IDs are shortened from the "NRG-6-Depth-SNL-Subdivision" Format
Test Conditions: Saturated samples (except as noted), ambient pressure and temperature.
Nominal Sample Dimensions: Length = 38.10 ; Diameter = 50.80 mm.

Depth, ft:	407.0	421.5	427.0	462.3	640.0	687.5	742.3	742.9	773.5	784.8
T/M Unit:	TSw1	TSw1	TSw1	TSw1	TSw1	TSw1	TSw1	TSw2	TSw2	TSw2
Date Tested:	6/4/93	6/4/93	6/4/93	7/29/93	7/29/93	7/29/93	7/29/93	7/29/93	7/29/93	7/29/93
Dry Bulk Density (g/cc):	2.237	2.170	2.209	2.171	2.185	2.233	2.281	2.268	2.223	2.270
Saturated Bulk Density (g/cc):	2.344	2.296	2.326	2.296	2.306	2.340	2.370	2.357	2.321	2.358
Average Grain Density (g/cc):	2.547	2.529	2.527	2.519	2.530	2.535	2.526	2.528	2.523	2.511
Porosity via Grain Density (%):	12.2	14.2	12.6	13.8	13.6	11.9	9.7	10.3	11.9	9.6
Ultimate Tensile Stress (MPa):	5.1	4.1	4.0	5.2	5.1	8.7	14.5	13.0	7.9	12.5

Depth, ft:	785.6	848.0	908.2	934.0	934.0	956.8	963.3	969.3	971.4
T/M Unit:	TSw2	TSw2	TSw2	TSw2	TSw2	TSw2	TSw2	TSw2	TSw2
Date Tested:	7/29/93	7/29/93	7/29/93	7/29/93	7/30/93	7/30/93	7/30/93	7/30/93	7/30/93
Dry Bulk Density (g/cc):	2.274	2.344	2.310	2.251	2.258	2.124	2.184	2.208	2.277
Saturated Bulk Density (g/cc):	2.360	2.432	2.406	2.363	2.372	2.276	2.315	2.330	2.375
Average Grain Density (g/cc):	8.6	8.8	9.7	11.2	11.4	15.2	13.1	12.2	9.8
Porosity via Grain Density (%):	9.3	10.0	10.5	12.6	12.4	16.4	14.1	13.5	10.4
Ultimate Tensile Stress (MPa):	14.1	7.9	8.8	10.8	4.0	5.3	3.2	7.5	11.7

Table 4

SUMMARY DATA SHEET: NRG-6 BOREHOLE

Porosity Values for Untestable Sample Intervals

Sample IDs are shortened from the "NRG-6-Depth-SNL-Subdivision" Format

Depth, ft:	495.0	502.8	539.2	539.8	554.0	564.9	649.6	673.4	906.0	940.5
T/M Unit:	TSw1	TSw1	TSw1	TSw1	TSw1	TSw1	TSw1	TSw1	TSw2	TSw2
Date Tested:	7/30/93	7/30/93	7/30/93	7/30/93	7/30/93	7/30/93	7/30/93	7/30/93	7/30/93	7/30/93
Dry Bulk Density (g/cc):	1.775	2.010	1.900	1.936	1.997	1.702	1.985	2.079	2.323	2.293
Average Grain Density (g/cc):	2.530	2.518	2.512	2.497	2.532	2.505	2.539	2.544	2.603	2.559
Porosity via Grain Density (%):	29.8	20.2	24.4	22.5	21.1	32.1	21.8	18.3	10.8	10.4

Depth, ft:	969.3	972.4	1085.0
T/M Unit:	TSw2	TSw2	TSw2
Date Tested:	7/30/93	7/30/93	7/30/93
Dry Bulk Density (g/cc):	2.157	2.247	2.108
Average Grain Density (g/cc):	2.553	2.547	2.555
Porosity via Grain Density (%):	15.5	11.8	17.5

Figure 7 shows the variation in porosity with depth. These data were compiled from all specimens studied. The vertical lines in the diagram indicate the boundaries between the thermal/mechanical units. The porosities ranged from 3 percent to 60 percent. The highest porosities and greatest variability were observed for the PTn thermal/mechanical unit.

All specimens tested in this study (with a few special exceptions) are ideally water saturated. However, the saturation is not 100%. Porosities computed using the saturated bulk density and dry bulk density yield consistently lower values than those computed using the average grain density and dry bulk density. In part, the differences can be attributed to an under-estimation of the saturated bulk density due to water loss on the surface of the specimen. However, these errors are small and cannot account for the total discrepancy. The major contribution to the differences is occluded porosity (isolated pores that are not filled during saturation). As a result, the specimens are not 100% saturated prior to mechanical testing; the saturations range between 80 and 95%.

3.1 Computerized Tomographic X-ray Images

Prior to testing, computerized tomographic X-ray (CT) imaging was performed on each of the specimens tested in unconfined compression. A single image was obtained through the center of the specimen parallel to the core axis. These data serve as a qualitative measure of the shape and distribution of the pores and density heterogeneity within the specimen. Typical CT images are shown in Figures 8, 9, 10 and 11. Figure 8 is a tomographic image of a TCw specimen recovered from a depth of 23.4 feet. On each end of the specimen, reference rock types were imaged. At the top of the specimen is a slice of Berea Sandstone (bulk density of 2.139 g cm^{-3}). The reference on the bottom of the test specimen is Tennessee Marble (bulk density of 2.692 g cm^{-3}). The scan clearly displays that the bedding in the Berea Sandstone is normal to the long axis of the scan. The Tennessee Marble, at the bottom of the specimen, is uniform in color; no features of the pore geometry are visible. The tomographic image of this TCw specimen is uniformly gray. There are no visible pores in this specimen; pores and low density zones would be seen as light gray or white patches. The porosity of this specimen was 4.8 percent.

Figure 9 is a tomographic image of a high porosity (53.3 percent) PTn specimen taken from a depth of 187.0 feet. In contrast to the image of the TCw specimen, the PTn has a lower density, as indicated by the lighter gray shades of its image. Elliptically shaped features of low density material with their long axis normal to the core axis are shown as

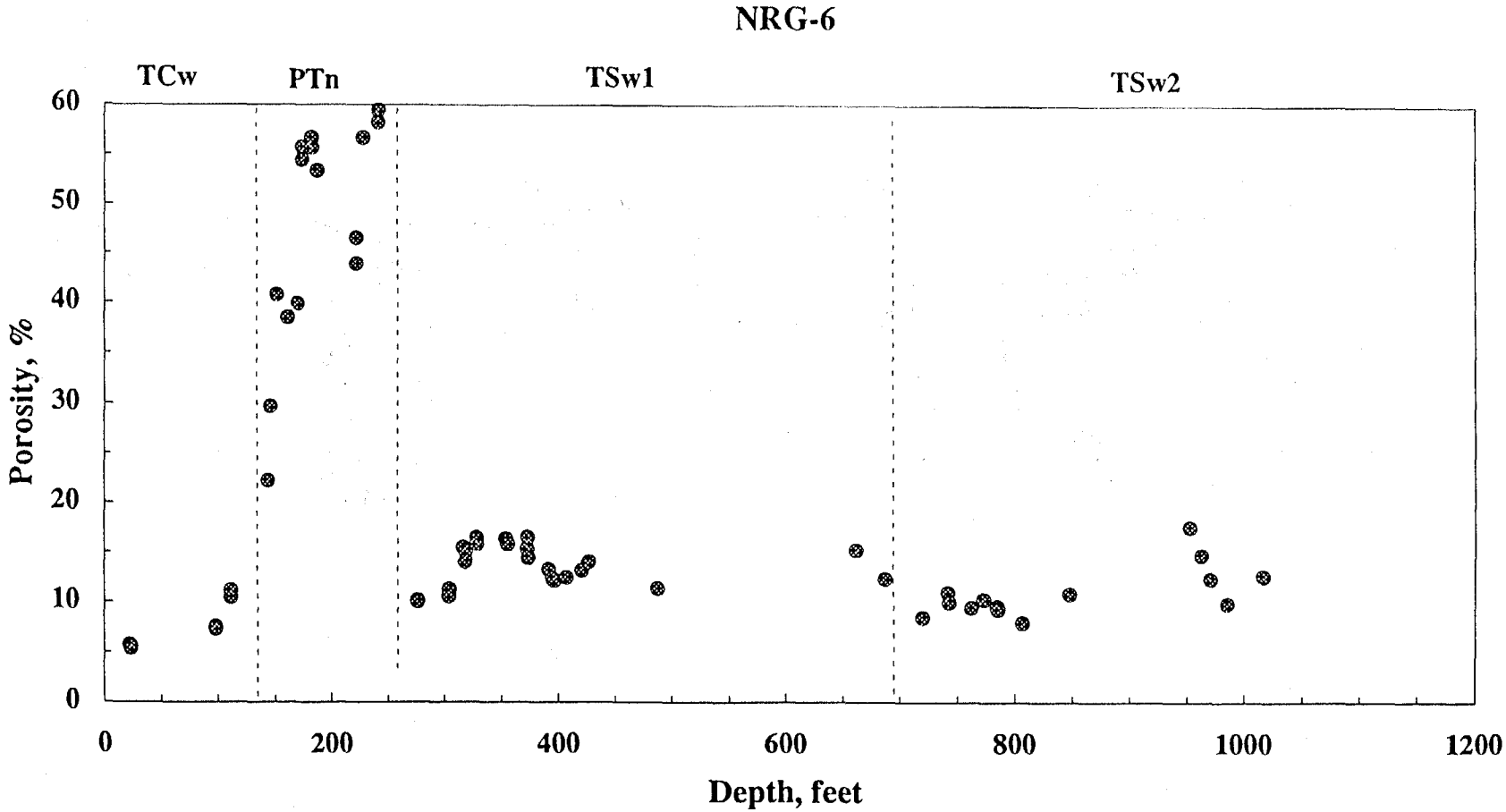

Figure 7: Porosity is shown as a function of depth of recovery for specimens from borehole USW NRG-6 at Yucca Mountain, NV. The boundaries between the thermal/mechanical units are shown as vertical dash lines.

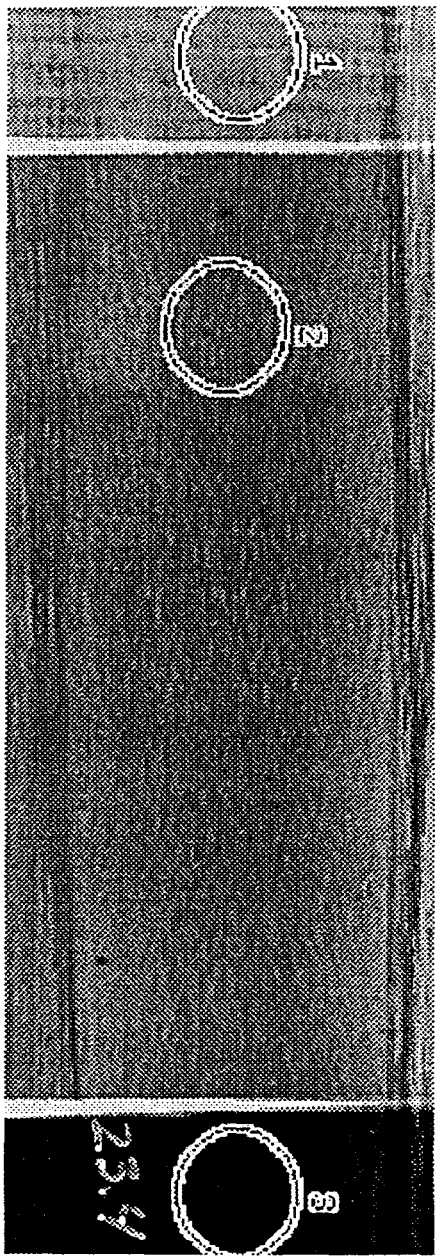

Figure 8: A tomographic image (CT scan) for a specimen of the Tiva Canyon unit (TCw) recovered from a depth of 23.4 feet from borehole USW NRG-6 at Yucca Mountain, NV.

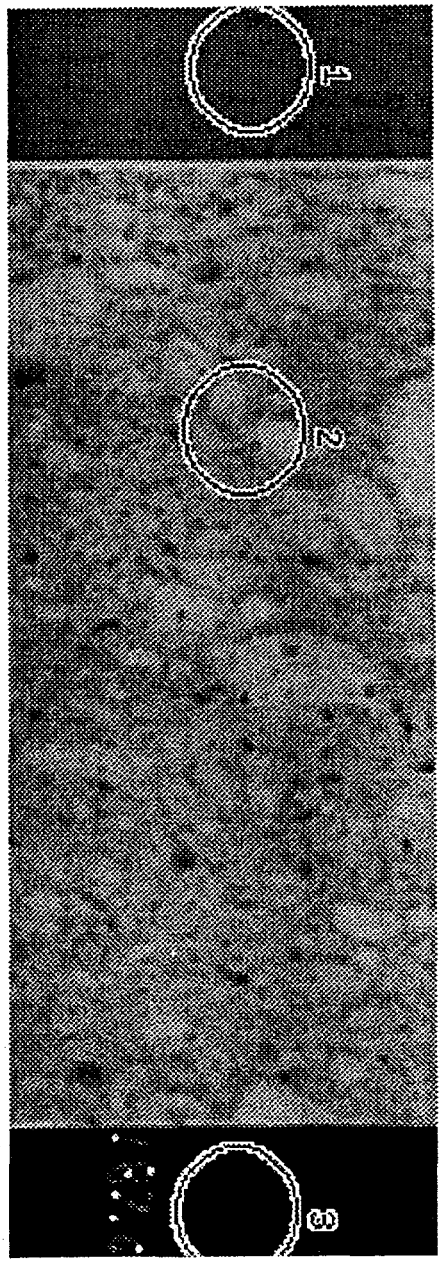

Figure 9: A tomographic image (CT scan) for a specimen of the Paintbrush Tuff (nonwelded) unit (PTn) recovered from a depth of 187.0 feet from borehole USW NRG-6 at Yucca Mountain, NV.

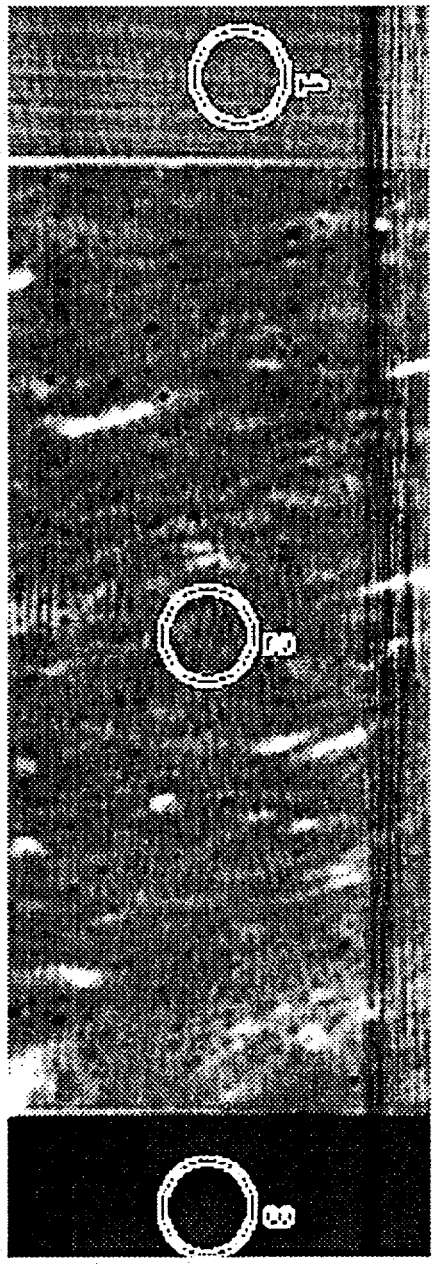

Figure 10: A tomographic image (CT scan) for a specimen of lithophysal Topopah Spring member tuff (TSw1) recovered from a depth of 372.6 feet from borehole USW NRG-6 at Yucca Mountain, NV.

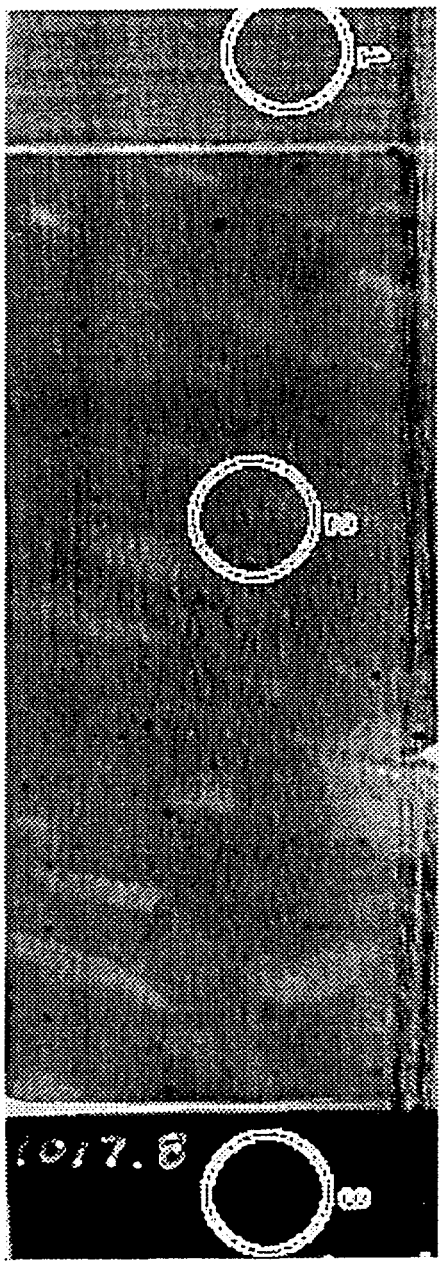

Figure 11: A tomographic image (CT scan) for a specimen of non-lithophysal Topopah Spring member tuff (TSw2) recovered from a depth of 1017.8 feet from borehole USW NRG-6 at Yucca Mountain, NV.

lighter gray and white objects in the image. The much darker, small fragments throughout the specimen are most likely high density lithic fragments.

Figures 10 and 11 are tomographic images of TSw1 and TSw2 specimens, respectively. The image in Figure 10 was obtained on a specimen of TSw1 recovered from a depth of 372.6 feet; Figure 11 shows an image for a specimen of TSw2 recovered from a depth of 1017.8 feet. The distribution, orientation, and shape of the visible features in the specimen of TSw1 are apparent as thin elliptical objects (mostly pores in this case) in the scan. The pores show a preferred orientation with their long axis at a high angle to the specimen axis. This is most likely due to compression of gas bubbles in the tuff during deposition. Irregular patches of low-density material are seen at the bottom of the figure. These may be a combination of vapor-phase altered zones and open pores. Figure 11 shows that the pores in thermal/mechanical unit TSw2 have been at least partially filled or altered. The visible pores are smaller than seen for the TSw1 specimen.

3.2 Compressional and Shear Wave Velocity Measurements

Compressional and shear wave velocity measurements were performed parallel and normal to the core axis for both dry and saturated conditions on all specimens tested in unconfined compression. Compressional and shear wave velocities were measured parallel to the core axis only for the specimens tested in confined compression. In some cases data were not collected due to the inability to transmit the waves through the specimen; the greatest difficulty was encountered measuring shear wave velocities under saturated conditions. Only dry velocities were measured on most PTn specimens.

A typical data set obtained on a specimen of TSw2 recovered from a depth of 773.5 feet is shown in Figures 12 and 13. These data are for the dry condition. The first trace in Figure 12 is the time series for the compressional wave propagated parallel to the core axis. The middle and lowest traces are shear waves propagated parallel to the core axis, with orthogonal polarizations. Using two polarizations enhances the reliability of the shear wave velocity measurement. Figure 13 shows the compressional and shear wave velocities measured normal to the core axis. The top trace is the compressional wave velocity and the lower trace is the shear wave velocity. These data exhibit no compressional or shear wave anisotropy. The mean compressional wave velocity for both propagation directions is 4.575 ± 0.002 km s^{-1}. The mean shear wave velocity is 2.884 ± 0.006, km s^{-1}.

The data presented in Figures 12 and 13 are typical of those collected on each specimen. These data are used to calculate the dynamic elastic moduli and are useful in the

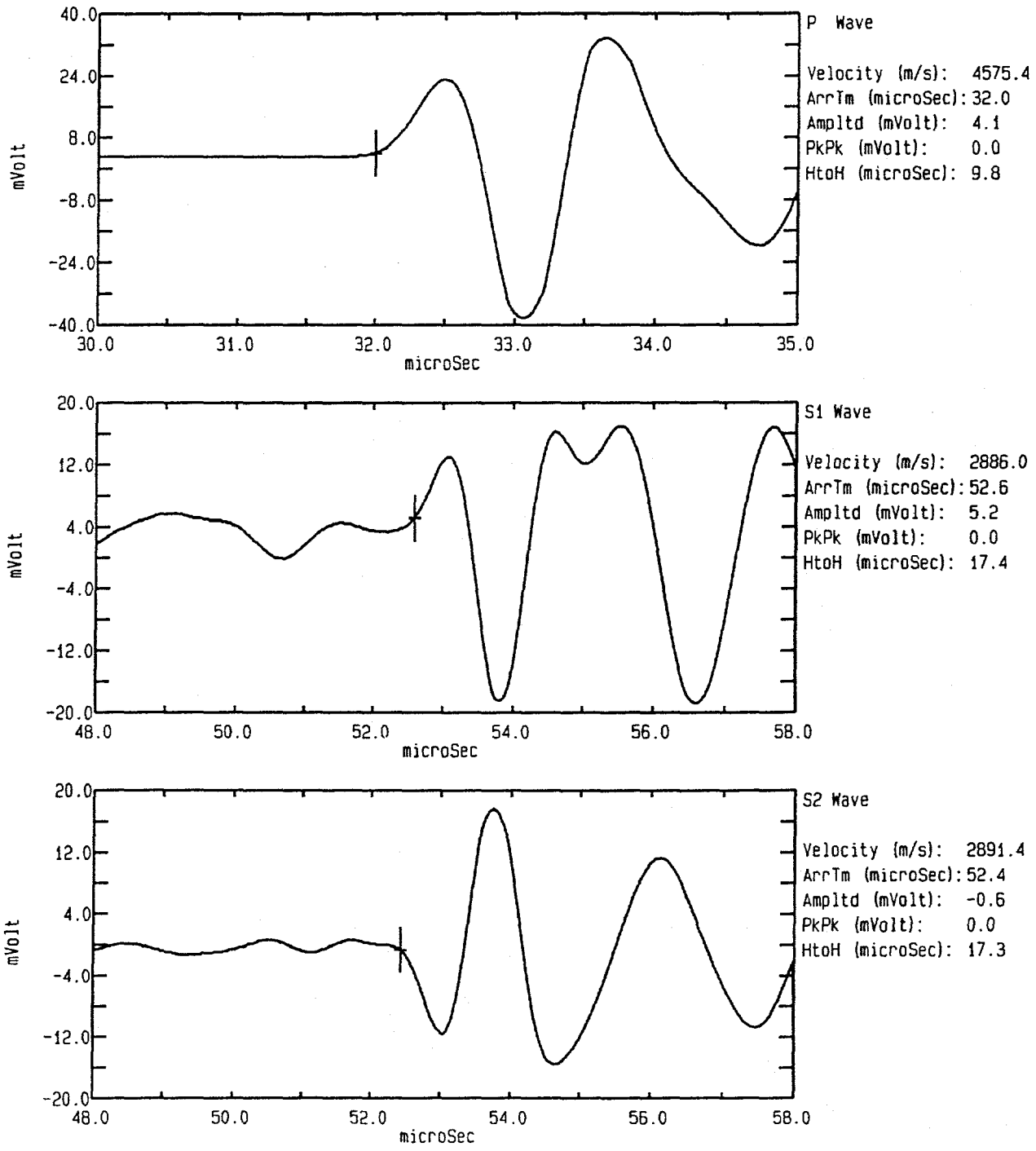

Figure 12: Time series plots for one compressional and two orthogonally polarized shear waves propagated parallel to the core axis of a Topopah Spring member tuff unit (TSw2) recovered from a depth of 773.5 feet from borehole USW NRG-6, Yucca Mountain, NV. The velocities are shown to the right of each time series. A cross indicates the onset of compressional and shear wave energy for each waveform.

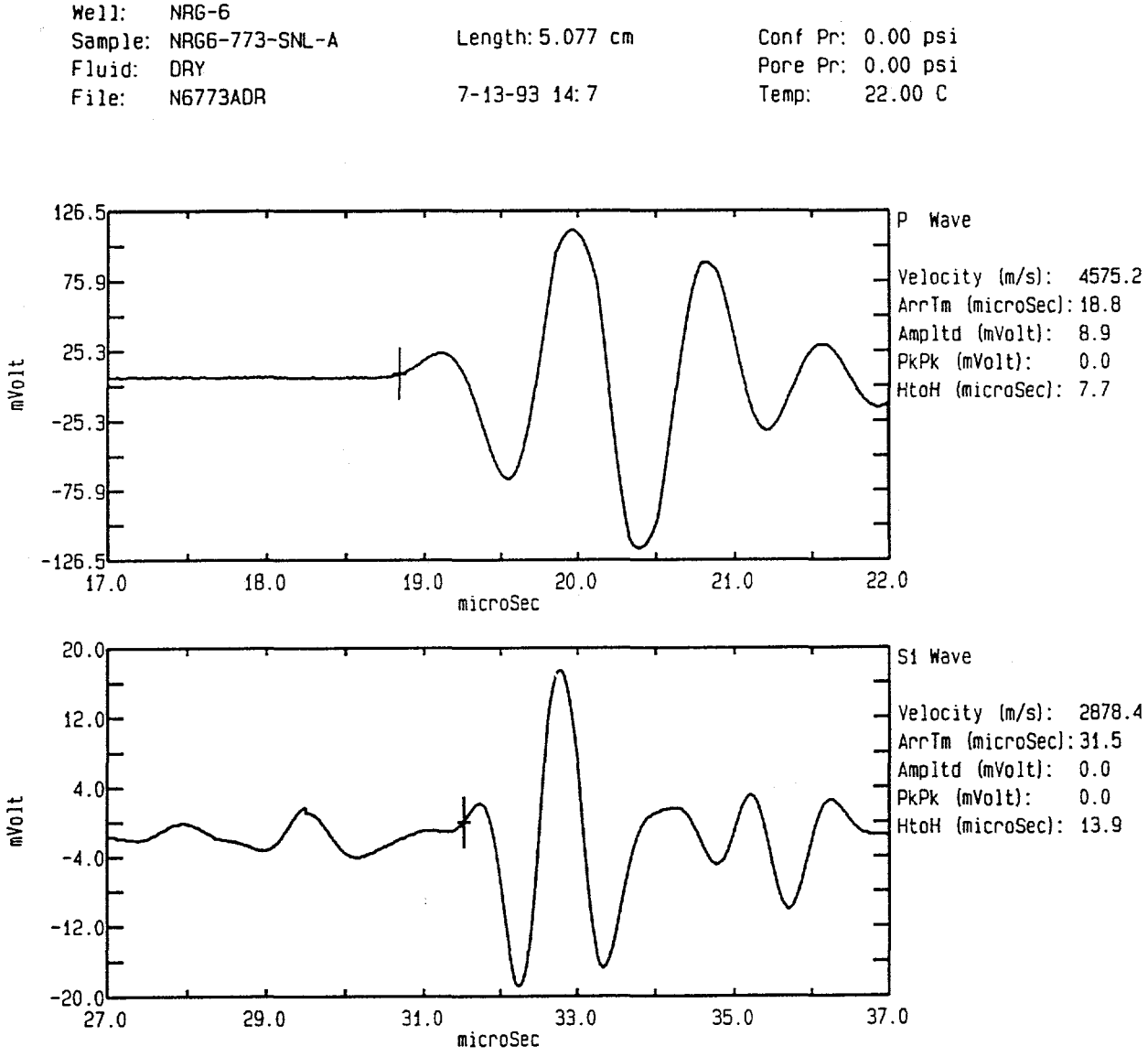

Figure 13: Time series plots for one compressional and one polarized shear wave propagated normal to the core axis from a specimen of Topopah Spring member tuff unit (TSw2) recovered from a depth of 773.5 feet from borehole USW NRG-6, Yucca Mountain, NV. The compressional and shear wave velocities are shown to the right of each time series. A cross indicates the onset of compressional and shear wave energy for each waveform.

interpretations of surface seismic and VSP data obtained in conjunction with the site characterization of Yucca Mountain.

The compressional and shear wave velocities measured for the dry condition for the specimens tested in uniaxial compression are shown in Figure 14. The velocities are plotted as a function of depth. The compressional wave velocities ranged between 3.5 and 4.7 km s^{-1} for all units except PTn. Similarly the shear wave velocities varied between 2.2 and 3.0 km s^{-1} for all specimens except PTn. There is some consistency in the trends observed in the data set. The compressional wave velocities were in excess of 4 km s^{-1} for TCw and TSw2. The compressional wave velocities for TSw1 tended to cluster below 4 km s^{-1}.

The compressional and shear wave anisotropy was computed from the velocity data collected in the dry condition. To calculate anisotropy, the velocity in the axial direction was subtracted from the corresponding mode in the radial direction and normalized to the velocity in the axial direction. A negative anisotropy indicates a greater velocity normal to the core axis than parallel to it. Figure 15 shows the anisotropy as a function of depth. The boundaries between the thermal/mechanical units are indicated with vertical dashed lines. The anisotropy varied from -14 percent to 5 percent. In general, the velocities were greater normal to the core axis than parallel to it. The most anisotropic rocks were the PTn and TSw1.

3.3 Unconfined Compression Tests

The plots of representative data sets for two specimens tested in unconfined compression are presented in Figures 16 and 17. Figure 16 shows the data for a relatively low porosity saturated specimen of the PTn (ϕ = 22 percent) recovered from a depth of 143.5 feet. Several specimens of PTn were tested in a room dry state due to the friable nature of the rock. The upper graph shows axial stress as a function of axial strain as the rock was loaded monotonically to failure. The specimen failed at a stress of 61.8 MPa; Young's modulus was 14.8 GPa. The lower graph shows radial strain as a function of axial strain; a Poisson's ratio of 0.13 was determined from these data.

TSw2 specimens exhibited much higher strengths than specimens of PTn. Figure 17 shows data collected on a specimen of TSw2 recovered from a depth of 806.8 feet. Axial stress and radial strain are plotted as a function of axial strain. Young's modulus was 31.7 GPa and the fracture strength was 261.9 MPa. The Poisson's ratio was computed over the same axial strain interval used to compute Young's modulus; Poisson's

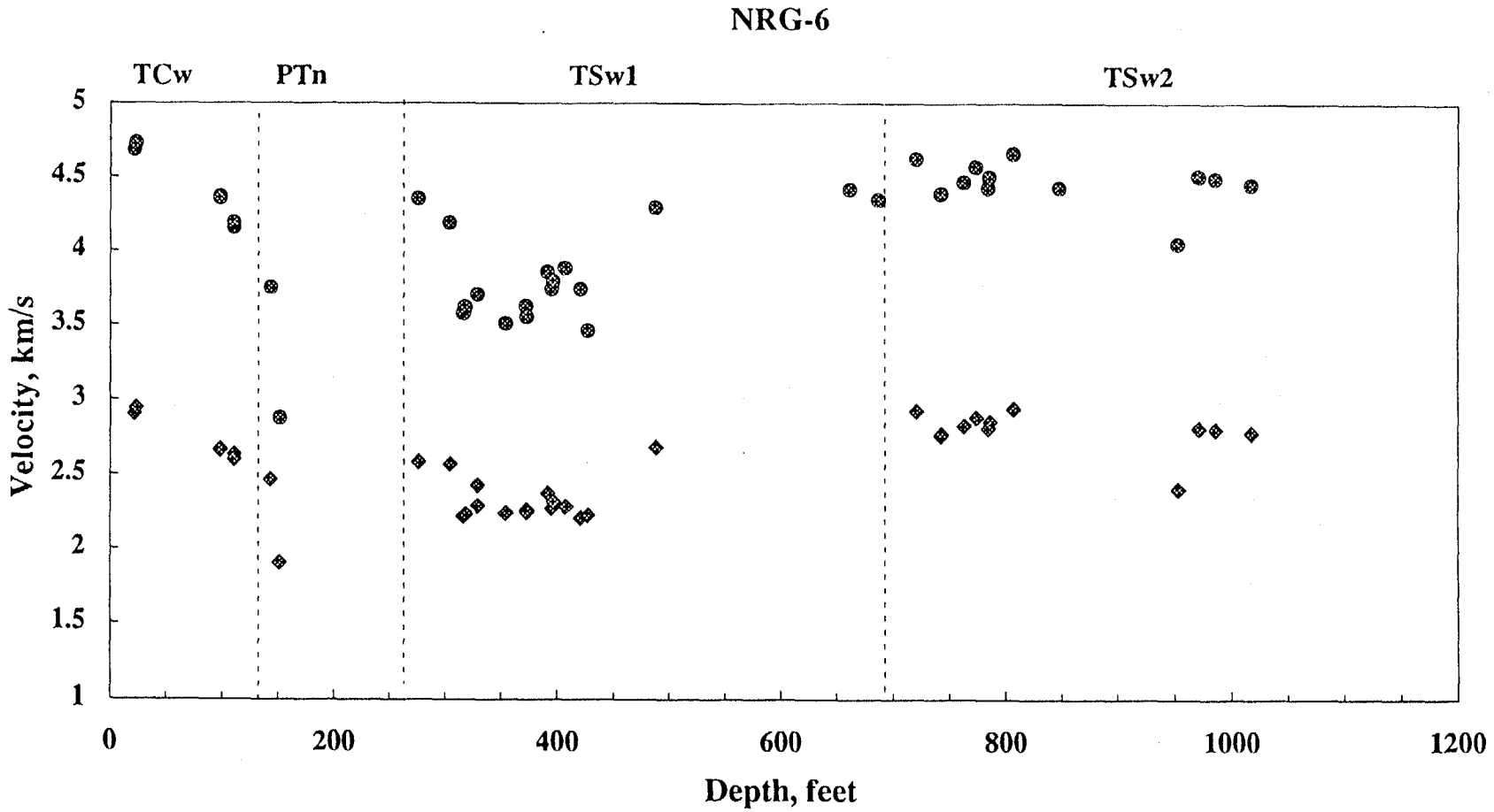

Figure 14: Compressional (circles) and shear wave (diamonds) velocities on specimens recovered from borehole USW NRG-6 are shown as a function of depth. Vertical dashed lines indicate boundaries between thermal/mechanical units.

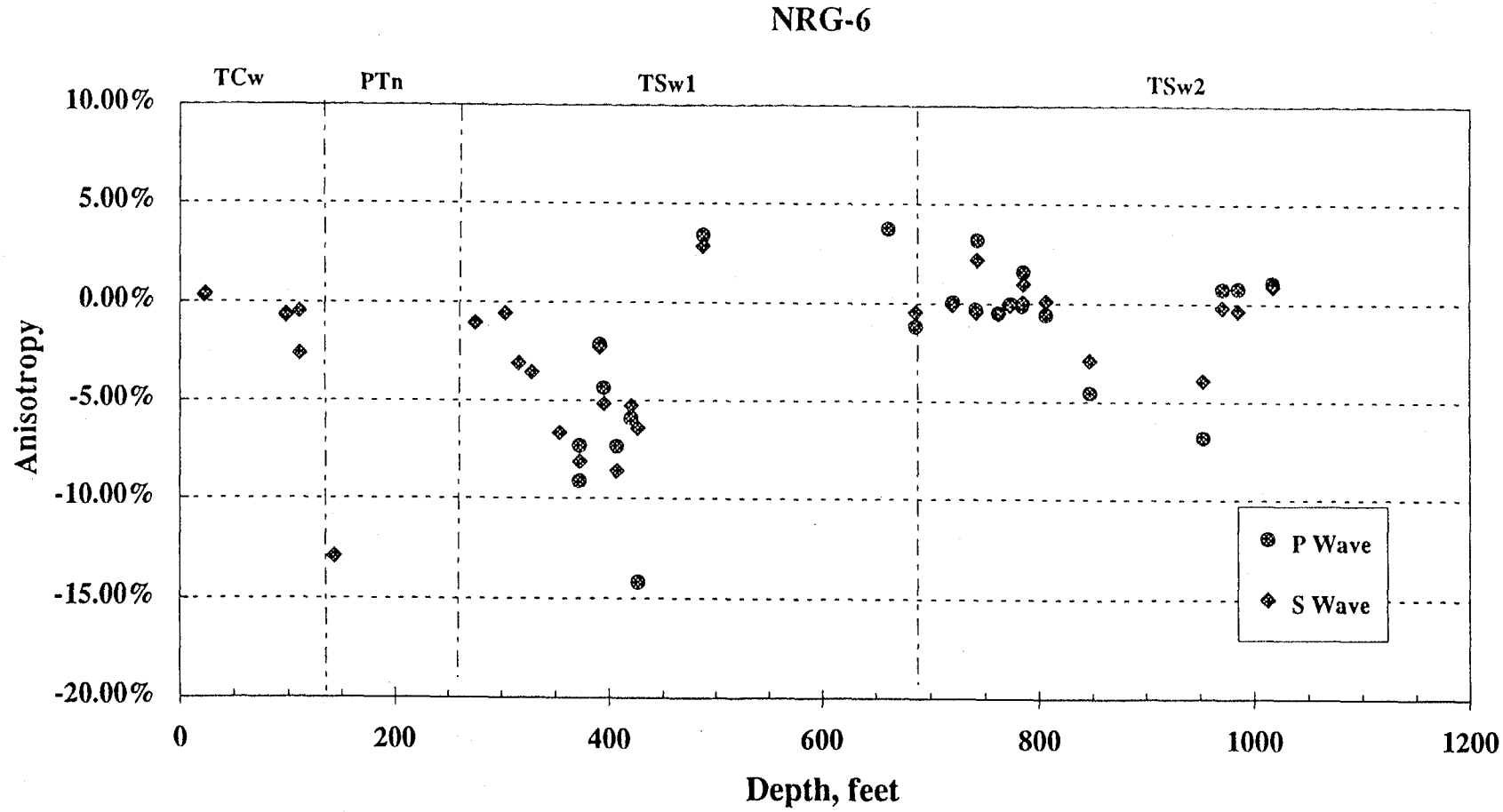

Figure 15: Compressional (P) and shear (S) wave anisotropy measured on specimens tested in unconfined compression from borehole USW NRG-6 are shown as a function of depth. Vertical dashed lines indicate boundaries between thermal/mechanical units.

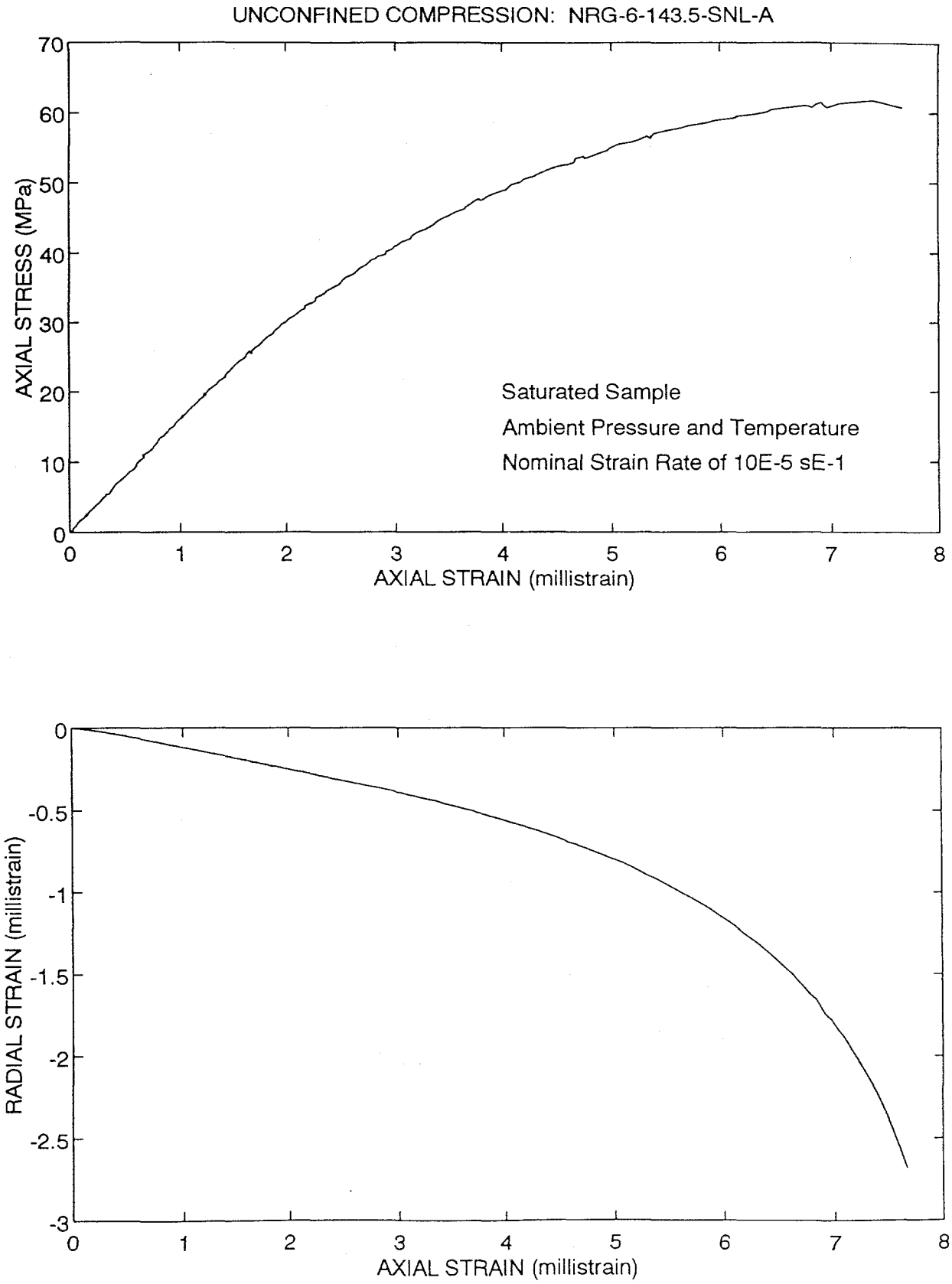

Figure 16: Axial stress and radial strain are plotted as a function of axial strain for a specimen of PTn tested in unconfined compression. The specimen was recovered from a depth of 143.5 feet from borehole USW NRG-6, Yucca Mountain, NV.

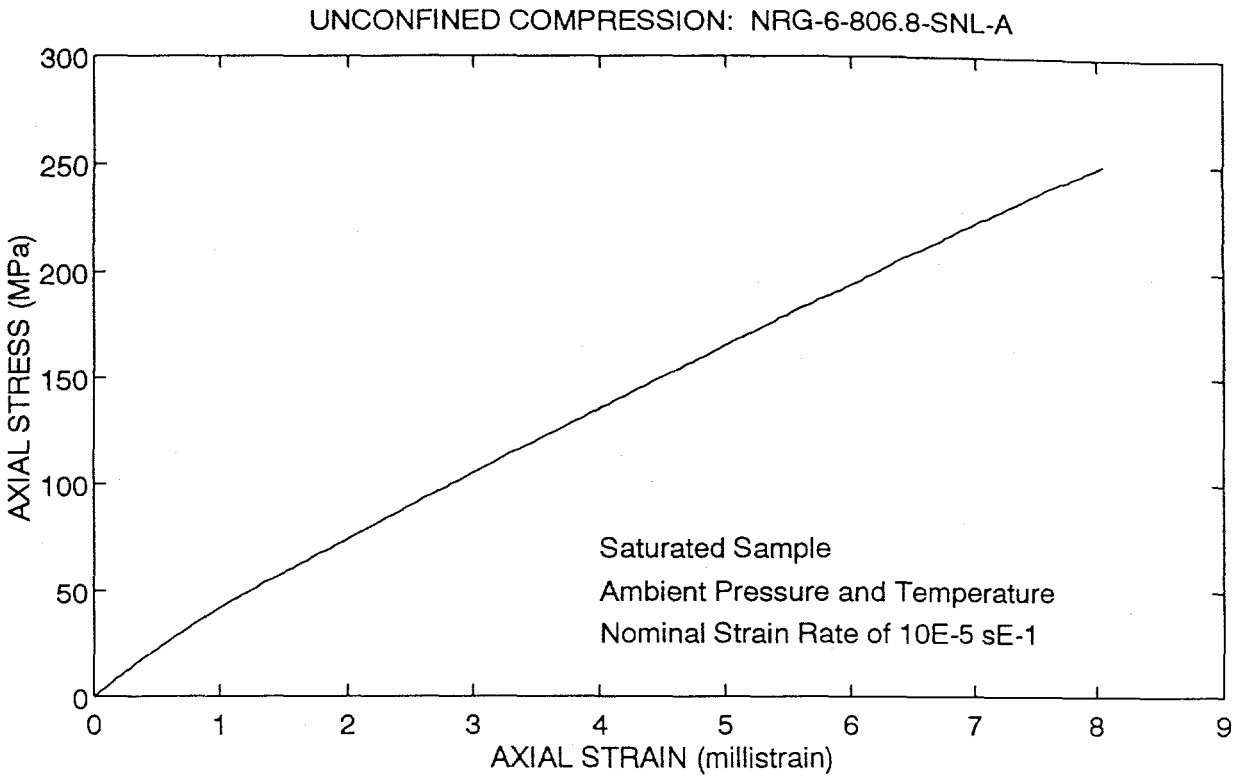

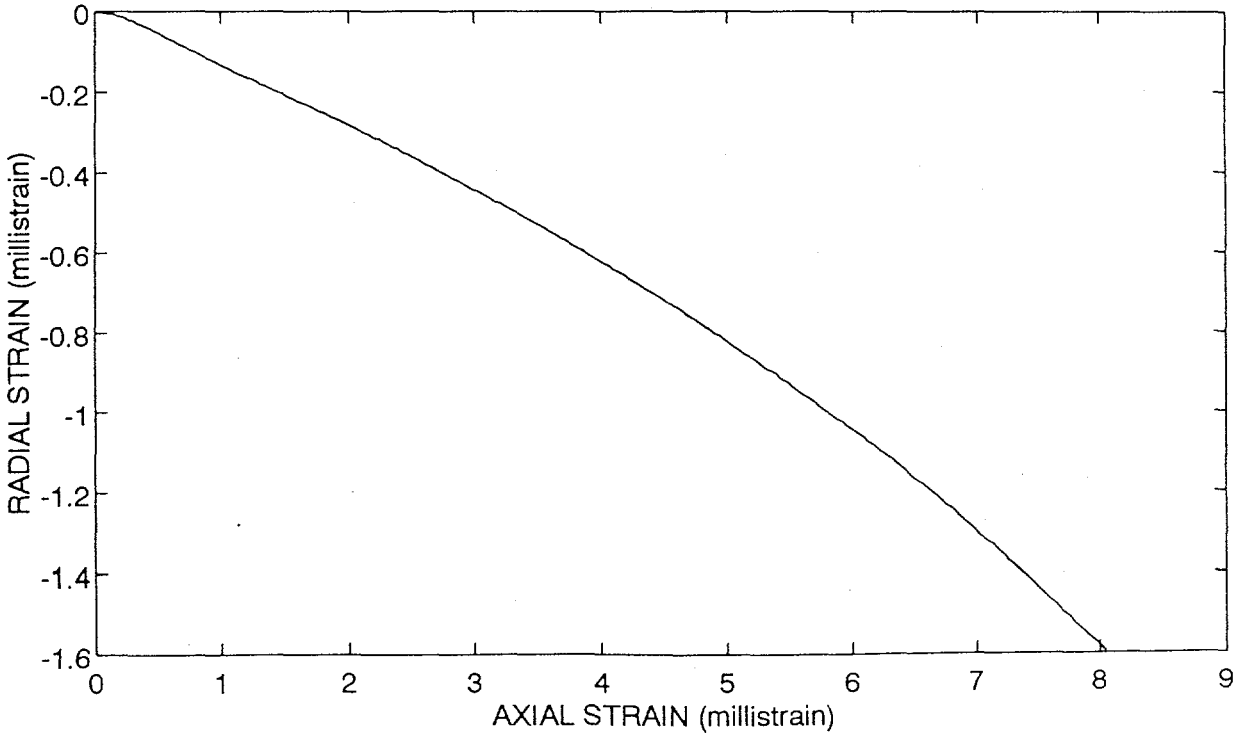

Figure 17. Axial stress and radial strain are plotted as a function of axial strain for an unconfined compression experiment performed on a specimen of TSw2. The specimen was recovered from a depth of 806.8 feet from borehole USW NRG-6, Yucca Mountain, NV.

ratio was 0.16.

The stress-strain data plots for all the unconfined compression tests are presented in Appendix I. An interesting feature results from an examination of the data collected during the unconfined compression tests. In most cases very little inelastic strain (dilatancy) is observed prior to failure. Many crystalline rocks begin to dilate at stresses as low as one-half the fracture strength. In these tuff specimens, very little dilatancy was observed until the specimens were very near failure as indicated by the small increase in the slope of the radial strain versus axial strain plot in Figure 17. This is particularly true for the TCw, TSw1, and TSw2 thermal/mechanical units. The manner in which cracks grow and interact in tuff is different from that observed in other crystalline rocks dominated by microcrack porosity (Brace et al., 1966).

The unconfined fracture strengths are plotted as a function of depth in Figure 18. TCw specimens typically exhibited the greatest strengths. Values in excess of 300 MPa were observed for this unit. In contrast, the weakest specimens were from the PTn unit. Fracture strengths less than 10 MPa were observed for most of these specimens. The largest variability was observed for TSw1 and TSw2. Strengths for these units varied from 25 MPa to 250 MPa. There was no consistent trend between strength and depth. There was, however, a cluster of relatively weak (40 to 110 MPa) specimens recovered from depths between 325 and 425 feet in the TSw1 unit.

Young's modulus was computed from the stress-axial strain data for each unconfined compression experiment over the interval of 10 to 50 percent of the fracture strength. These data are shown as a function of depth in Figure 19. The moduli varied between 1 and 40 GPa. As with the fracture strength, the lowest moduli were observed on specimens of PTn. There is no readily apparent correlation between depth and modulus. The modulus computed for TCw, TSw1, and TSw2 specimens scattered between 12.5 and 39.0 GPa. Dynamic elastic moduli for each of the specimens tested in unconfined compression was computed from the velocity and density data. In all cases, the dynamic moduli exceeded the static moduli. In Figure 20, the ratio of dynamic-to-static Young's modulus is shown as a function of fracture strength. In general, the specimens exhibiting the lowest fracture strengths displayed a correspondingly high dynamic-to-static Young's moduli. For specimens with fracture strengths less than 50 MPa the ratio of dynamic-to-static Young's modulus exceeded 1.5.

Test system checks using aluminum were performed prior to testing the suite of rock core and repeated each time a group of ten specimens had been tested. The checks verified the operation of the entire test system, including all devices and the data acquisition

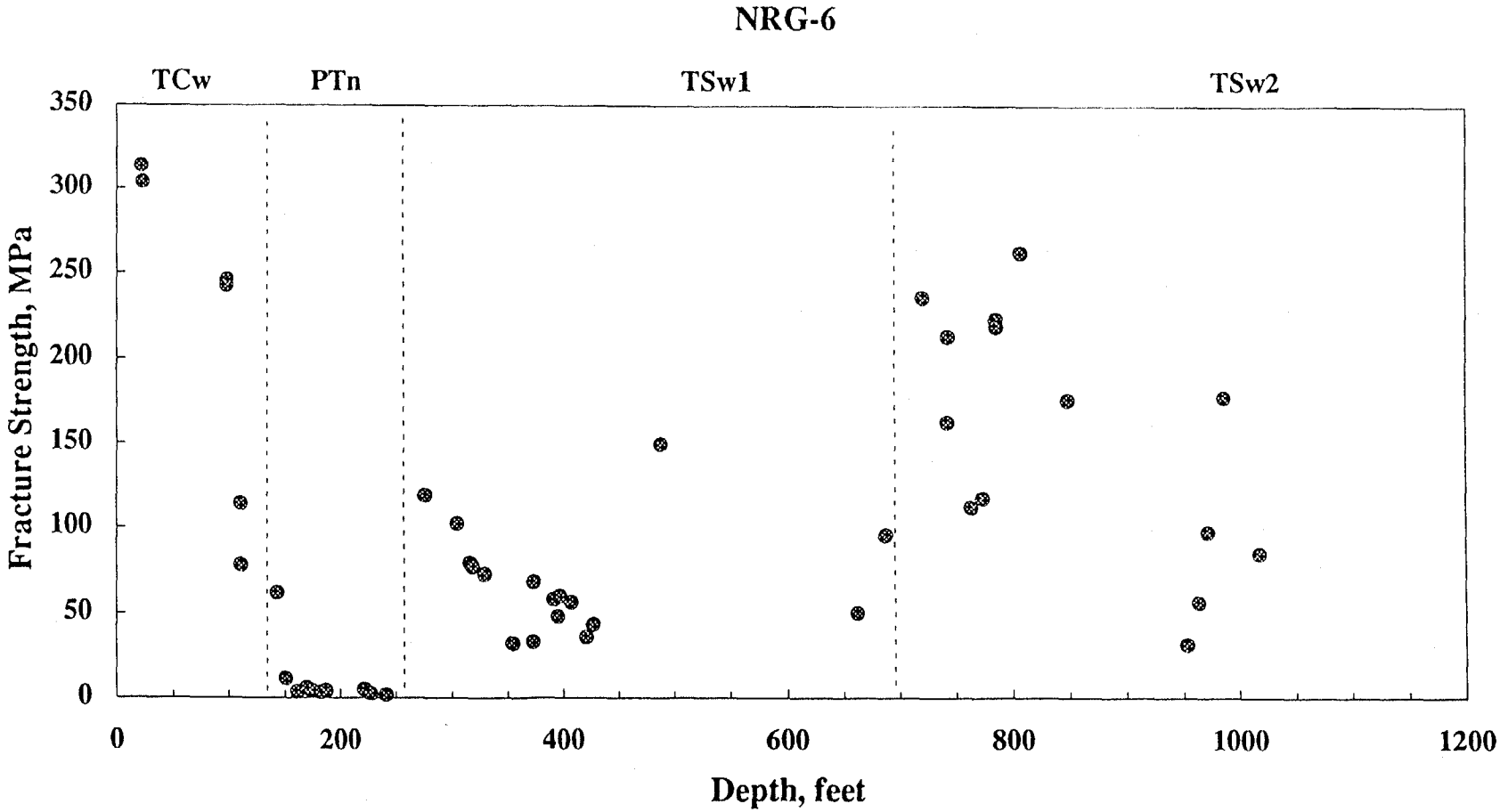

Figure 18: The fracture strengths for specimens of the Paintbrush tuff tested in unconfined compression are plotted as a function of the depth of recovery. The specimens were obtained from borehole USW NRG-6, Yucca Mountain, NV. The vertical dashed lines indicate the boundaries between thermal/mechanical units.

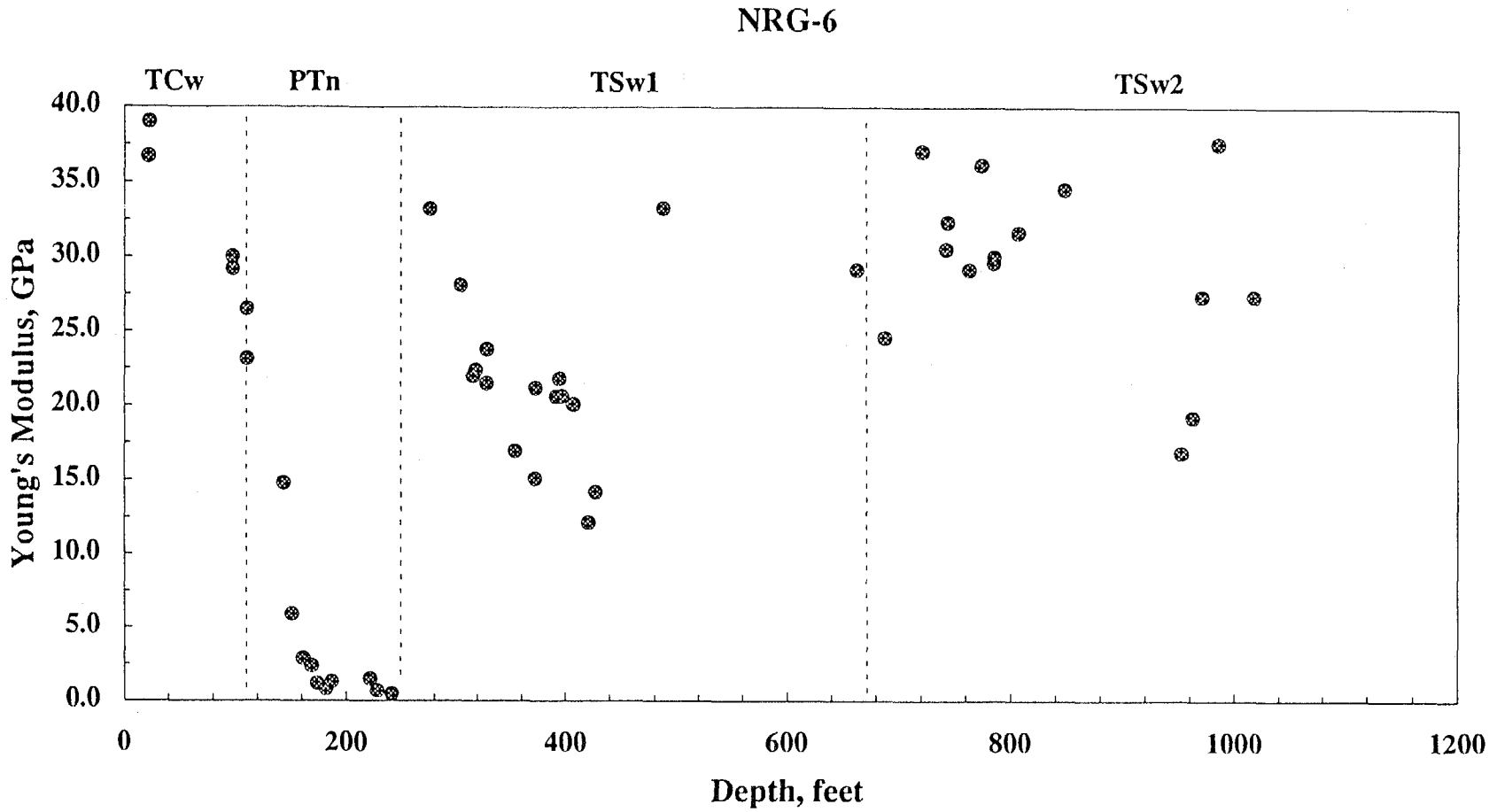

Figure 19: Young's moduli for specimens of the Paintbrush tuff tested in unconfined compression are plotted as a function of depth of recovery. The specimens were obtained from borehole USW NRG-6, Yucca Mountain, NV. The vertical dashed lines indicate the boundaries between thermal/mechanical units.

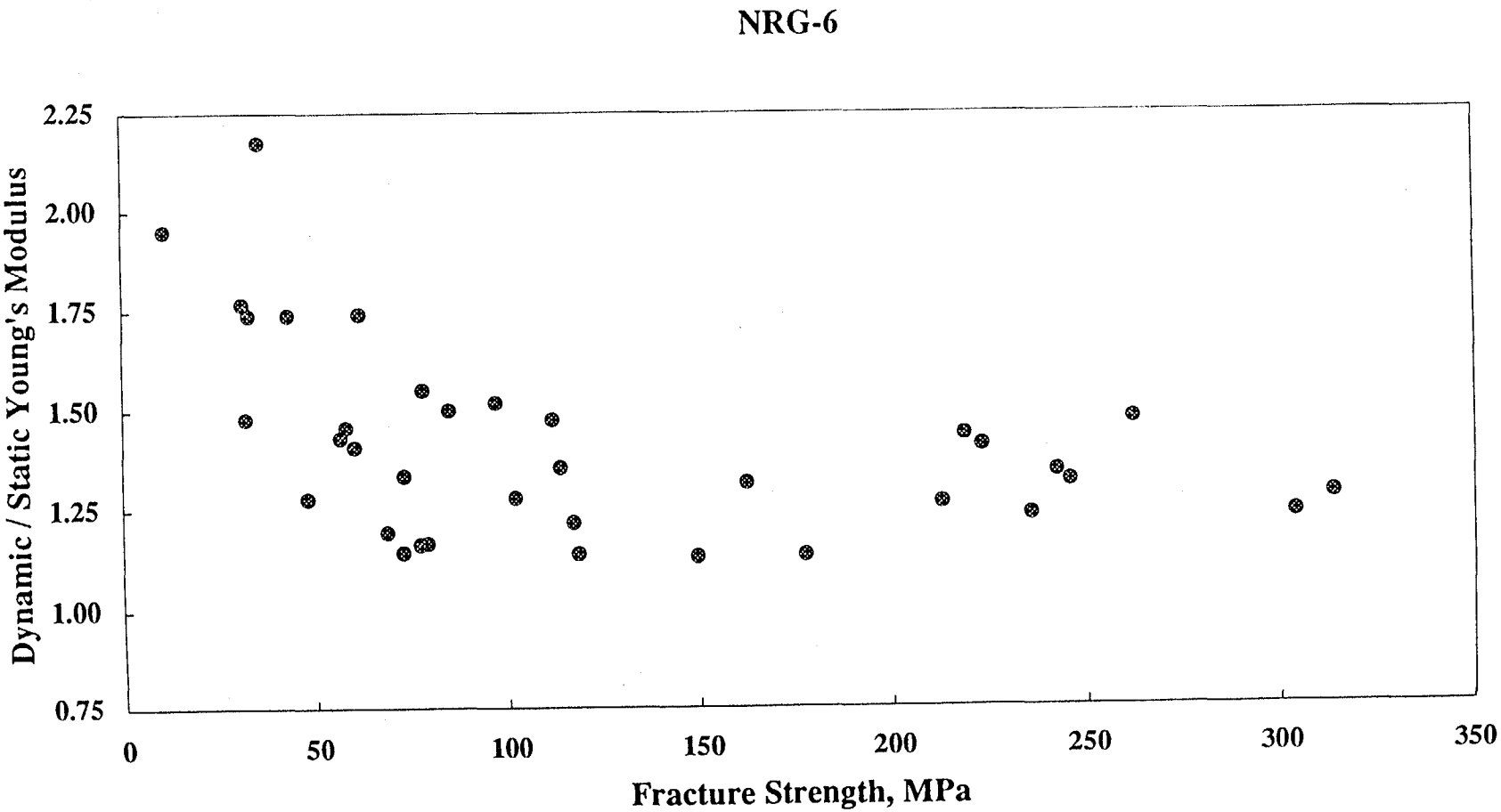

Figure 20: The ratio of dynamic to static Young's moduli for specimens of Paintbrush tuff tested in unconfined compression is plotted as a function of fracture strength. The specimens were prepared from cores recovered from borehole USW NRG-6, Yucca Mountain, NV.

and processing software. These experiments were run in an identical manner to the unconfined compression tests. An aluminum specimen with the same nominal dimensions as the tuff specimens was tested in unconfined compression up to one-half its yield stress. The results of these experiments showed that the system performed satisfactorily throughout the suite of measurements on the tuff specimens from the USW NRG-6 borehole. The Young's modulus and Poisson's ratio for each system check is given in Appendix II.

3.4 Confined Compression Tests

Small diameter specimens obtained from cores recovered at depths of 22.2 and 416.0 feet, from the TCw and TSw1 thermal/mechanical units respectively, were tested in confined compression. Twelve specimens were measured from the 22.2 foot interval. Four specimens were tested at each of the following confining pressures: 0, 5 and 10 MPa. In spite of the fact that all of the specimens were machined from the same core, there is some heterogeneity that contributes to scatter in the data at each confining pressure. There is a definite trend of increasing fracture strength with increasing confining pressure.

Eight confined compression experiments were performed on TSw1 specimens recovered from a depth of 416.0 feet. Four specimens were tested at confining pressures of 5 MPa and four specimens were tested at 10 MPa. No unconfined compression tests were performed on small diameter cores from this depth. There is more heterogeneity in these specimens than in the TCw specimens and the scatter in the fracture strengths at each confining pressure is greater. Deviations from the general trends are directly related to the presence of heterogeneities (lithophysal cavities) in the weaker specimens. The mean fracture strength at each confining pressure increases with increasing confining pressure. The stress and strain data for these experiments are presented graphically in Appendix II. Stress difference is plotted as a function of axial strain. Radial strain is also plotted as a function of axial strain.

3.5 Indirect Tensile Strength Tests

Thirty-nine indirect tensile strength tests were performed. The tensile strengths ranged between 0.2 and 16.0 MPa. The weakest specimens were from the nonwelded PTn thermal/mechanical unit. The greatest strengths were observed in the TCw welded tuff. TSw1 and TSw2 exhibited a wide variety of strengths. In general, TSw1 was weaker than TSw2. However, there was significant scatter in TSw2. These data are presented

graphically as a function of depth of recovery in Figure 21.

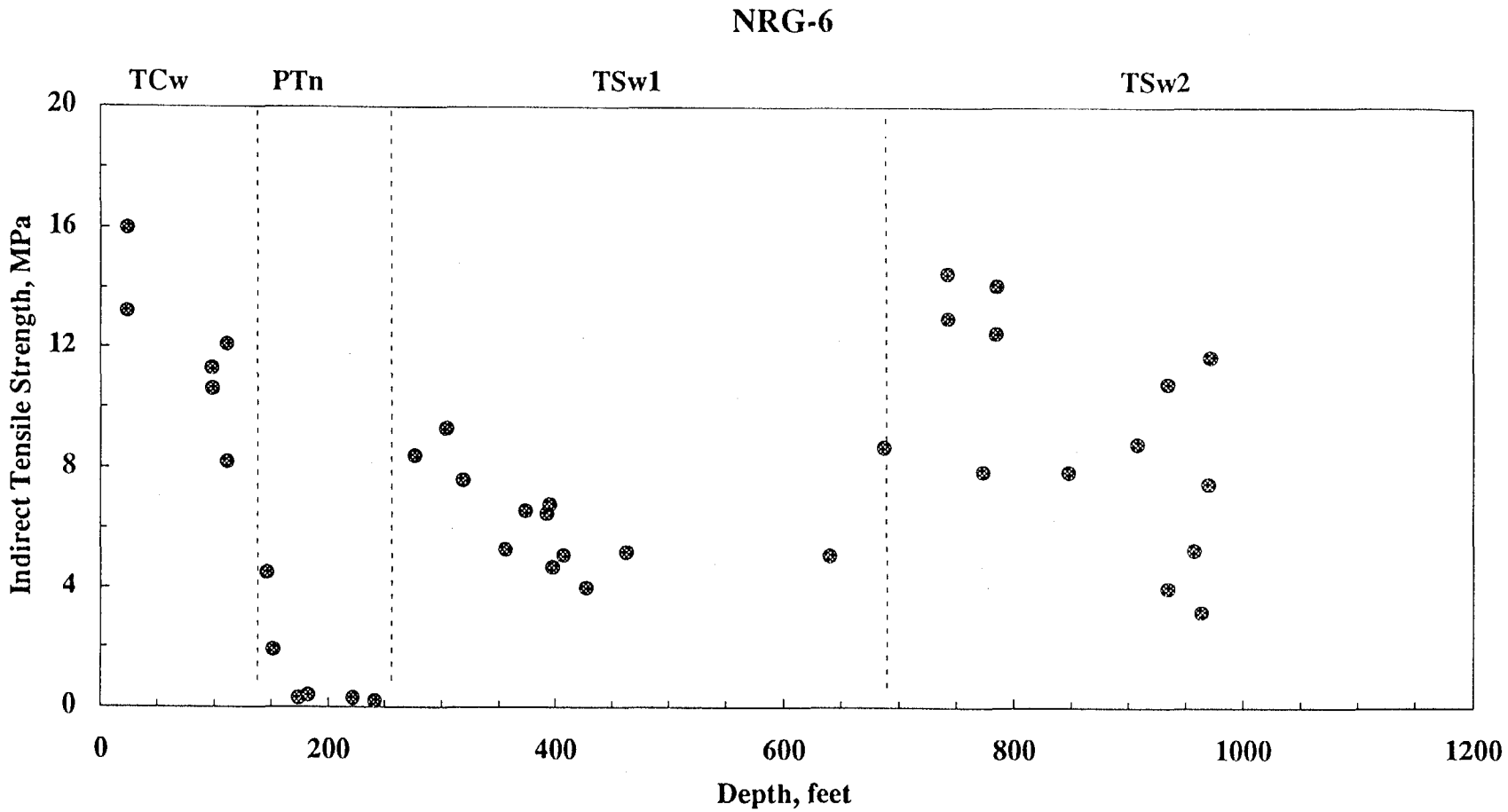

Figure 21: The indirect tensile strengths of specimens of Paintbrush tuff are plotted as a function of depth of recovery. The specimens were from borehole USW NRG-6, Yucca Mountain, NV.

4.0 REFERENCES

American Society for Testing and Materials, 1990

Standard test Method for True Specific Gravity of Refractory Materials by Water Immersion, ASTM C 135-86. (NNA.910522.0040)

American Society for Testing and Materials, 1993

Standard Test Method for Triaxial Compressive Strength of Undrained Rock Core Specimens Without Pore Pressure Measurements, ASTM D 2664-86. (MOL.19940819.0013)

American Society for Testing and Materials, 1993

Standard Test Method for Elastic Moduli of Intact Rock Core Specimens in Uniaxial Compression, ASTM D 3148-93. (MOL.19940819.0014)

American Society for Testing and Materials, 1993

Standard Test Method for Splitting Tensile Strength of Intact Rock Core Specimens, ASTM D 3967-92. (MOL.19940819.0015)

American Society for Testing and Materials, 1993

Standard test Method for Specific Gravity of Soils, ASTM D 854-92. (MOL.19940819.0016)

Brace, W. F, B. Paulding, and C.H. Scholz, 1966,

Dilatancy in the fracture of crystalline rocks, J. Geophys. Res., 68 (12): 3790. (MOL.19940805.0099)

Cheng, C.H. and D.H. Johnston, 1981

Dynamic and static moduli. Geophys. Res. Let. 8:39-42. (NNA.910923.0006)

Haupt, R.W., R.J. Martin, III, X. Tang, W.J. Dupree and R.H. Price, 1992

Modulus dispersion and attenuation in tuff and granite. Proceedings of the 33rd U.S. Symposium on Rock Mechanics. 899-908. (NNA.930824.0002)

Holcomb and McNamee, 1984

Displacement Gage for the Rock Mechanics Laboratory, SAND84-0651, Sandia National Laboratories, Albuquerque, NM. (NNA.910523.0022)

International Society for Rock Mechanics, 1981

Suggested Methods for Determining the Strength of Rock Materials in Triaxial Compression, In Rock Characterization Testing and Monitoring - ISRM Suggested Methods, 123-127. (MOL.19940805.0084)

International Society for Rock Mechanics, 1981

Suggested Methods for Determining the Uniaxial Compressive Strength and Deformability of Rock Materials - ISRM Suggested Methods, 113-116. (MOL.19941103.0001)

Ortiz, T. S., R. L. Williams, F. B. Nimick, B. C. Whittet, and D. L. South, 1985

A Three Dimensional Model of Reference Thermal/Mechanical and Hydrologic Stratigraphy at Yucca Mountain, Southern Nevada, SAND84-1076, Sandia National Laboratories, Albuquerque, NM. (NNA.890315.0013)

Price, R. H., and S. J. Bauer, 1985

Analysis of the Elastic and Strength Properties of Yucca Mountain Tuff, Nevada, In: Research and Engineering Applications in Rock Masses, Vol. 1, Proc. 26th U.S. Symposium on Rock Mechanics, Eileen Ashworth (ed.), 89-96. (HQS.880517.1697)

Simmons, G. and W.F. Brace, 1965

Comparison of static and dynamic measurements of compressibility of rocks. J. Geophys. Res. 70:5649-5656. (NNA.910923.0007)

APPENDIX I

Stress vs Axial Strain and Radial Strain vs Axial Strain Plots for Unconfined Compression Experiments

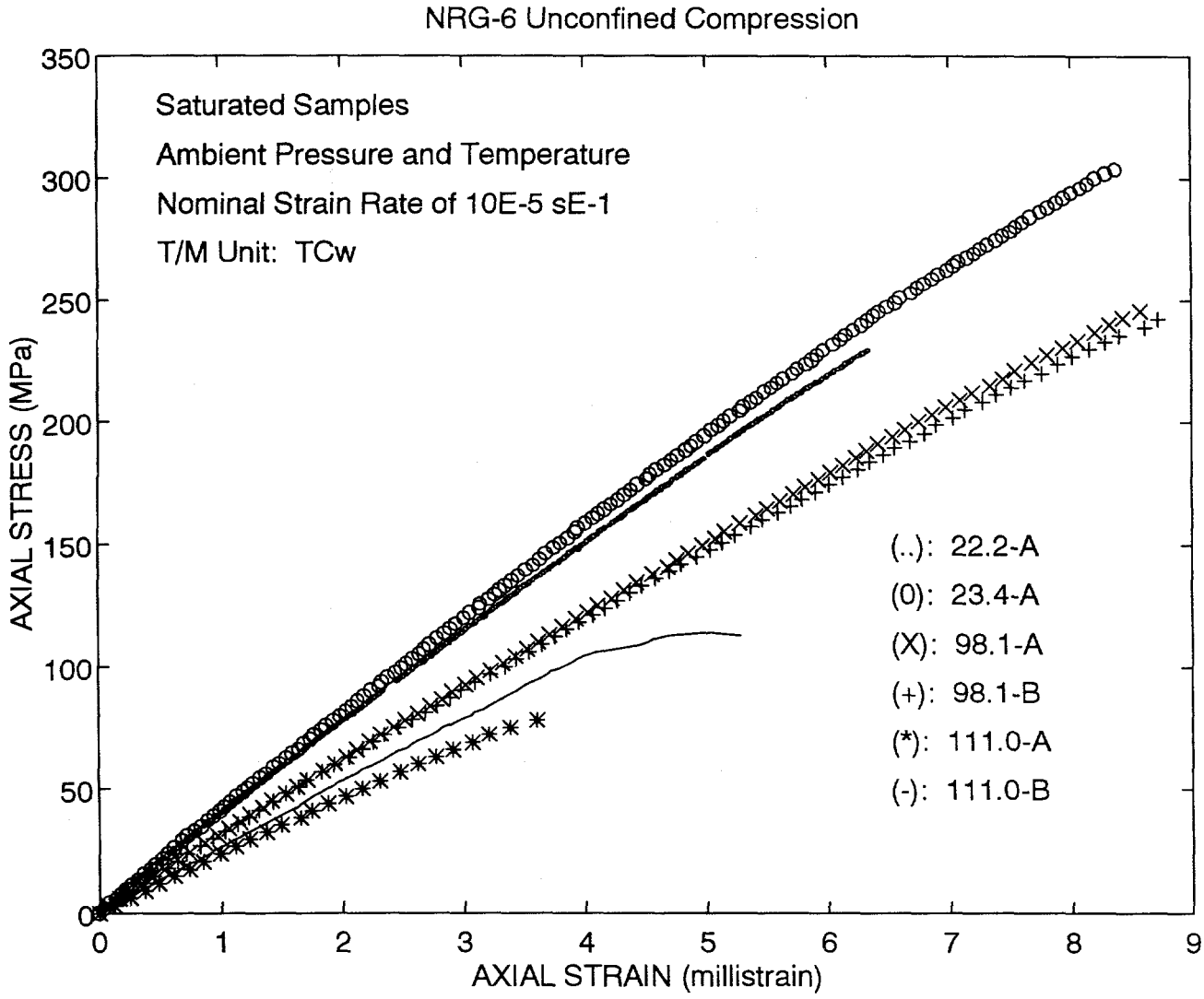
NRG-6 Unconfined Compression
Saturated Samples
Ambient Pressure and Temperature
Nominal Strain Rate of 10E-5 sE-1
T/M Unit: TCw
(..): 22.2-A
(0): 23.4-A
(X): 98.1-A
(+): 98.1-B
(*): 111.0-A
(-): 111.0-B
AXIAL STRESS (MPa)
AXIAL STRAIN (millistrain)
0
50
100
150
200
250
300
350
0
1
2
3
4
5
6
7
8
9

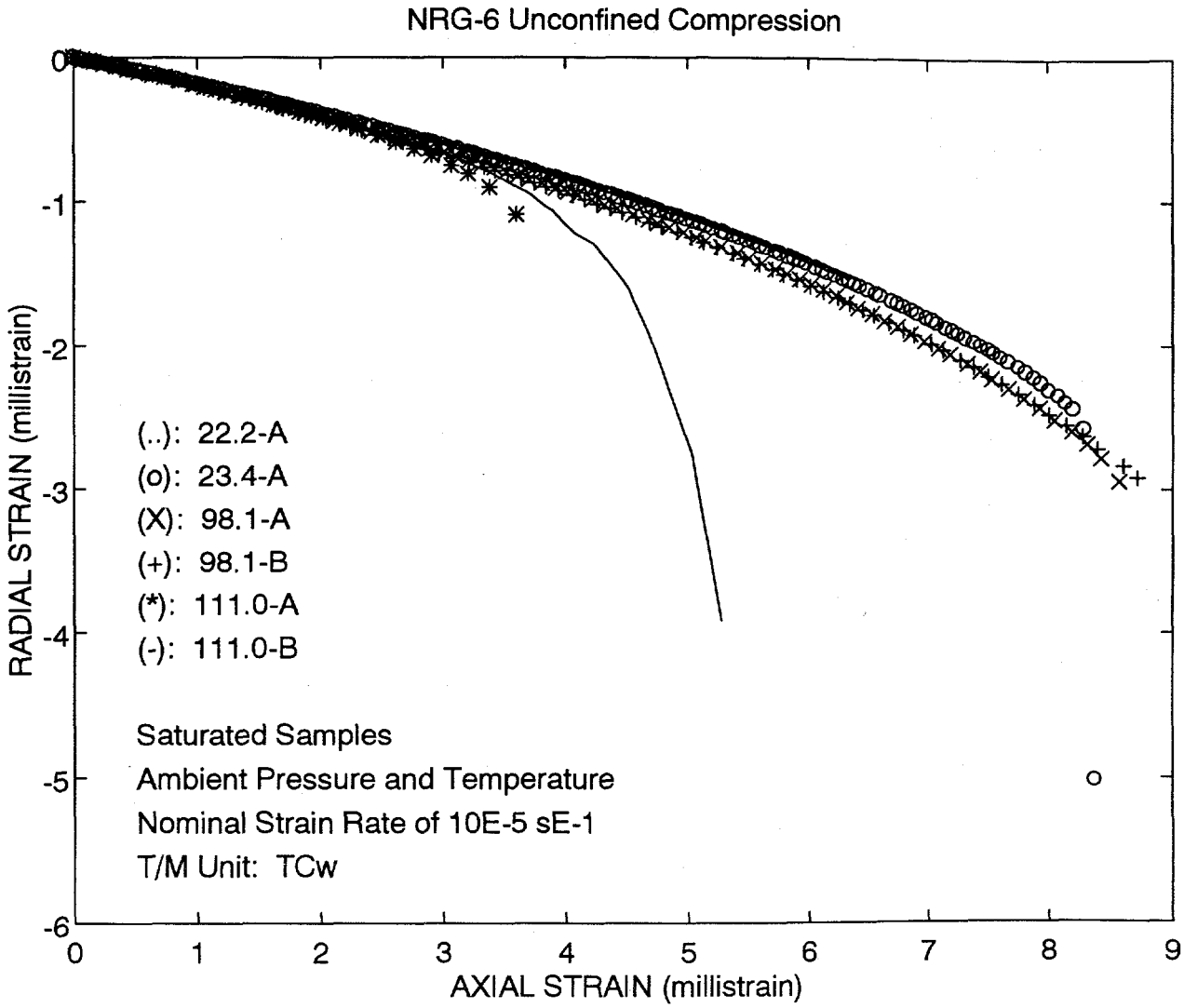
NRG-6 Unconfined Compression
RADIAL STRAIN (millistrain)
AXIAL STRAIN (millistrain)
0
-1
-2
-3
-4
-5
-6
0
1
2
3
4
5
6
7
8
9
(..): 22.2-A
(o): 23.4-A
(X): 98.1-A
(+): 98.1-B
(*): 111.0-A
(-): 111.0-B
Saturated Samples
Ambient Pressure and Temperature
Nominal Strain Rate of 10E-5 sE-1
T/M Unit: TCw

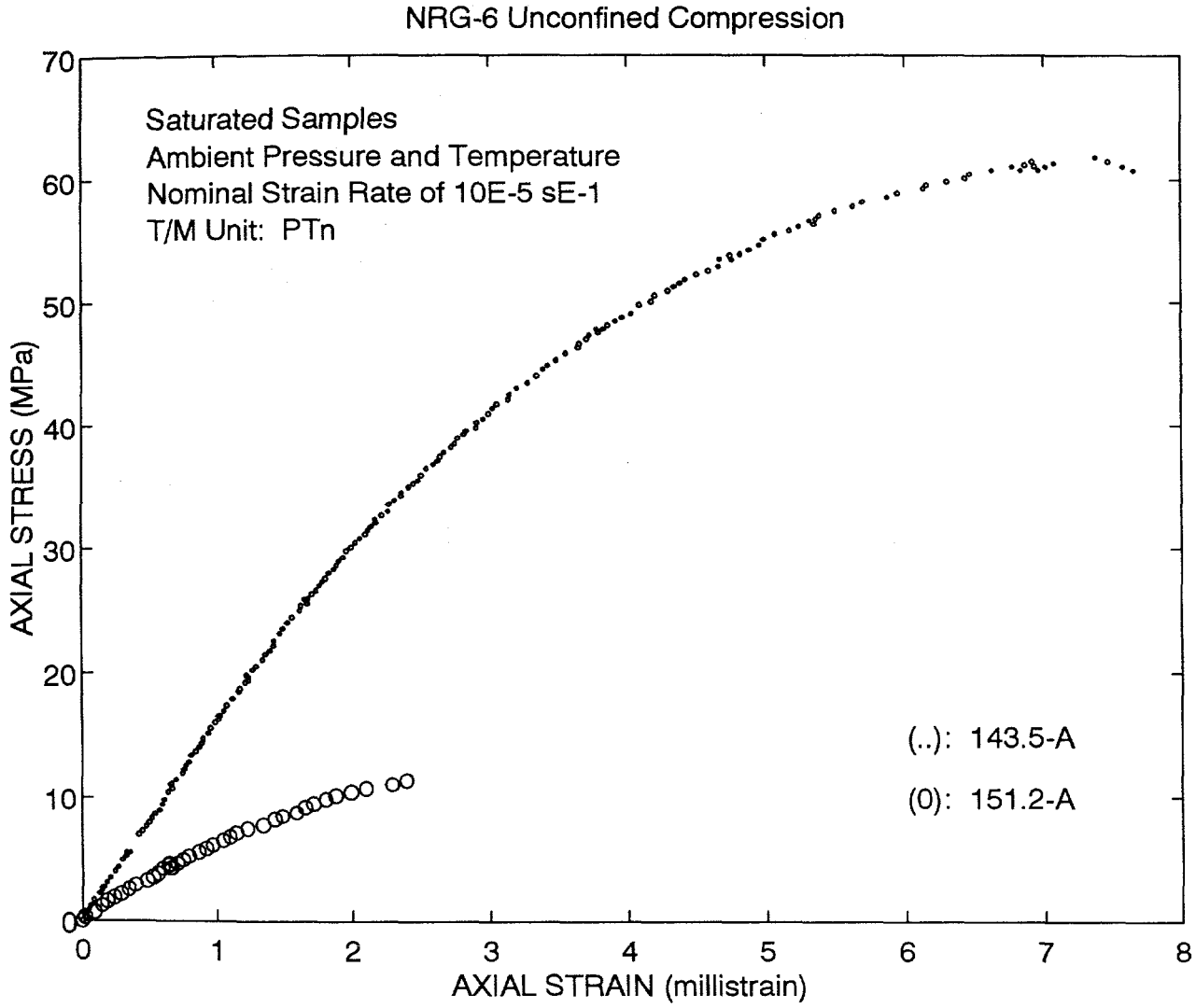
NRG-6 Unconfined Compression
Saturated Samples
Ambient Pressure and Temperature
Nominal Strain Rate of 10E-5 sE-1
T/M Unit: PTn
(..): 143.5-A
(0): 151.2-A
AXIAL STRESS (MPa)
AXIAL STRAIN (millistrain)
0
10
20
30
40
50
60
70
0
1
2
3
4
5
6
7
8

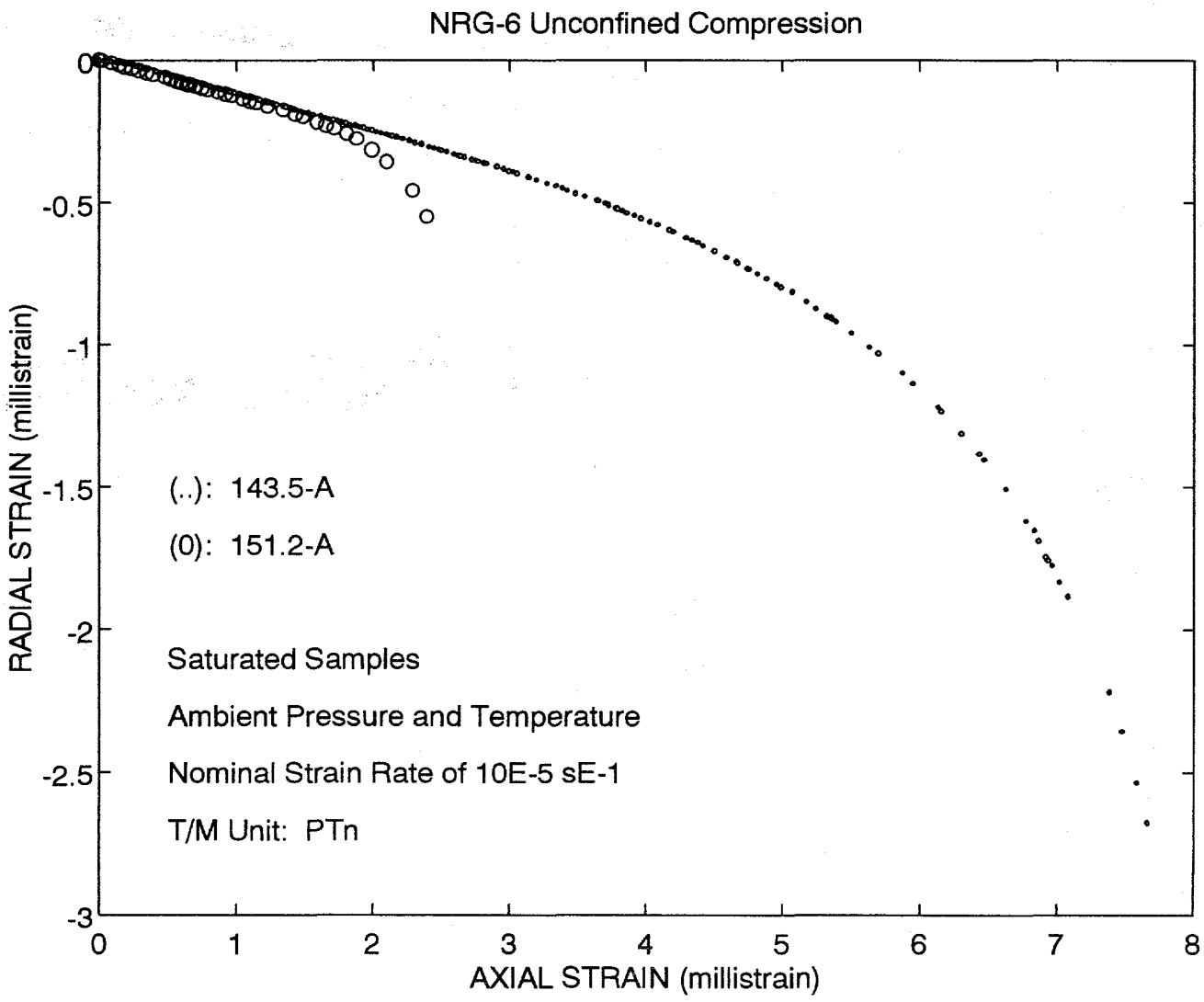
NRG-6 Unconfined Compression
RADIAL STRAIN (millistrain)
AXIAL STRAIN (millistrain)
0
-0.5
-1
-1.5
-2
-2.5
-3
0
1
2
3
4
5
6
7
8
(..): 143.5-A
(0): 151.2-A
Saturated Samples
Ambient Pressure and Temperature
Nominal Strain Rate of 10E-5 sE-1
T/M Unit: PTn

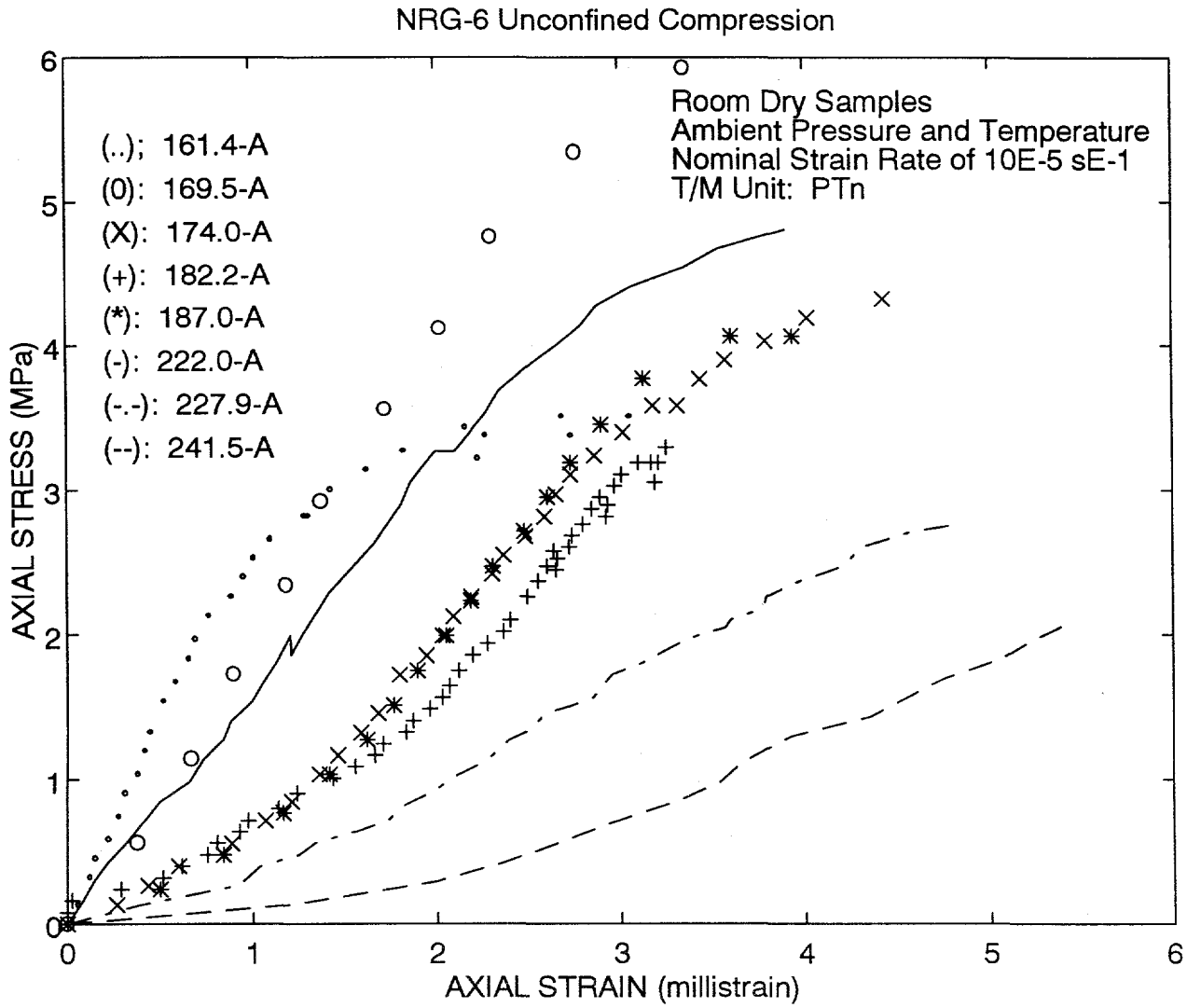
NRG-6 Unconfined Compression
Room Dry Samples
Ambient Pressure and Temperature
Nominal Strain Rate of 10E-5 sE-1
T/M Unit: PTn
(..); 161.4-A
(0): 169.5-A
(X): 174.0-A
(+): 182.2-A
(*): 187.0-A
(-): 222.0-A
(-.-): 227.9-A
(--): 241.5-A
AXIAL STRESS (MPa)
AXIAL STRAIN (millistrain)
0
1
2
3
4
5
6

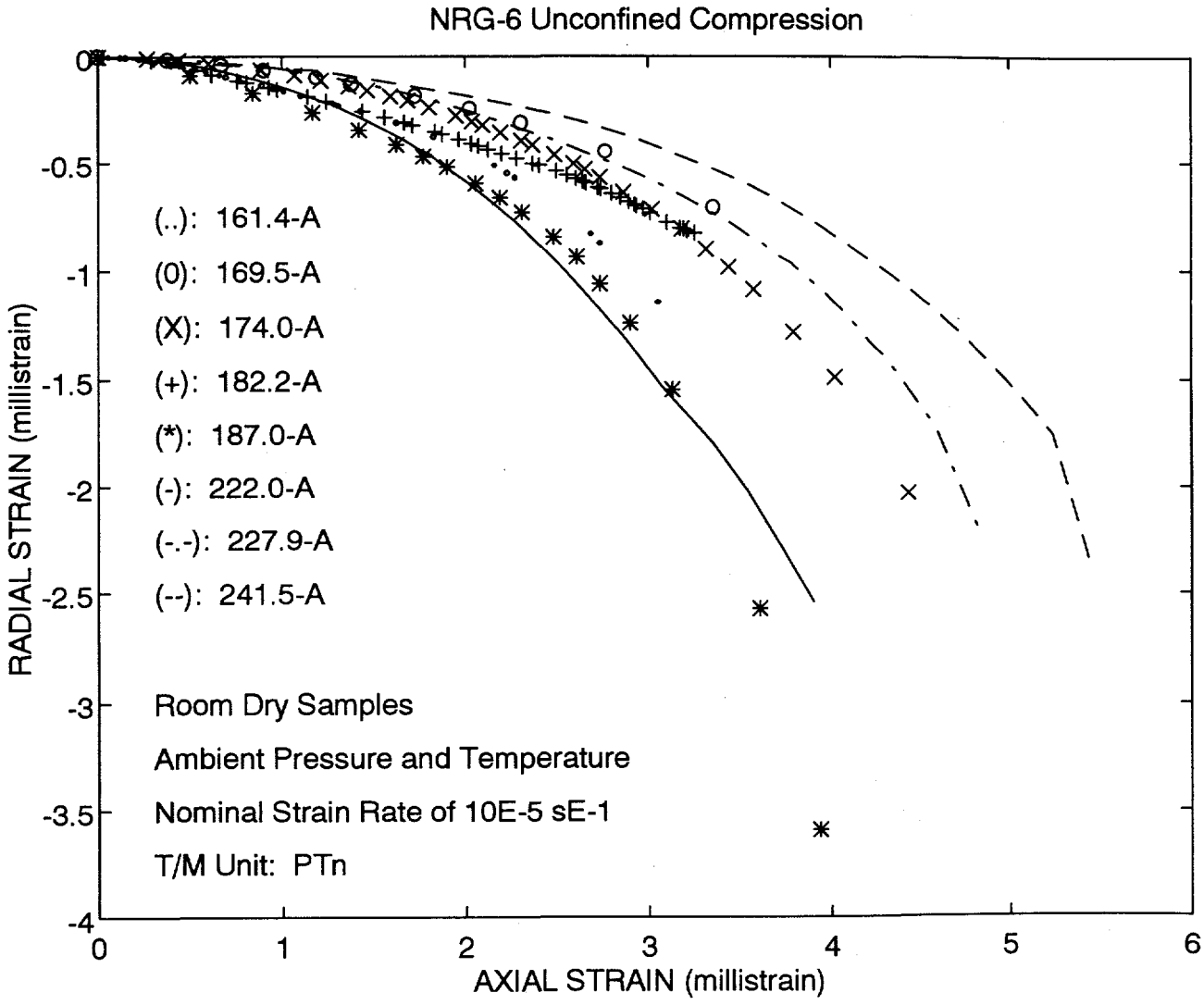
NRG-6 Unconfined Compression
RADIAL STRAIN (millistrain)
AXIAL STRAIN (millistrain)
0
-0.5
-1
-1.5
-2
-2.5
-3
-3.5
-4
0
1
2
3
4
5
6
(..): 161.4-A
(0): 169.5-A
(X): 174.0-A
(+): 182.2-A
(*): 187.0-A
(-): 222.0-A
(-.-): 227.9-A
(--): 241.5-A
Room Dry Samples
Ambient Pressure and Temperature
Nominal Strain Rate of 10E-5 sE-1
T/M Unit: PTn

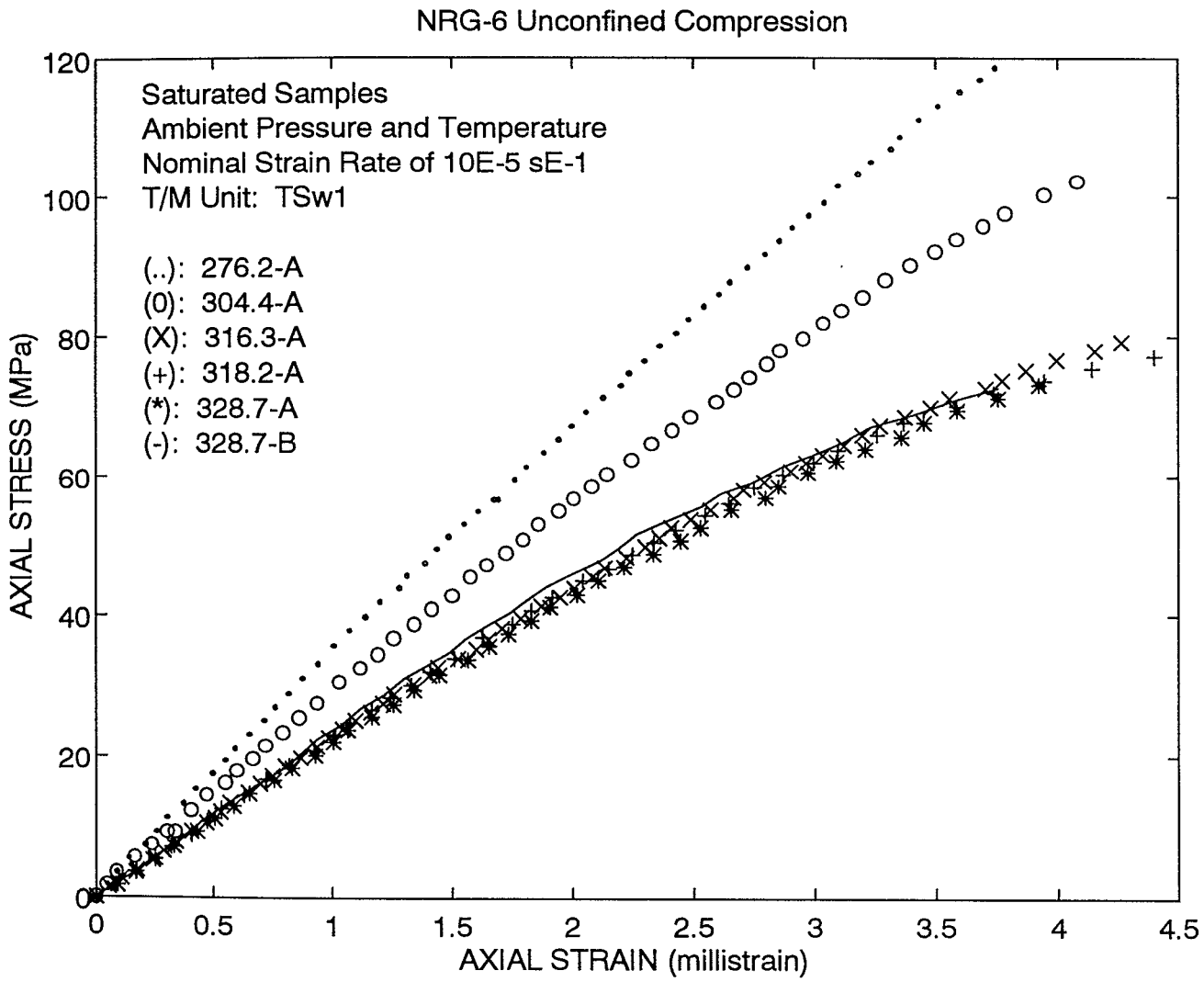
NRG-6 Unconfined Compression
Saturated Samples
Ambient Pressure and Temperature
Nominal Strain Rate of 10E-5 sE-1
T/M Unit: TSw1
(..): 276.2-A
(0): 304.4-A
(X): 316.3-A
(+): 318.2-A
(*): 328.7-A
(-): 328.7-B
AXIAL STRESS (MPa)
AXIAL STRAIN (millistrain)
0
20
40
60
80
100
120
0
0.5
1
1.5
2
2.5
3
3.5
4
4.5

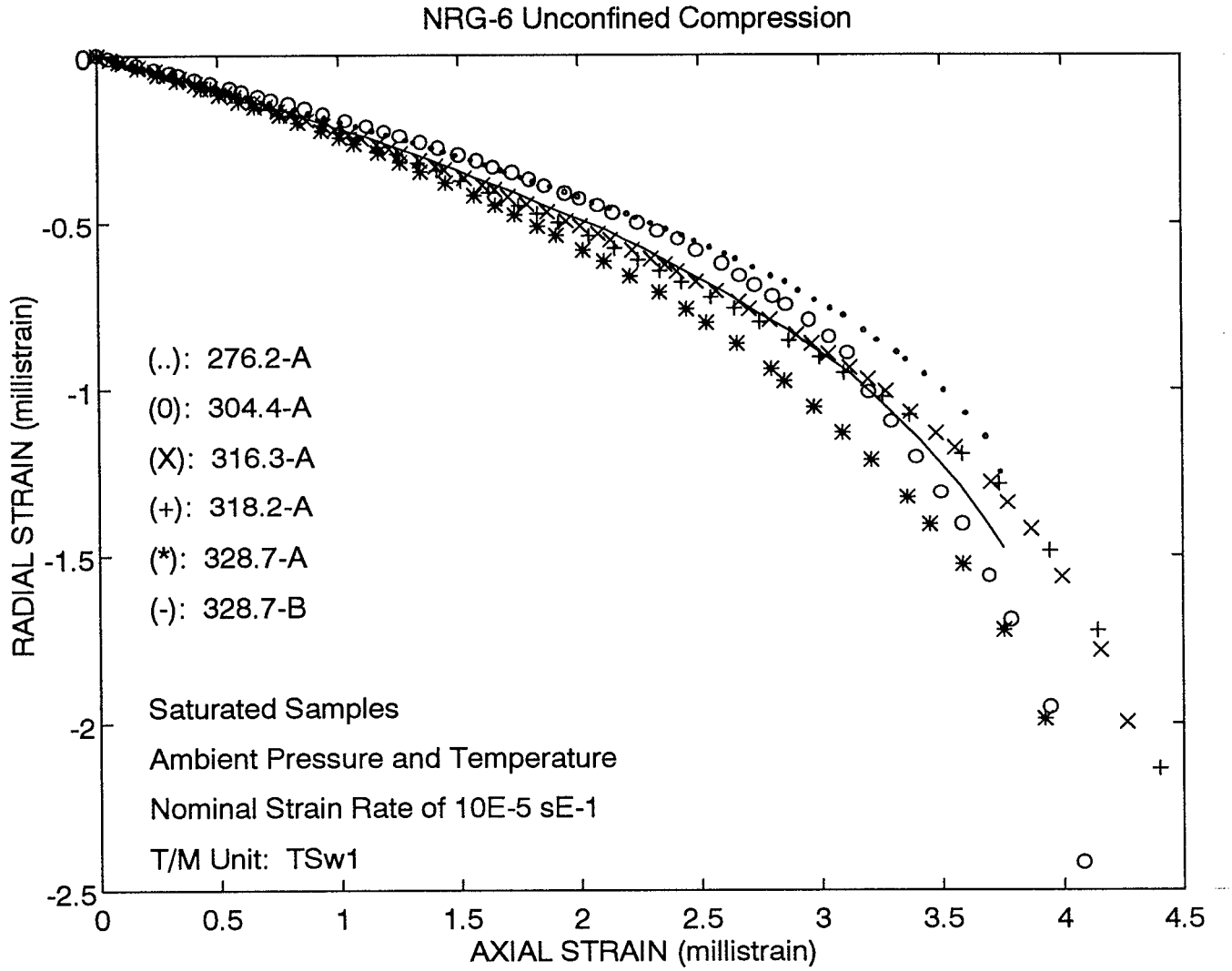
NRG-6 Unconfined Compression
RADIAL STRAIN (millistrain)
AXIAL STRAIN (millistrain)
0
-0.5
-1
-1.5
-2
-2.5
0
0.5
1
1.5
2
2.5
3
3.5
4
4.5
(..): 276.2-A
(0): 304.4-A
(X): 316.3-A
(+): 318.2-A
(*): 328.7-A
(-): 328.7-B
Saturated Samples
Ambient Pressure and Temperature
Nominal Strain Rate of 10E-5 sE-1
T/M Unit: TSw1

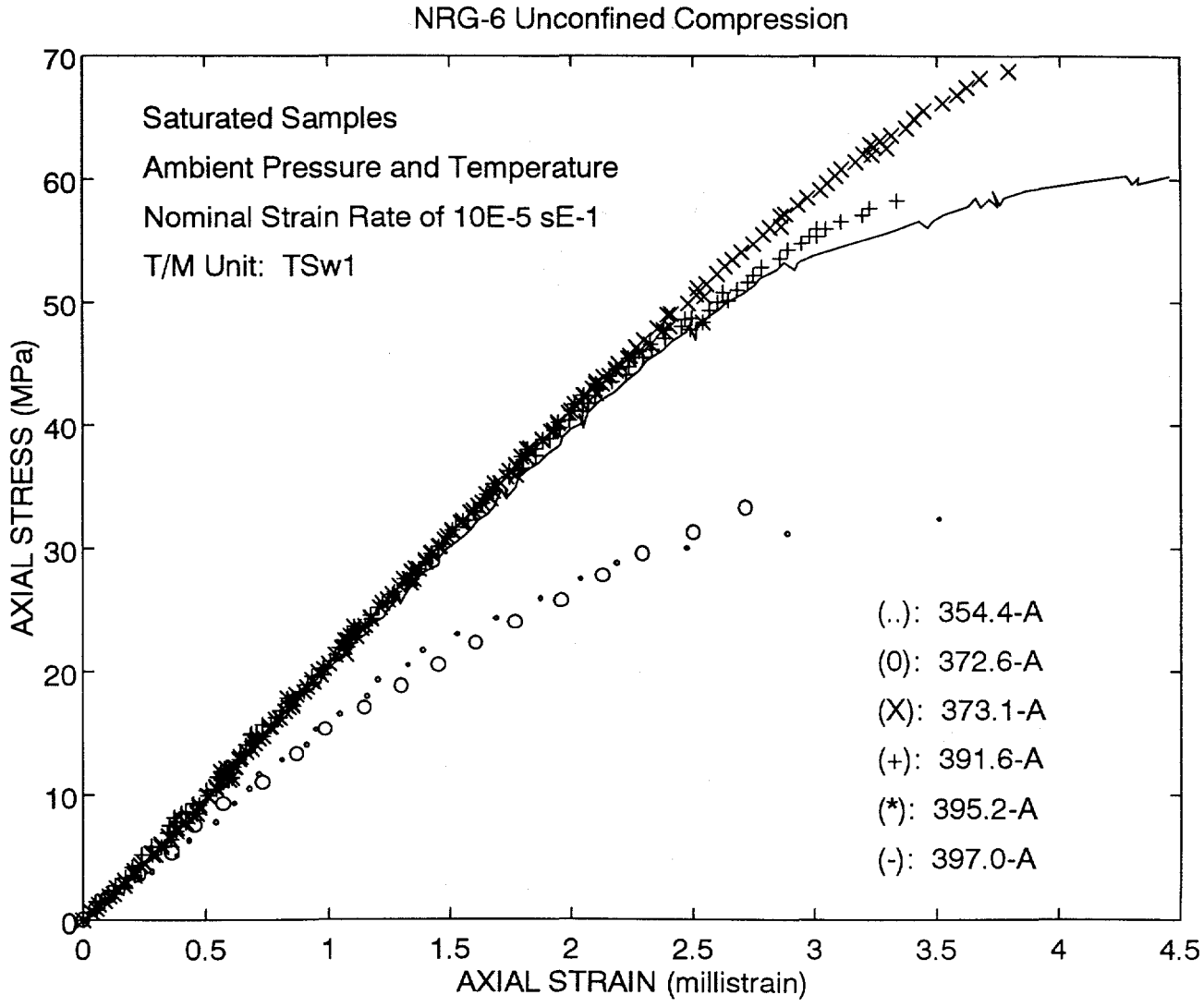
NRG-6 Unconfined Compression
Saturated Samples
Ambient Pressure and Temperature
Nominal Strain Rate of 10E-5 sE-1
T/M Unit: TSw1
(..): 354.4-A
(0): 372.6-A
(X): 373.1-A
(+): 391.6-A
(*): 395.2-A
(-): 397.0-A
AXIAL STRESS (MPa)
AXIAL STRAIN (millistrain)
0
10
20
30
40
50
60
70
0
0.5
1
1.5
2
2.5
3
3.5
4
4.5

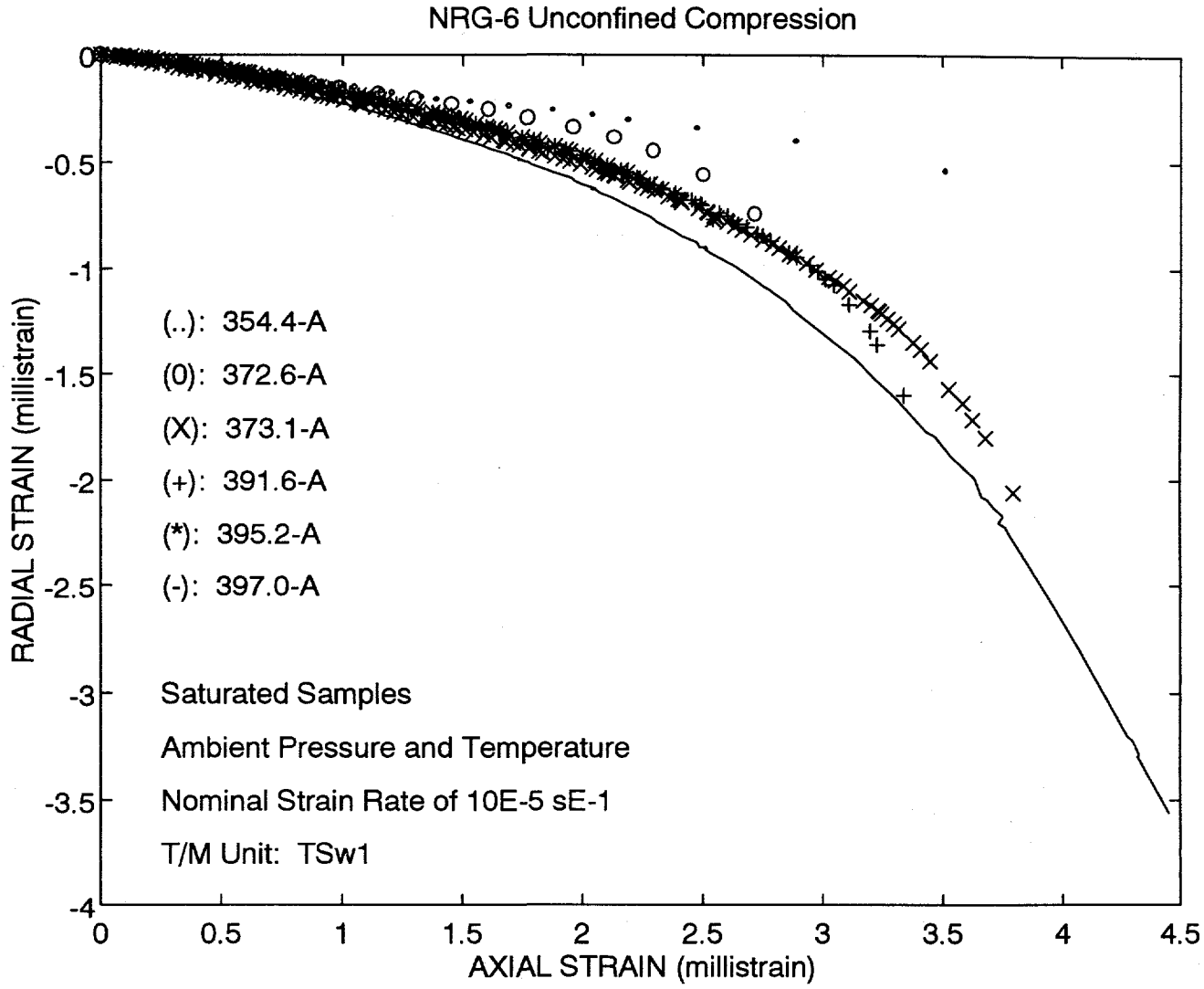
NRG-6 Unconfined Compression
RADIAL STRAIN (millistrain)
AXIAL STRAIN (millistrain)
0
-0.5
-1
-1.5
-2
-2.5
-3
-3.5
-4
0
0.5
1
1.5
2
2.5
3
3.5
4
4.5
(..): 354.4-A
(0): 372.6-A
(X): 373.1-A
(+): 391.6-A
(*): 395.2-A
(-): 397.0-A
Saturated Samples
Ambient Pressure and Temperature
Nominal Strain Rate of 10E-5 sE-1
T/M Unit: TSw1

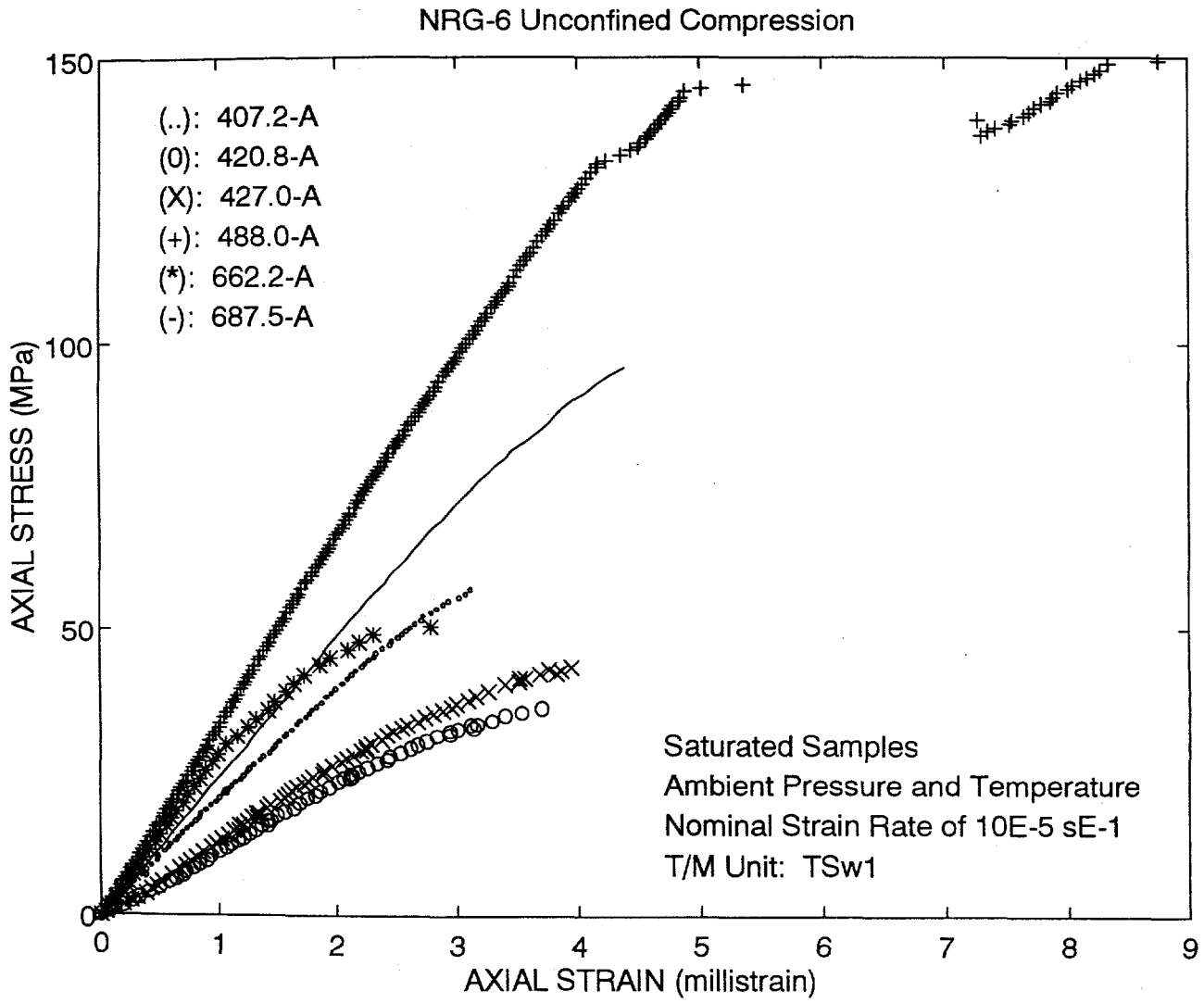
NRG-6 Unconfined Compression
(..): 407.2-A
(0): 420.8-A
(X): 427.0-A
(+): 488.0-A
(*): 662.2-A
(-): 687.5-A
Saturated Samples
Ambient Pressure and Temperature
Nominal Strain Rate of 10E-5 sE-1
T/M Unit: TSw1
AXIAL STRESS (MPa)
AXIAL STRAIN (millistrain)
0
50
100
150
0
1
2
3
4
5
6
7
8
9

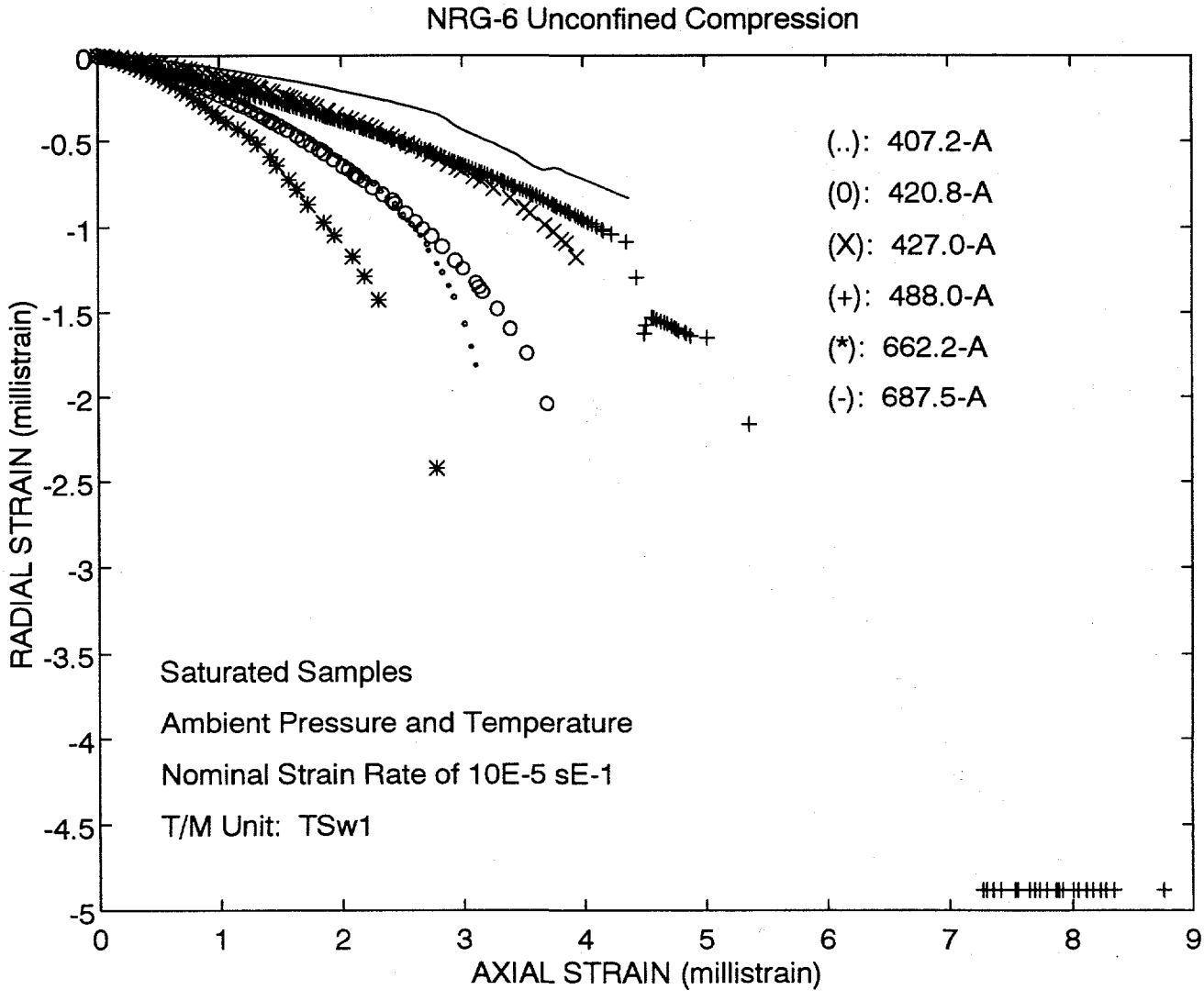
NRG-6 Unconfined Compression
RADIAL STRAIN (millistrain)
AXIAL STRAIN (millistrain)
0
-0.5
-1
-1.5
-2
-2.5
-3
-3.5
-4
-4.5
-5
0
1
2
3
4
5
6
7
8
9
(..): 407.2-A
(0): 420.8-A
(X): 427.0-A
(+): 488.0-A
(*): 662.2-A
(-): 687.5-A
Saturated Samples
Ambient Pressure and Temperature
Nominal Strain Rate of 10E-5 sE-1
T/M Unit: TSw1

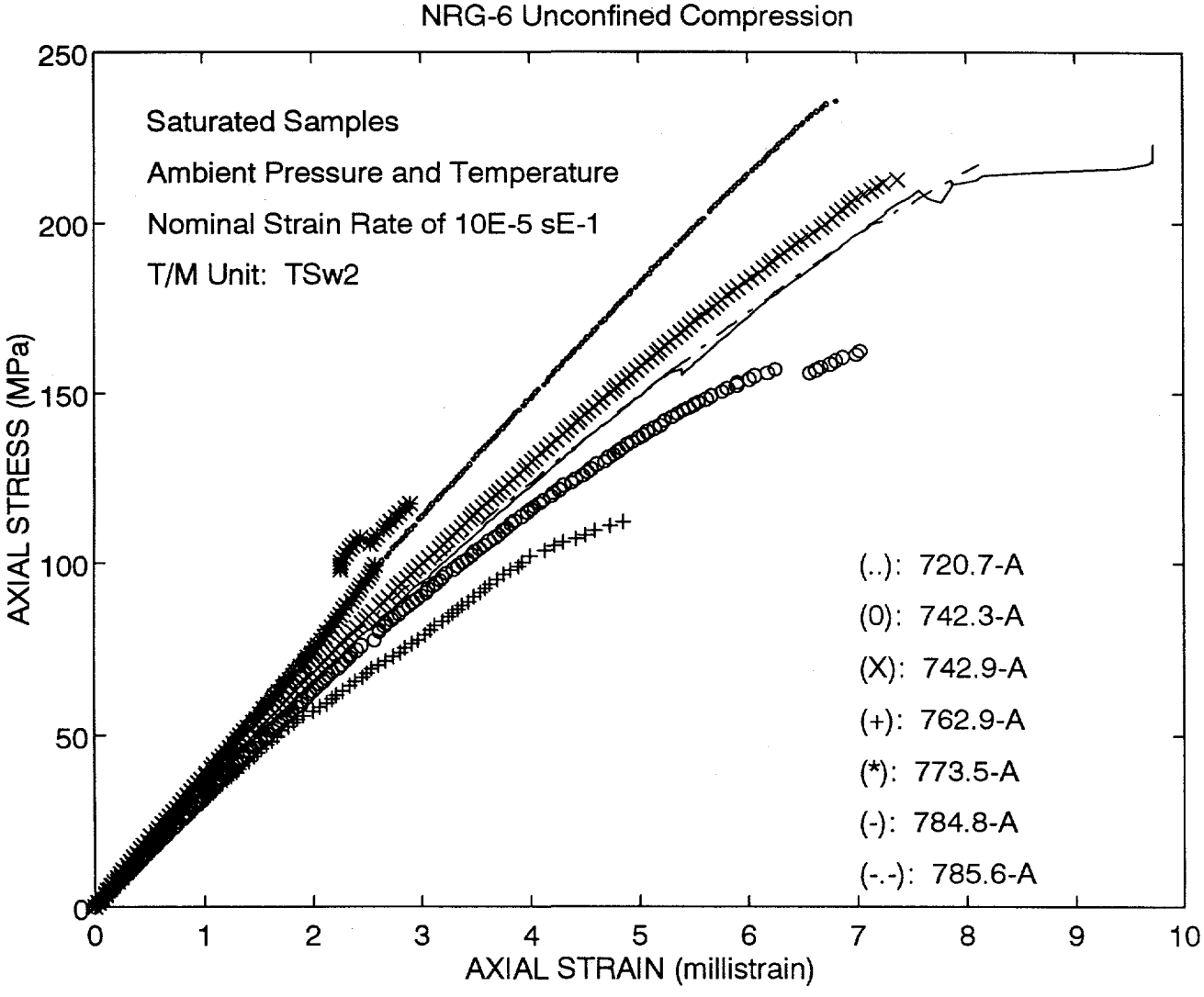
NRG-6 Unconfined Compression
Saturated Samples
Ambient Pressure and Temperature
Nominal Strain Rate of 10E-5 sE-1
T/M Unit: TSw2
(..): 720.7-A
(0): 742.3-A
(X): 742.9-A
(+): 762.9-A
(*): 773.5-A
(-): 784.8-A
(-.-): 785.6-A
AXIAL STRESS (MPa)
AXIAL STRAIN (millistrain)
0
50
100
150
200
250
0
1
2
3
4
5
6
7
8
9
10

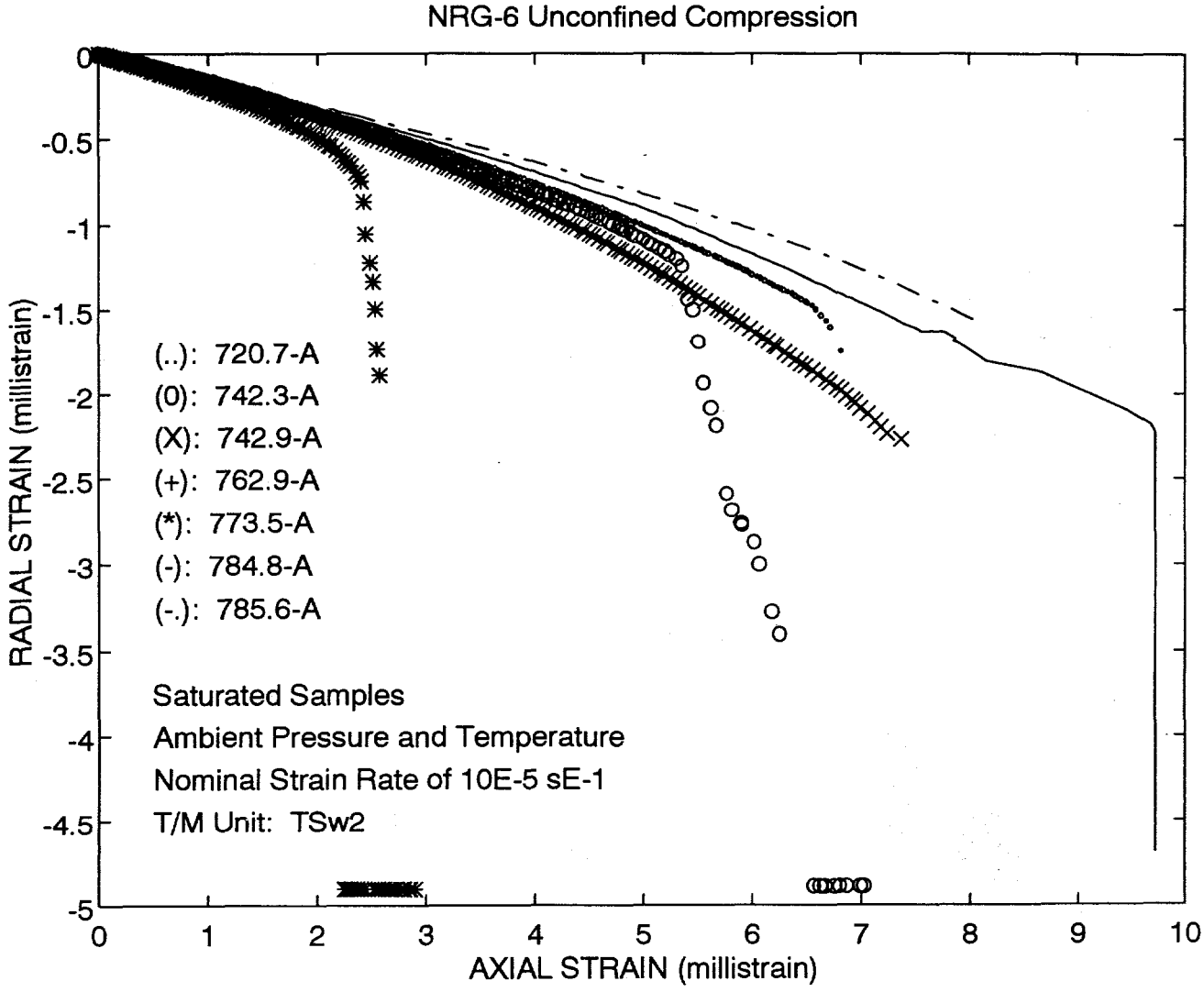
NRG-6 Unconfined Compression
RADIAL STRAIN (millistrain)
AXIAL STRAIN (millistrain)
0
-0.5
-1
-1.5
-2
-2.5
-3
-3.5
-4
-4.5
-5
0
1
2
3
4
5
6
7
8
9
10
(..): 720.7-A
(0): 742.3-A
(X): 742.9-A
(+): 762.9-A
(*): 773.5-A
(-): 784.8-A
(-.): 785.6-A
Saturated Samples
Ambient Pressure and Temperature
Nominal Strain Rate of 10E-5 sE-1
T/M Unit: TSw2

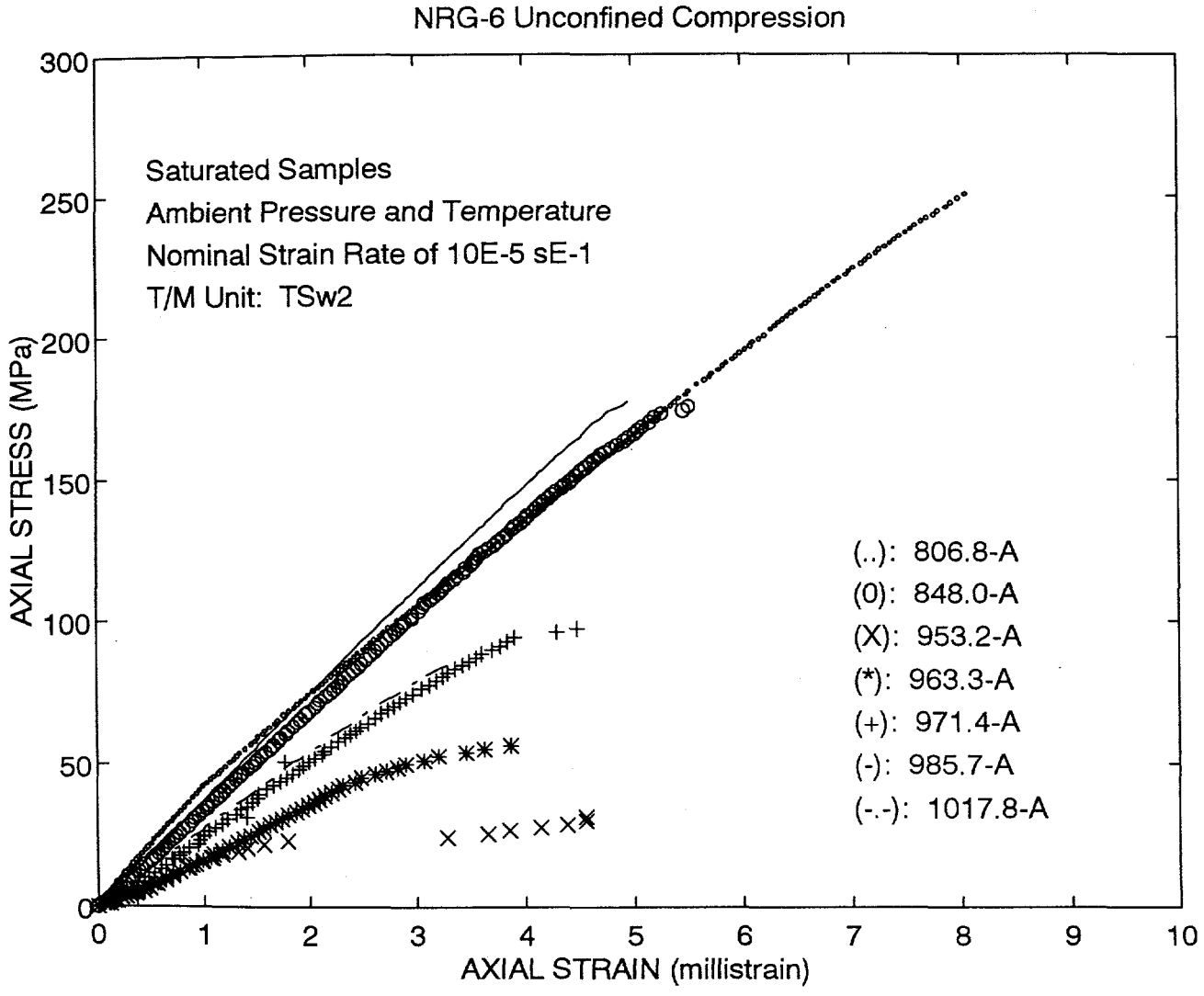
NRG-6 Unconfined Compression
Saturated Samples
Ambient Pressure and Temperature
Nominal Strain Rate of 10E-5 sE-1
T/M Unit: TSw2
(..): 806.8-A
(0): 848.0-A
(X): 953.2-A
(*): 963.3-A
(+): 971.4-A
(-): 985.7-A
(-.-): 1017.8-A
AXIAL STRESS (MPa)
AXIAL STRAIN (millistrain)
0
50
100
150
200
250
300
0
1
2
3
4
5
6
7
8
9
10

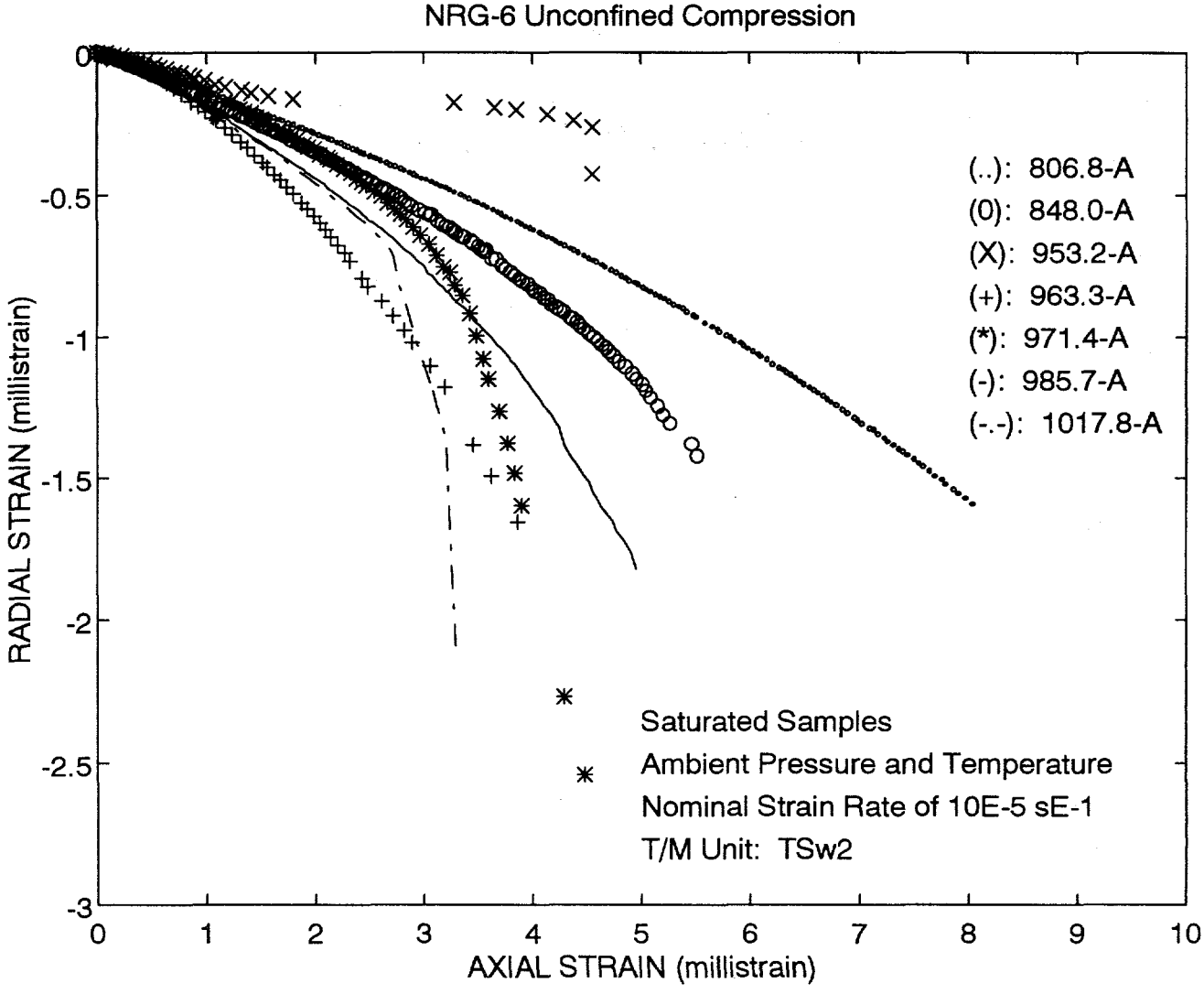
NRG-6 Unconfined Compression
RADIAL STRAIN (millistrain)
AXIAL STRAIN (millistrain)
0
-0.5
-1
-1.5
-2
-2.5
-3
0
1
2
3
4
5
6
7
8
9
10
(..): 806.8-A
(0): 848.0-A
(X): 953.2-A
(+): 963.3-A
(*): 971.4-A
(-): 985.7-A
(-.-): 1017.8-A
Saturated Samples
Ambient Pressure and Temperature
Nominal Strain Rate of 10E-5 sE-1
T/M Unit: TSw2

APPENDIX II

Stress vs Axial Strain and Radial Strain vs Axial Strain Plots for Confined Compression Experiments

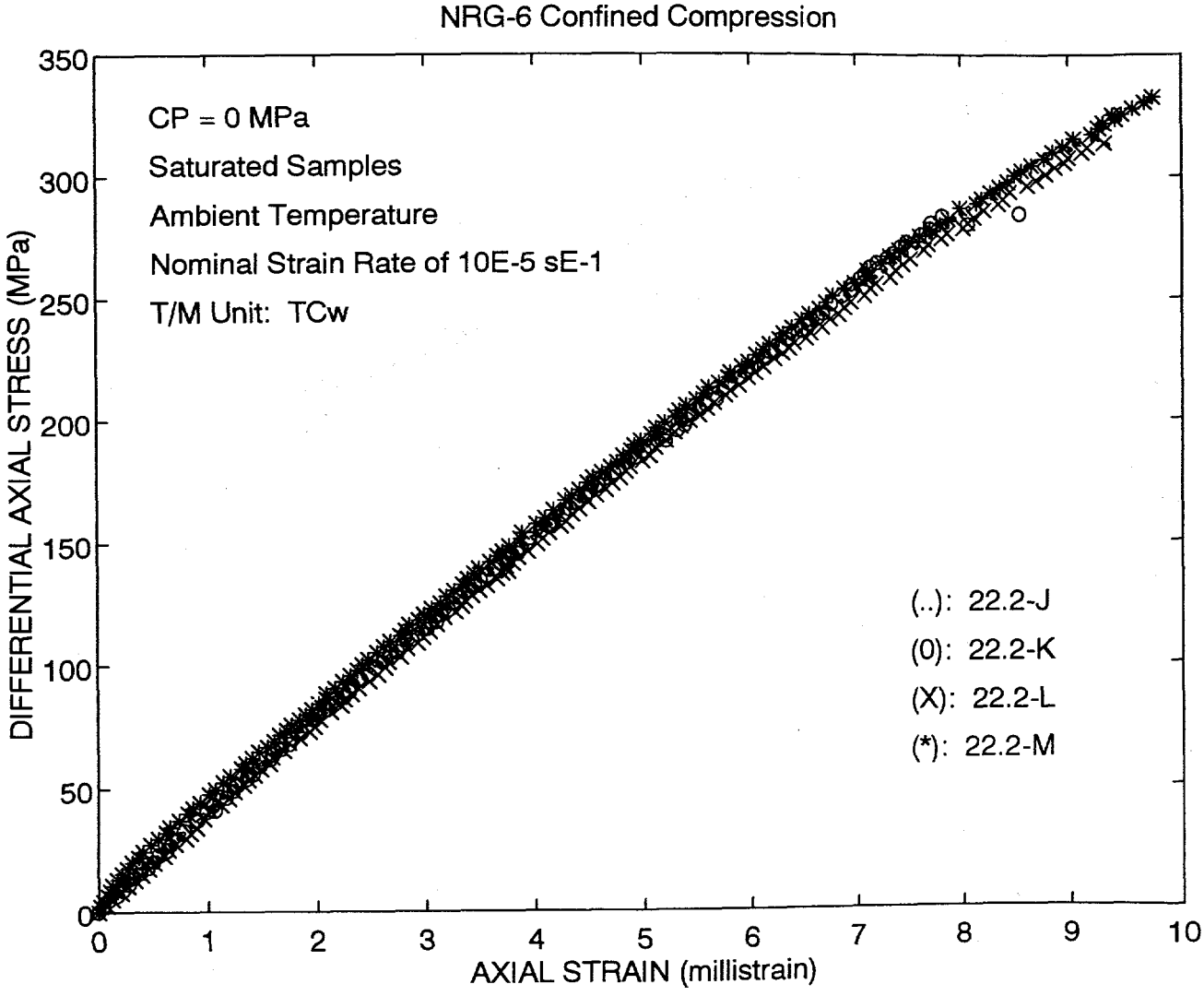
NRG-6 Confined Compression
CP = 0 MPa
Saturated Samples
Ambient Temperature
Nominal Strain Rate of 10E-5 sE-1
T/M Unit: TCw
(..): 22.2-J
(0): 22.2-K
(X): 22.2-L
(*): 22.2-M
DIFFERENTIAL AXIAL STRESS (MPa)
AXIAL STRAIN (millistrain)
0
50
100
150
200
250
300
350
0
1
2
3
4
5
6
7
8
9
10

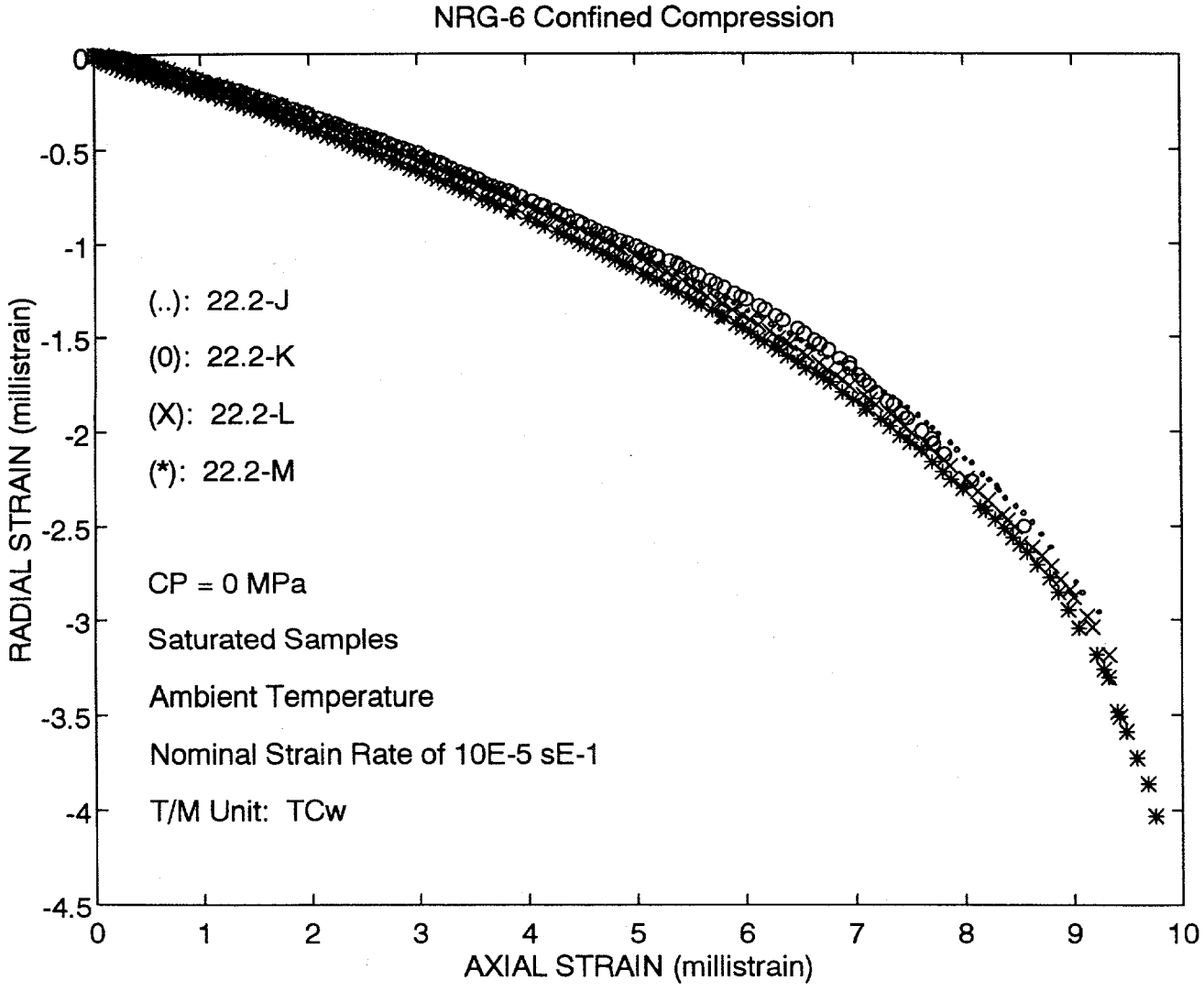
NRG-6 Confined Compression
RADIAL STRAIN (millistrain)
AXIAL STRAIN (millistrain)
0
-0.5
-1
-1.5
-2
-2.5
-3
-3.5
-4
-4.5
0
1
2
3
4
5
6
7
8
9
10
(..): 22.2-J
(0): 22.2-K
(X): 22.2-L
(*): 22.2-M
CP = 0 MPa
Saturated Samples
Ambient Temperature
Nominal Strain Rate of 10E-5 sE-1
T/M Unit: TCw

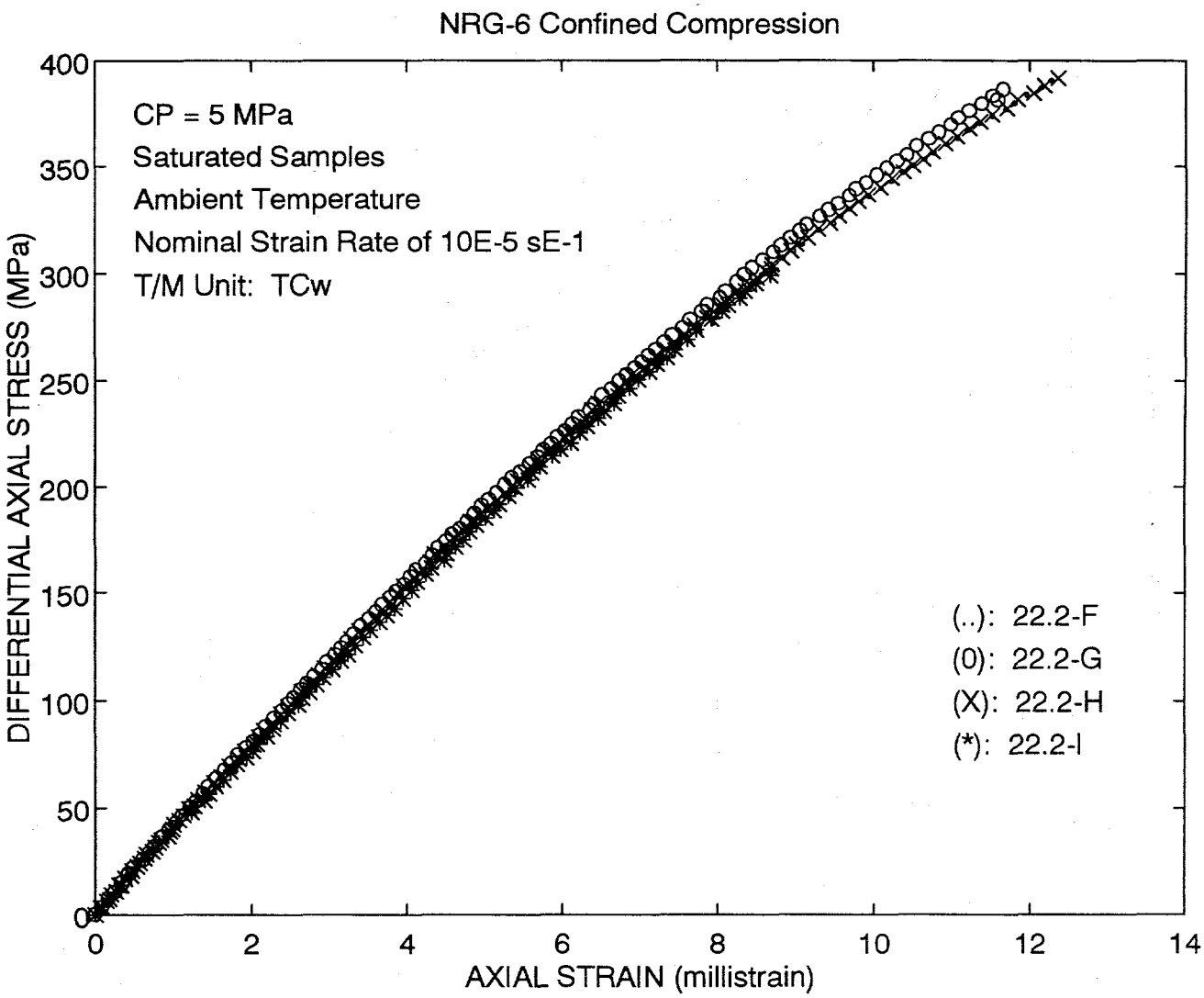
NRG-6 Confined Compression
CP = 5 MPa
Saturated Samples
Ambient Temperature
Nominal Strain Rate of 10E-5 sE-1
T/M Unit: TCw
(..): 22.2-F
(0): 22.2-G
(X): 22.2-H
(*): 22.2-I
DIFFERENTIAL AXIAL STRESS (MPa)
AXIAL STRAIN (millistrain)
0
50
100
150
200
250
300
350
400
0
2
4
6
8
10
12
14

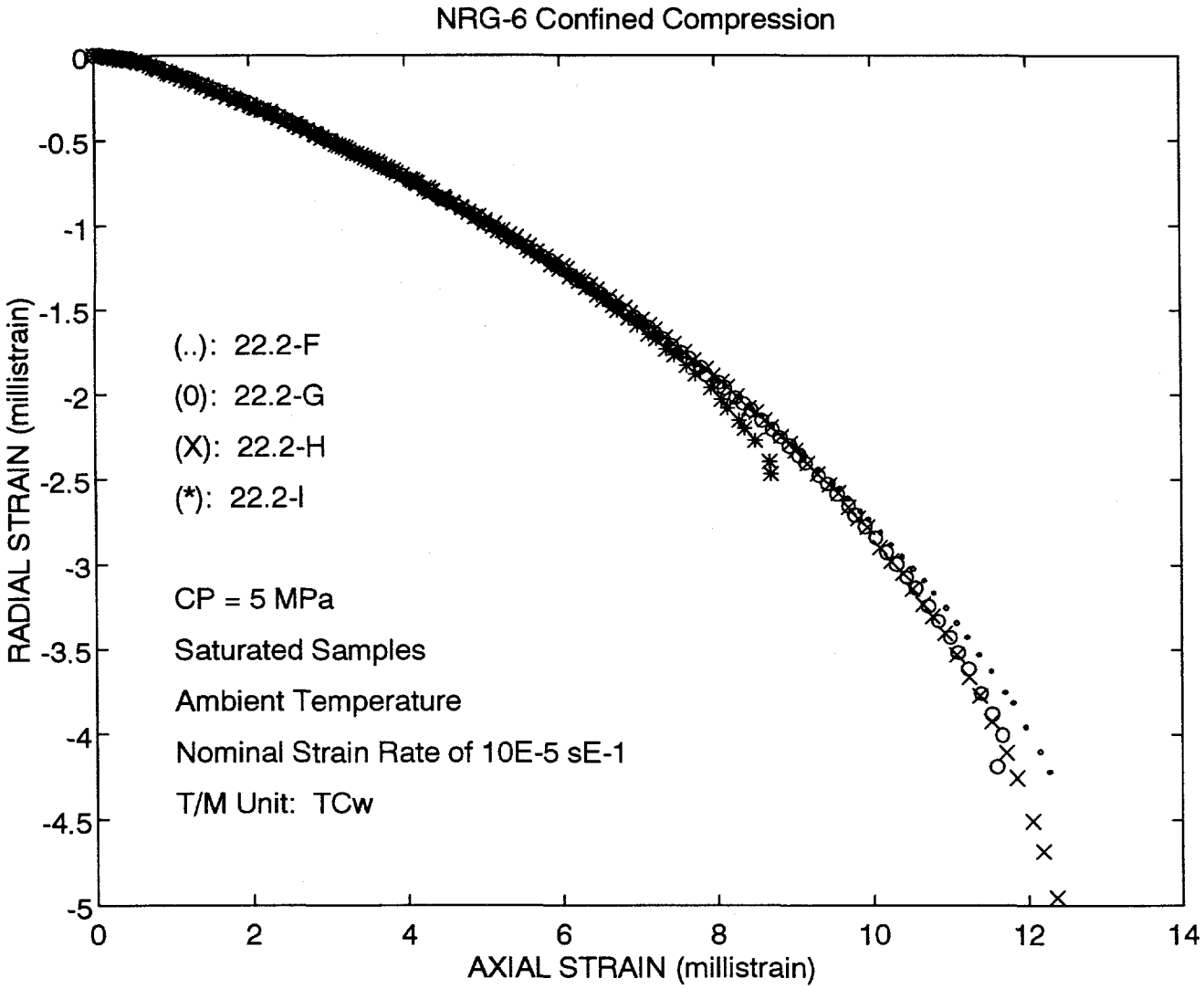
NRG-6 Confined Compression
RADIAL STRAIN (millistrain)
AXIAL STRAIN (millistrain)
0
-0.5
-1
-1.5
-2
-2.5
-3
-3.5
-4
-4.5
-5
0
2
4
6
8
10
12
14
(..): 22.2-F
(0): 22.2-G
(X): 22.2-H
(*): 22.2-I
CP = 5 MPa
Saturated Samples
Ambient Temperature
Nominal Strain Rate of 10E-5 sE-1
T/M Unit: TCw

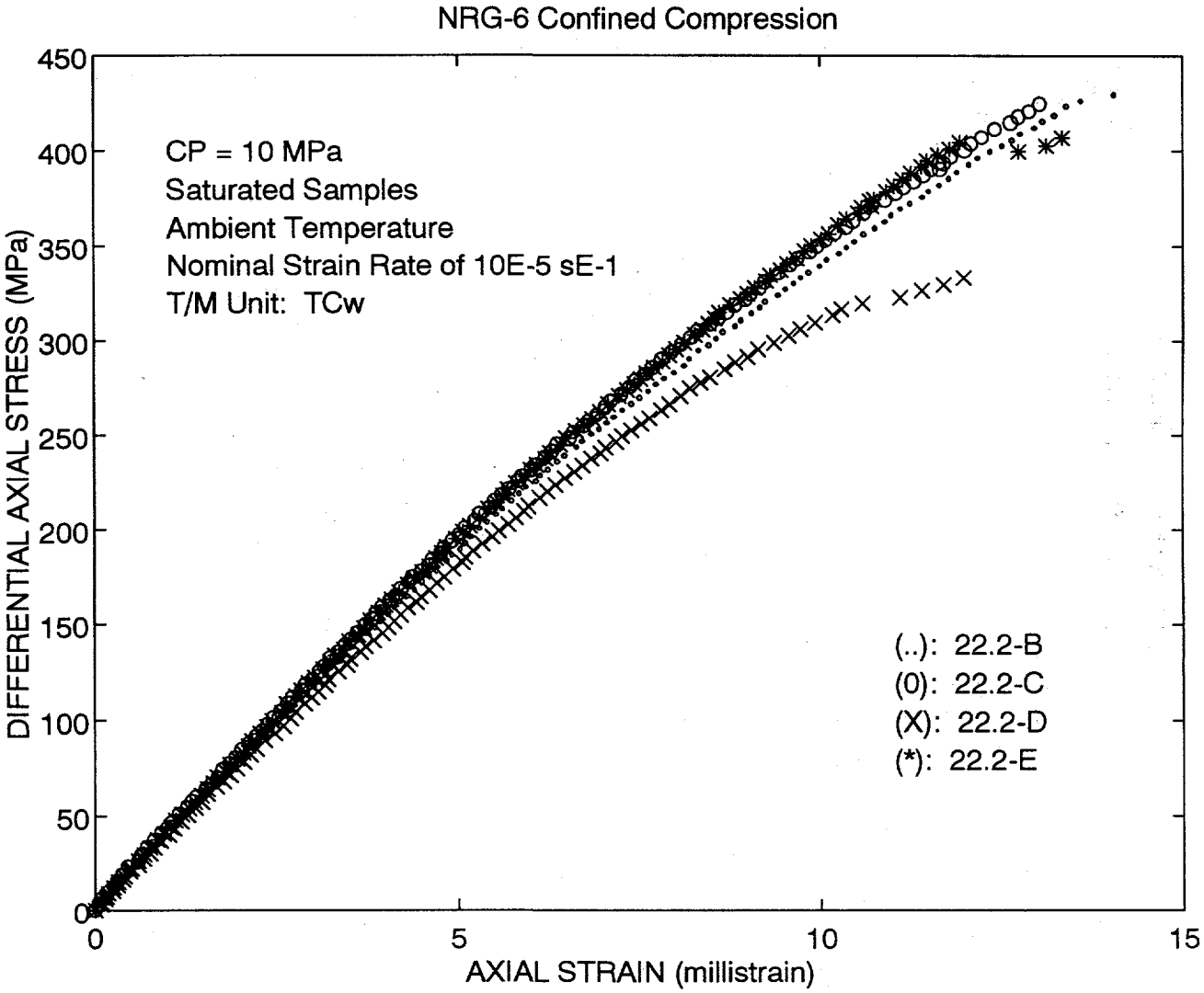
NRG-6 Confined Compression
CP = 10 MPa
Saturated Samples
Ambient Temperature
Nominal Strain Rate of 10E-5 sE-1
T/M Unit: TCw
(..): 22.2-B
(0): 22.2-C
(X): 22.2-D
(*): 22.2-E
DIFFERENTIAL AXIAL STRESS (MPa)
AXIAL STRAIN (millistrain)
0
50
100
150
200
250
300
350
400
450
0
5
10
15

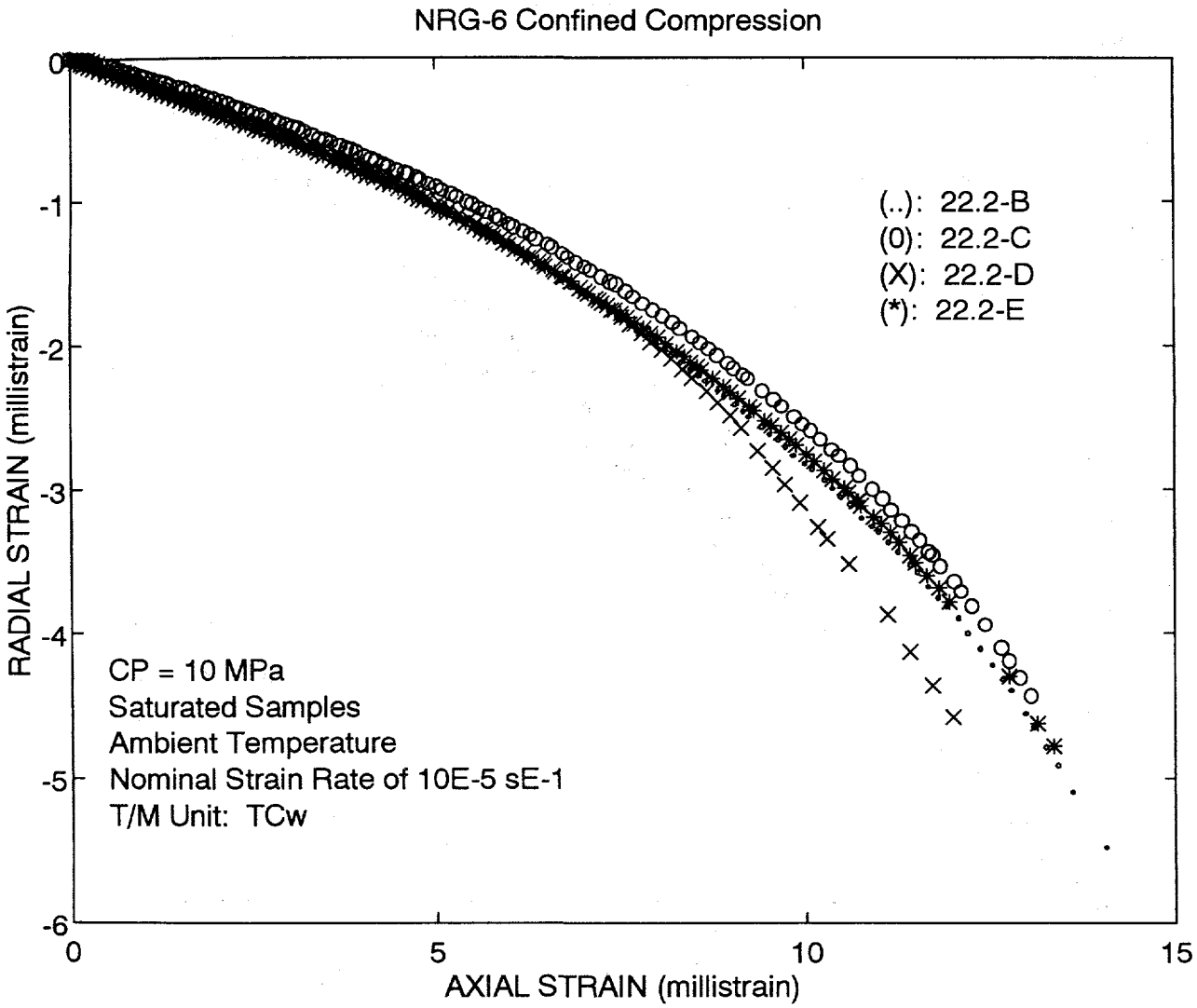
NRG-6 Confined Compression
RADIAL STRAIN (millistrain)
AXIAL STRAIN (millistrain)
0
-1
-2
-3
-4
-5
-6
0
5
10
15
(..): 22.2-B
(0): 22.2-C
(X): 22.2-D
(*): 22.2-E
CP = 10 MPa
Saturated Samples
Ambient Temperature
Nominal Strain Rate of 10E-5 sE-1
T/M Unit: TCw

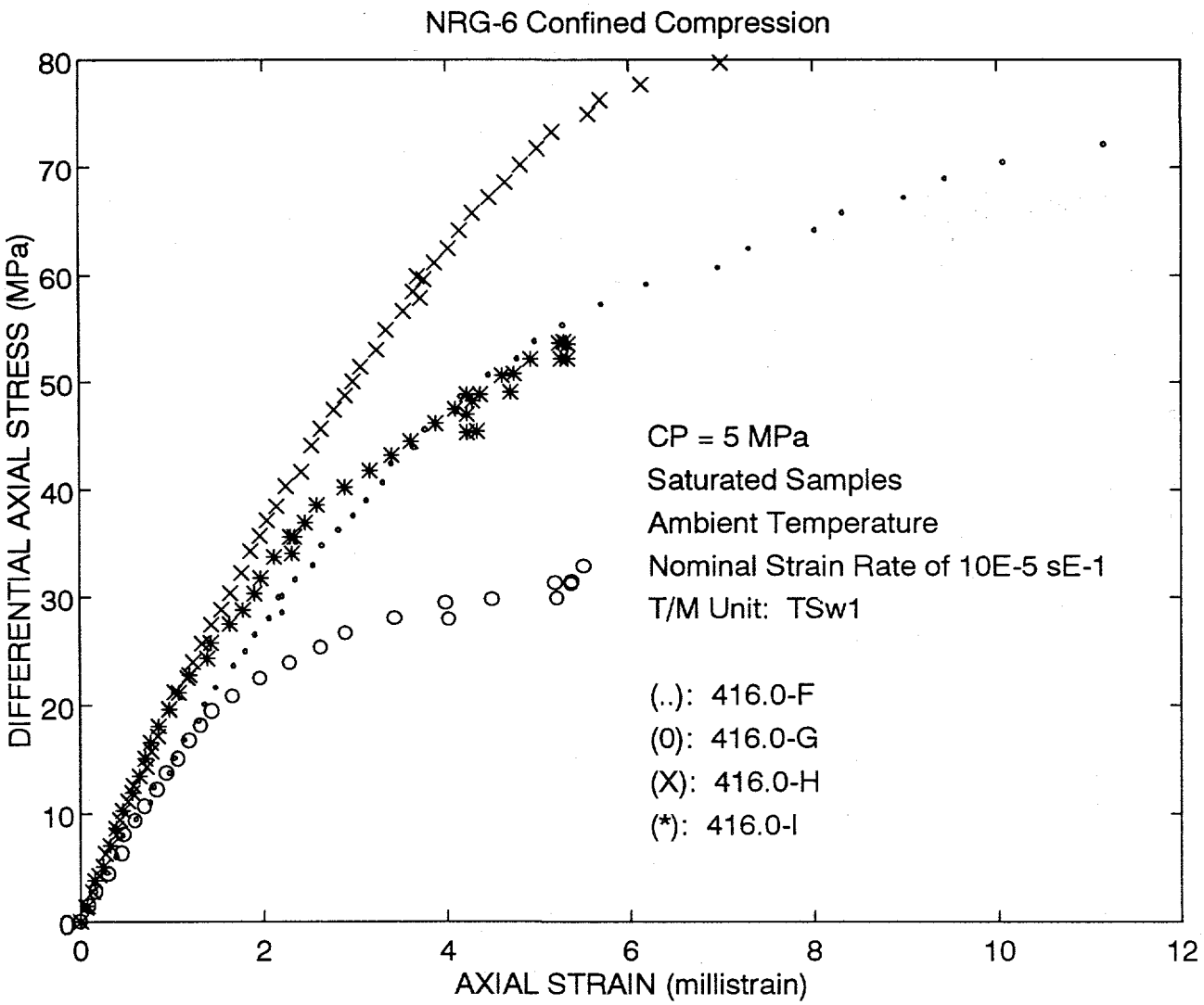
NRG-6 Confined Compression
DIFFERENTIAL AXIAL STRESS (MPa)
AXIAL STRAIN (millistrain)
0
10
20
30
40
50
60
70
80
0
2
4
6
8
10
12
CP = 5 MPa
Saturated Samples
Ambient Temperature
Nominal Strain Rate of 10E-5 sE-1
T/M Unit: TSw1
(..): 416.0-F
(0): 416.0-G
(X): 416.0-H
(*): 416.0-I

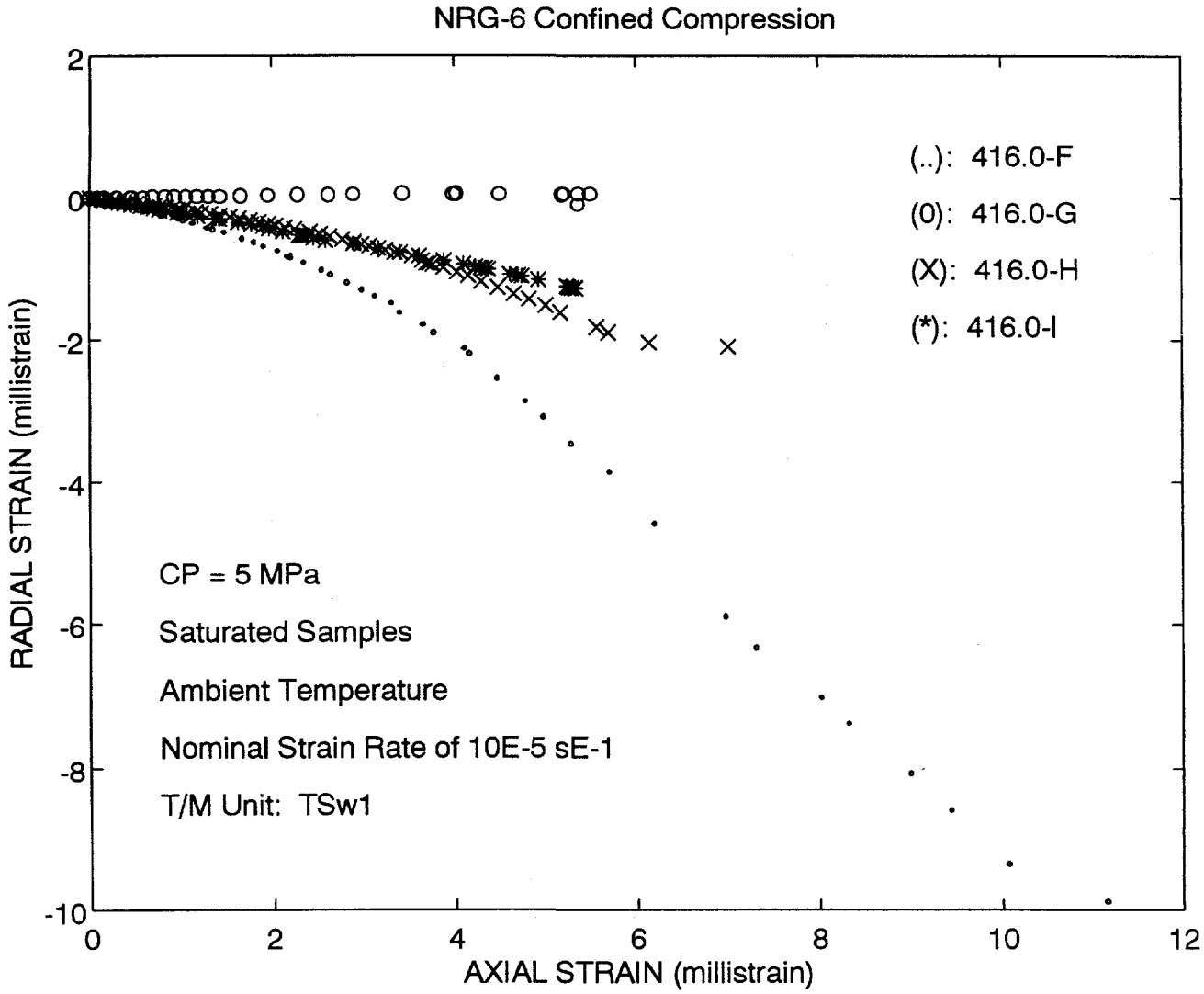
NRG-6 Confined Compression
RADIAL STRAIN (millistrain)
AXIAL STRAIN (millistrain)
2
0
-2
-4
-6
-8
-10
0
2
4
6
8
10
12
(..): 416.0-F
(0): 416.0-G
(X): 416.0-H
(*): 416.0-I
CP = 5 MPa
Saturated Samples
Ambient Temperature
Nominal Strain Rate of 10E-5 sE-1
T/M Unit: TSw1

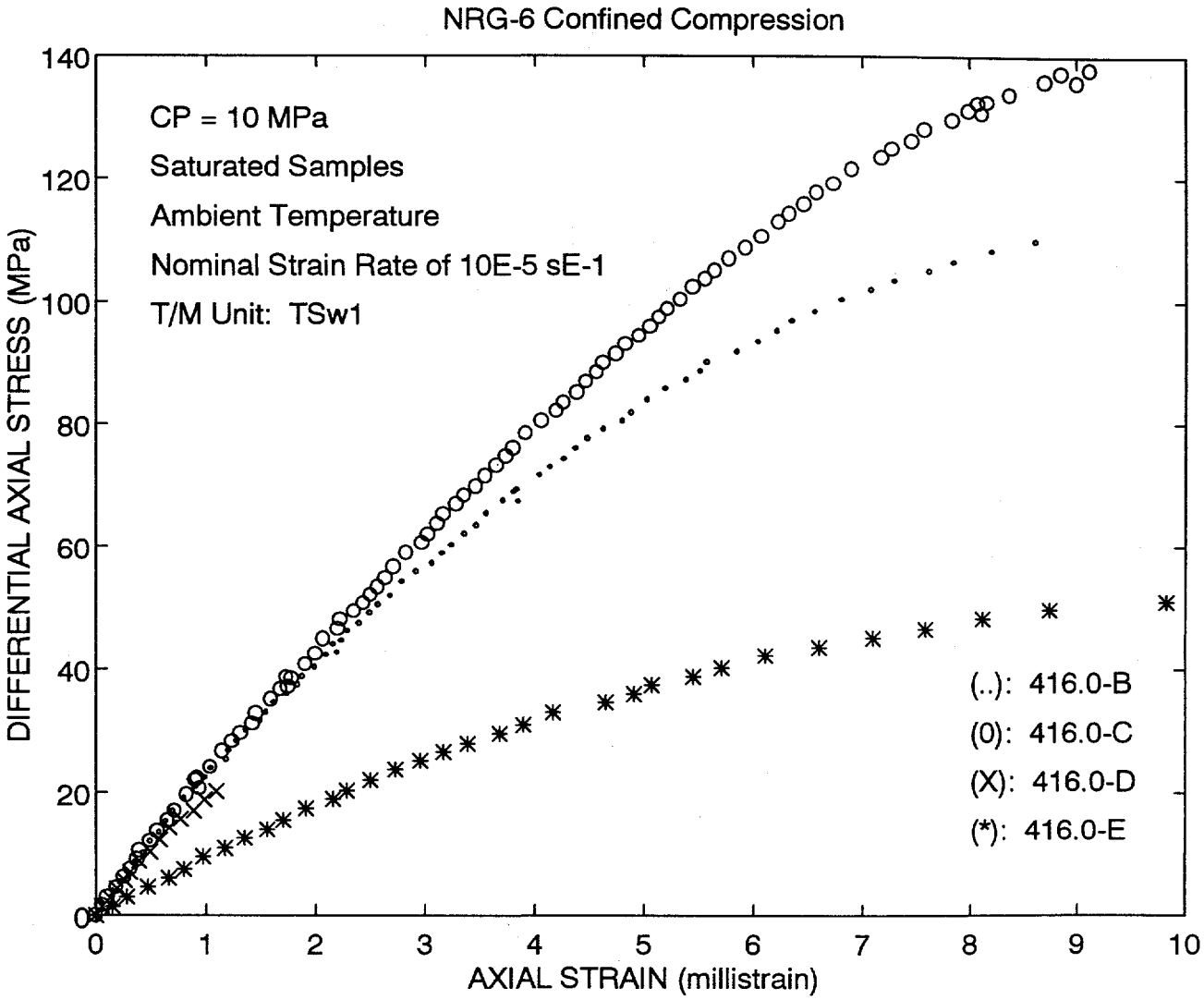
NRG-6 Confined Compression
CP = 10 MPa
Saturated Samples
Ambient Temperature
Nominal Strain Rate of 10E-5 sE-1
T/M Unit: TSw1
(..): 416.0-B
(0): 416.0-C
(X): 416.0-D
(*): 416.0-E
DIFFERENTIAL AXIAL STRESS (MPa)
AXIAL STRAIN (millistrain)
0
20
40
60
80
100
120
140
0
1
2
3
4
5
6
7
8
9
10

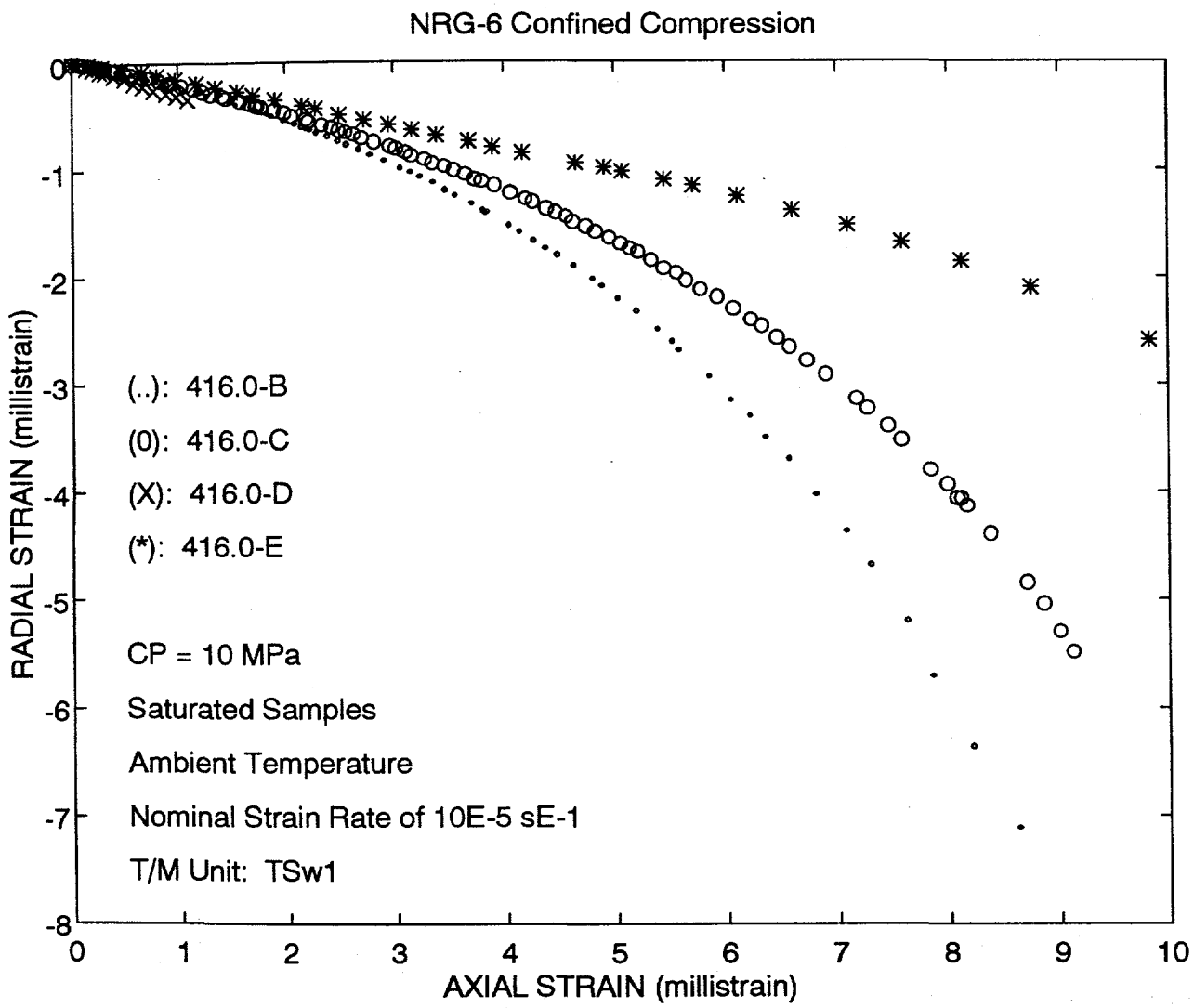
NRG-6 Confined Compression
RADIAL STRAIN (millistrain)
AXIAL STRAIN (millistrain)
0
-1
-2
-3
-4
-5
-6
-7
-8
0
1
2
3
4
5
6
7
8
9
10
(..): 416.0-B
(0): 416.0-C
(X): 416.0-D
(*): 416.0-E
CP = 10 MPa
Saturated Samples
Ambient Temperature
Nominal Strain Rate of 10E-5 sE-1
T/M Unit: TSw1

APPENDIX III

System Checks Using an Aluminum Standard Specimen

System Checks Using an Aluminum Standard Specimen

Unconfined compression experiments were performed on a specimen of 6061-T6511 aluminum. The specimen was monotonically loaded at a constant strain rate of 10^{-5} s^{-1} to 138 MPa, (i.e., approximately one-half of its yield stress). Young's modulus and Poisson's ratio were computed from the stress and strain data. The purpose of the system checks is to ensure that the entire system is performing correctly and that the reported data are accurate.

A system check involves performing the uniaxial compression experiment on aluminum and comparing the observed Young's modulus and Poisson's ratio with the standard values reported for the material. If the measured values deviate by more than ± 5 percent from the published reference values, corrective measures are taken and no further experiments are performed on tuff until the aluminum calibration experiment yields acceptable elastic constants.

Typical results from a calibration experiment are shown in Figure A-1. Axial stress and radial strain are plotted as a function of axial strain for an aluminum specimen with the same nominal dimensions as the tuff. These data were collected using the procedure specified for the unconfined compression experiments. The specimen is cyclically loaded to one-half its yield stress at a strain rate of 10^{-5} s^{-1}; Young's modulus and Poisson's ratio are computed from the data.

A summary of the system checks performed during the course of the study of the specimens from the USW NRG-6 borehole are presented in Table A-1. The results indicate that the system performed within the specified accuracy during the course of the study. However, for the system check performed on May 13, 1993, Poisson's ratio exceeded the ± 5 percent specification. Several corrective measures were taken. Initially, the specimen was rotated 90° and retested. These data showed that the system was performing satisfactorily. In order to further investigate the reason for the deviation several measures were taken to identify the problem. First, the LVDTs were recalibrated. The calibration factors for the LVDTs were within specification. Second, the spring and the screw adjustment on the radial deformation gage were examined. The adjustment screw was remachined to correct wear that had occurred during the previous suite of experiments. A subsequent system check on May 14, 1993, produced an acceptable system check.

Compressional and shear wave velocities were measured on the aluminum standard specimen. These data were used to compute the dynamic Young's modulus and Poisson's ratio. These values are also shown in Table A-1. The fact that these values for both

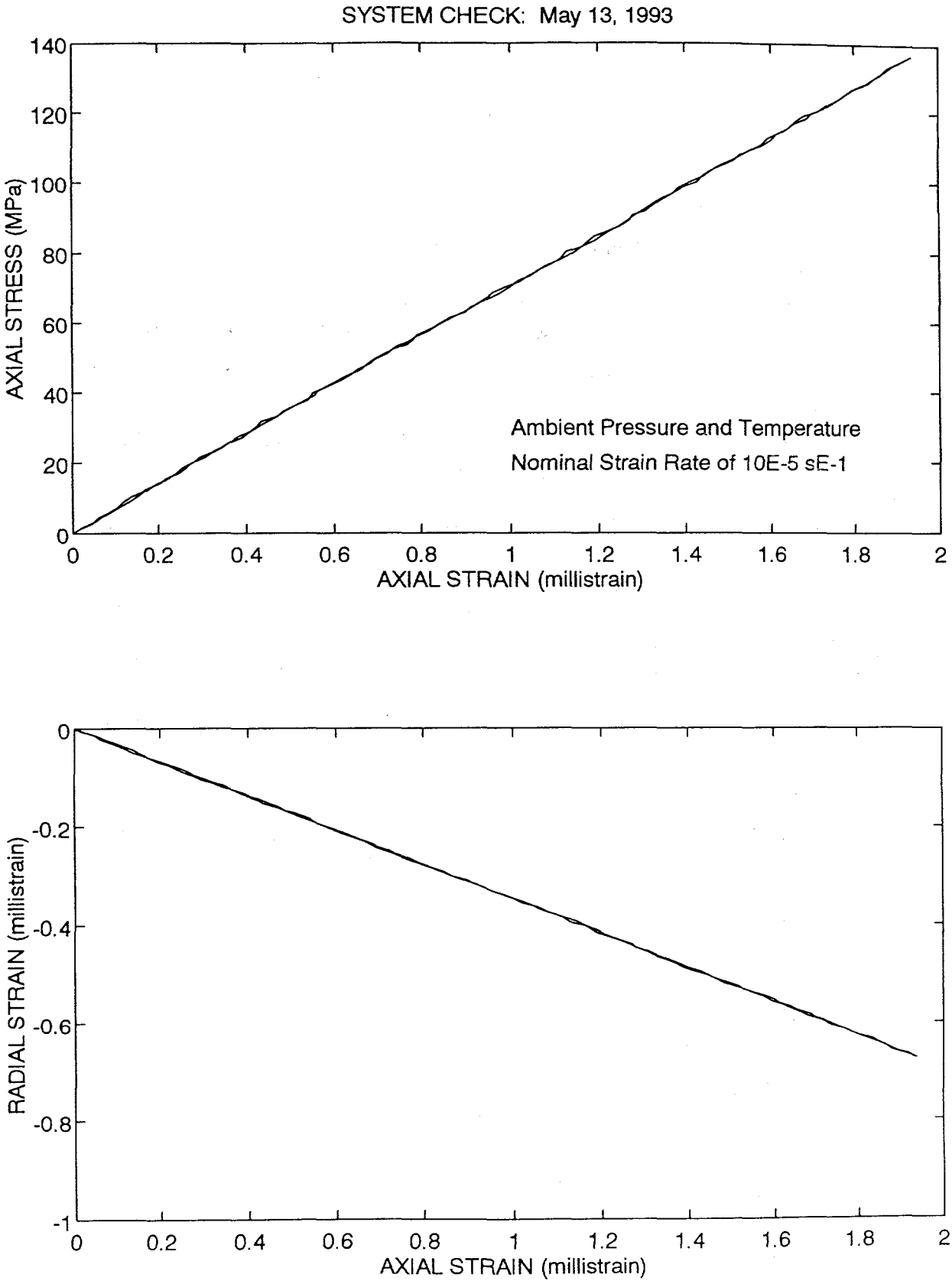

Figure A-1: Axial stress and radial strain are plotted as a function of axial strain for a specimen of 6061-T6511 aluminum cyclically loaded in unconfined compression.

Table A-1

USW NRG-6
System Checks
Aluminum Standard - 6061 T6511

Date	Young's Modulus GPa	Deviation %	Poisson's Ratio	Deviation %
3-May-93	69.92	0.4%	0.34	3.0%
	69.97	0.4%	0.34	3.0%
11-May-93	70.61	1.3%	0.34	3.0%
13-May-93	70.45	1.1%	0.348	5.5%
	69.87	0.3%	0.345	4.5%
14-May-93	68.95	-1.0%	0.34	3.0%
9-Jun-93	69.46	-0.3%	0.34	3.0%
23-Jun-93	70.04	0.5%	0.34	3.0%
2-Jul-93	68.73	-1.4%	0.34	3.0%
28-Jul-93	69.39	-0.4%	0.34	3.0%
Reference	69.66		0.33	
Dynamic	71.02		0.34	

Young's modulus and Poisson's ratio are larger than those given in the literature, suggests that there are minor variations in the properties of aluminum supplied by the manufacturer. The elastic moduli for nonporous materials are frequently computed from the compressional and shear wave velocities. These dynamic values should be used in conjunction with the static measurements . In many cases, the manufacturer's data are obtained for tension experiments and empirically corrected for compression, which can also lead to a discrepancy.

APPENDIX IV

Information from the Reference Information Base Used in this Report

This report contains no information from the Reference Information Base.

Candidate Information for the Reference Information Base

This report contains no information for the Reference Information Base.

Candidate Information for the Geographic Nodal Information Study and Evaluation System

This report contains candidate information for the Geographic Nodal Information Study and Evaluation System (GeNESIS) in Tables 1, 2, 3, and 4. The data have been submitted to the SNL Participant Data Archive (PDA) and are indexed in the Automated Technical Data Tracking system (ATDT). The data packages have the following Data Tracking Numbers (DTN): SNL02030193001.001, SNL02030193001.002, SNL02030193001.004, and SNL02030193001.008.

YUCCA MOUNTAIN SITE CHARACTERIZATION PROJECT

DISTRIBUTION LIST

1 D.A. Dreyfus (RW-1)
Director
OCRWM
US Department of Energy
1000 Independence Avenue SW
Washington, DC 20585

1 L.H. Barrett (RW-2)
Acting Deputy Director
OCRWM
US Department of Energy
1000 Independence Avenue SW
Washington, DC 20585

1 J.D. Saltzman (RW-4)
Office of Strategic Planning and International Programs
OCRWM
US Department of Energy
1000 Independence Avenue SW
Washington, DC 20585

1 J.D. Saltzman (RW-5)
Office of External Relations
OCRWM
US Department of Energy
1000 Independence Avenue SW
Washington, DC 20585

1 Samuel Rousso (RW-10)
Office of Program and Resource Mgt.
OCRWM
US Department of Energy
1000 Independence Avenue SW
Washington, DC 20585

1 J. C. Bresee (RW-10)
OCRWM
US Department of Energy
1000 Independence Avenue SW
Washington, DC 20585

1 R.M. Nelson (RW-20)
Office of Geologic Disposal
OCRWM
US Department of Energy
1000 Independence Avenue, SW
Washington, DC 20585

1 S. J. Brocoum (RW-22)
Analysis and Verification Division
OCRWM
US Department of Energy
1000 Independence Avenue SW
Washington, DC 2585

1 D. Shelor (RW-30)
Office of Systems and Compliance
OCRWM
US Department of Energy
1000 Independence Avenue, SW
Washington, DC 20585

1 J. Roberts (RW-33)
Director, Regulatory Compliance Division
OCRWM
US Department of Energy
1000 Independence Avenue, SW
Washington, DC 20585

1 G. J. Parker (RW-332)
Reg. Policy/Requirements Branch
OCRWM
US Department of Energy
1000 Independence Avenue, SW
Washington, DC 20585

1 R. A. Milner (RW-40)
Office of Storage and Transporation
OCRWM
US Department of Energy
1000 Independence Avenue, SW
Washington, DC 20585

1 S. Rousso (RW-50)
Office of Contract Business Management
OCRWM
US Department of Energy
1000 Independence Avenue, SW
Washington, DC 20585

1 T. Wood (RW-52)
Director, M&O Management Division
OCRWM
US Department of Energy
1000 Independence Avenue, SW
Washington, DC 20585

4 Victoria F. Reich, Librarian
Nuclear Waste Technical Review Board
1100 Wilson Blvd, Suite 910
Arlington, VA 22209

5 R.M. Nelson Jr, Acting Project Manager
Yucca Mountain Site Characterization Office
US Department of Energy
P.O. Box 98608--MS 523
Las Vegas, NV 89193-8608

1 C. L. West, Director
Office of External Affairs
DOE Nevada Field Office
US Department of Energy
P.O. Box 98518
Las Vegas, NV 89193-8518

8 Technical Information Officer
DOE Nevada Field Office
US Department of Energy
P.O. Box 98518
Las Vegas, NV 89193-8518

1 P. K. Fitzsimmons, Technical Advisor
Office of Assistant Manager for Environmental Safety and Health
DOE Nevada Field Office
US Department of Energy
P.O. Box 98518
Las Vegas, NV 89193-8518

1 D. R. Elle, Director
Environmental Protection and Division
DOE Nevada Field Office
US Department of Energy
P.O. Box 98518
Las Vegas, NV 89193-8518

1 Repository Licensing & Quality Assurance
Project Directorate
Division of Waste Management
US NRC
Washington, DC 20555

1 Senior Project Manager for Yucca Mountain
Repository Project Branch
Division of Waste Management
US NRC
Washington, DC 20555

1 NRC Document Control Desk
Division of Waste Management
US NRC
Washington, DC 20555

1 Philip S. Justus
NRC Site Representive
301 E Stewart Avenue, Room 203
Las Vegas, NV 89101

1 E. P. Binnall
Field Systems Group Leader
Building 50B/4235
Lawrence Berkeley Laboratory
Berkeley, CA 94720

1 Center for Nuclear Waste Regulatory Analyses
6220 Culebra Road
Drawer 28510
San Antonio, TX 78284

3 W. L. Clarke
Technical Project Officer - YMP
Attn: YMP/LRC
Lawrence Livermore National Laboratory
P.O. Box 5514
Livermore, CA 94551

1 J. A. Blink
Deputy Project Leader
Lawrence Livermore National Laboratory
101 Convention Center Drive
Suite 820, MS 527
Las Vegas, NV 89109

4 J. A. Canepa
Technical Project Officer - YMP
N-5, Mail Stop J521
Los Alamos National Laboratory
P.O. Box 1663
Los Alamos, NM 87545

1 H. N. Kalia
Exploratory Shaft Test Manager
Los Alamos National Laboratory
Mail Stop 527
101 Convention Center Dr., #820
Las Vegas, NV 89101

1 N. Z. Elkins
Deputy Technical Project Officer
Los Alamos National Laboratory
Mail Stop 527
101 Convention Center Dr., #820
Las Vegas, NV 89101

5 L. E. Shephard
Technical Project Officer - YMP
Sandia National Laboratories
Organization 6302, M/S 1333
P.O. Box 5800
Albuquerque, NM 87185

1 J. F. Devine
Asst Director of Engineering Geology
US Geological Survey
106 National Center
12201 Sunrise Valley Drive
Reston, VA 22092

1 L. R. Hayes
Technical Project Officer
Yucca Mountain Project Branch
MS 425
US Geological Survey
P.O. Box 25046
Denver, CO 80225

1 V. R. Schneider
Asst. Chief Hydrologist--MS 414
Office of Program Coordination and Technical Support
US Geological Survey
12201 Sunrise Valley Drive
Reston, VA 22092

1 J. S. Stuckless
Geologic Division Coordinator
MS 913
Yucca Mountain Project
US Geological Survey
P.O. Box 25046
Denver, CO 80225

1 D. H. Appel, Chief
Hydrologic Investigations Program
MS 421
US Geological Survey
P.O. Box 25046
Denver, CO 80225

1 E. J. Helley
Branch of Western Regional Geology
MS 427
US Geological Survey
345 Middlefield Road
Menlo Park, CA 94025

1 R. W. Craig, Chief
Nevada Operations Office
US Geological Survey
101 Convention Center Drive
Suite 860, MS 509
Las Vegas, NV 89109

1 D. Zesiger
US Geological Survey
101 Conventional Center Drive
Suite 860, MS 509
Las Vegas, NV 89109

1 G. L. Ducret, Associate Chief
Yucca Mountain Project Division
US Geological Survey
P.O. Box 25046
421 Federal Center
Denver, CO 80225

1 A. L. Flint
US Geological Survey
MS 721
P.O. Box 327
Mercury, NV 89023

1 D. A. Beck
Water Resources Division, USGS
6770 S Paradise Road
Las Vegas, NV 89119

1 P. A. Glancy
US Geological Survey
Federal Building, Room 224
Carson City, NV 89701

1 Sherman S.C. Wu
US Geological Survey
2255 N. Gemini Drive
Flagstaff, AZ 86001

1 J. H. Sass - USGS
Branch of Tectonophysics
2255 N Gemini Drive
Flagstaff, AZ 86001

1 DeWayne Campbell
Technical Project Officer - YMP
US Bureau of Reclamation
Code D-3790
P.O. Box 25007
Denver, CO 80225

1 J. M. LaMonaca
Records Specialist
US Geological Survey
421 Federal Center
P.O. Box 25046
Denver, CO 80225

1 W. R. Keefer - USGS
913 Federal Center
P.O. Box 25046
Denver, CO 80225

1 M. D. Voegele
Technical Project Officer - YMP
SAIC
101 Convention Center Drive
Suite 407
Las Vegas, NV 89109

2 L. D. Foust
Nevada Site Manager
TRW Environmental Safety Systems
101 Convention Center Drive
Suite 540, MS 423
Las Vegas, NV 89109

1 C. E. Ezra
YMP Support Office Manager
EG&G Energy Measurements Inc
MS V-02
P.O. Box 1912
Las Vegas, NV 89125

1 Jan Docka
Roy F. Weston Inc
955 L'Enfant Plaza SW
Washington, DC 20024

1 Technical Information Center
Roy F. Weston Inc
955 L'Enfant Plaza SW
Washington, DC 20024

1 D. Hedges, Vice President, QA
Roy F. Weston Inc
4425 Spring Mountain Road
Suite 300
Las Vegas, NV 89102

1 D. L. Fraser, General Manager
Reynolds Electrical & Engineering Co, Inc
MS 555
P.O. Box 98521
Las Vegas, NV 89193-8521

1 B. W. Colston, President and General Manager
Las Vegas Branch
Raytheon Services Nevada
MS 416
P.O. Box 95487
Las Vegas, NV 89193-5487

1 R. L. Bullock
Technical Project Officer - YMP
Raytheon Services Nevada
Suite P-250, MS 403
101 Convention Center Drive
Las Vegas, NV 89109

PASS Program
Pacific Northwest Laboratories
P.O. Box 999
Richland, WA 99352

1 A. T. Tamura
Science and Technology Division
OSTI
US Department of Energy
P.O. Box 62
Oak Ridge, TN 37831

1 Carlos G. Bell Jr
Professor of Civil Engineering
Civil and Mechanical Engineering Dept.
University of Nevada, Las Vegas
4505 S Maryland Parkway
Las Vegas, NV 89154

1 P. J. Weeden, Acting Director
Nuclear Radiation Assessment Div.
US EPA
Environmental Monitoring
Systems Lab
P.O. Box 93478
Las Vegas, NV 89193-3478

1 ONWI Library
Battelle Columbus Laboratory
Office of Nuclear Waste Isolation
505 King Avenue
Columbus, OH 43201

1 T. Hay, Executive Assistant
Office of the Governor
State of Nevada
Capitol Complex
Carson City, NV 89710

3 R. R. Loux
Executive Director
Agency for Nuclear Projects
State of Nevada
Evergreen Center, Suite 252
1802 N. Carson Street
Carson City, NV 89710

1 C.H. Johnson
Technical Program Manager
Agency for Nuclear Projects
State of Nevada
Evergreen Center, Suite 252
1802 N. Carson Street
Carson City, NV 89710

1 John Fordham
Water Resources Center
Desert Research Institute
P.O. Box 60220
Reno, NV 89506

1 David Rhode
Desert Research Institute
P.O. Box 60220
Reno, NV 89506

1 Eric Anderson
Mountain West Research-
Southwest Inc
2901 N Central Avenue #1000
Phoenix, AZ 85012-2730

1 The Honorable Cyril Schank
Chairman
Churchill County Board of
Commissioners
190 W First Street
Fallon, NV 89406

1 Dennis Bechtel, Coordinator
Nuclear Waste Division
Clark County Department of
Comprehensive Planning
301 E Clark Avenue, Suite 570
Las Vegas, NV 89101

1 Juanita D. Hoffman
Nuclear Waste Repository
Oversight Program
Esmeralda County
P.O. Box 490
Goldfield, NV 89013

1 Eureka County Board of Commissioners
Yucca Mountain Information
Office
P.O. Box 714
Eureka, NV 89316

1 Brad Mettam
Inyo County Yucca Mountain
Repository Assessment Office
Drawer L
Independence, CA 93526

1 Lander County Board of
Commissioners
315 South Humbolt
Battle Mountain, NV 89820

1 Vernon E. Poe
Office of Nuclear Projects
Mineral County
P.O. Box 1026
Hawthorne, NV 89415

1 Les W. Bradshaw
Program Manager
Nye County Repository
P.O. Box 429
Tonopah, NV 89049

1 Florindo Mariani
White Pine County Nuclear
Waste Project Office
457 Fifth Street
Ely, NV 89301

1 Judy Foremaster
City of Caliente Nuclear Waste
Project Office
P.O. Box 158
Caliente, NV 89008

1 Phillip A. Niedzielski-Eichner
Nye County Nuclear Waste
Repository Project Office
P.O. Box 221274
Chantilly, VA 22022-1274

1 Jason Pitts
Lincoln County Nuclear Waste
Project Office
Lincoln County Courthouse
Pioche, NV 89043

1 Economic Development Dept.
City of Las Vegas
400 E. Stewart Avenue
Las Vegas, NV 89101

1 Commmunity Planning and
Development
City of North Las Vegas
P.O. Box 4086
North Las Vegas, NV 89030

1 Community Development and
Planning
City of Boulder City
P.O. Box 61350
Boulder City, NV 89006

1 Commission of the European
Communities
200 Rue de la Loi
B-1049 Brussells
BELGIUM

2 M. J. Dorsey, Librarian
YMP Research and Study Center
Reynolds Electrical &
Engineering Co Inc
MS 407
P.O. Box 98521
Las Vegas, NV 89193-8521

1 Amy Anderson
Argonne National Laboratory
Building 362
9700 S Cass Avenue
Argonne, IL 60439

1 Steve Bradhurst
[redacted]

1 Michael L. Baughman
[redacted]

1 Glenn Van Roekel
Director of Community
Development
City of Caliente
P.O. Box 158
Caliente, NV 89008

1	Ray Williams, Jr [redacted]		MS	
		1	1325	L.S. Costin, 6313
		2	1330	G.M. Gerstner-Miller, 6352 100/1232713/SAND93- 4020/QA
1	Nye County District Attorney P.O. Box 593 Tonopah, NV 89049	8	1330	G.M. Gerstner-Miller DRMS Files SNL02030193001.001 SNL02030103001.002 SNL02030103001.004 SNL02030103001.008
1	William Offutt Nye County Manager Tonopah, NV 89049	20	1330	WMT Library, 6352
		1	1324	P.B. Davies, 6115
1	Charles Thistlethwaite, AICP Associate Planner Inyo County Planning Department Drawer L Independence, CA 93526	1	0827	P.J. Hommert, 1502
		1	1375	D.A. Dahlgren, 4400
		20	1325	R.H. Price, 6313
1	R. F. Pritchett Technical Project Officer - YMP Reynolds Electrical & Engineering Company Inc MS 408 P.O. Box 98521 Las Vegas, NV 89193-8521	5	0899	Technical Library, 13414
		1	0619	Technical Publications, 12613
		2	0100	Document Processing for DOE/OSTI, 7613-2
		1	9018	Central Technical Files, 8523-2
1	Dr. Moses Karakouzian [redacted]			
10	R.J. Martin III New England Research Inc 76 Olcott Drive White River Junction, VT 05001			